國 立 交 通 大 學

電機與控制工程學系

博 士 論 文

基於腦波之駕駛員認知反應估測
及其在安全駕駛的應用

EEG-Based Assessment of Driver Cognitive Responses and Its Application to Driving Safety

研 究 生：吳 瑞 成

指導教授：林 進 燈

中 華 民 國 九 十 四 年 七 月

基於腦波之駕駛員認知反應估測及其在安全駕駛的應用

EEG-Based Assessment of Driver Cognitive Responses and Its Application to Driving Safety

研 究 生：吳瑞成　　Student： Ruei-Cheng Wu

指導教授：林進燈 博士　　Advisor： Dr. Chin-Teng Lin

國 立 交 通 大 學

電 機 與 控 制 工 程 學 系

博 士 論 文

A Dissertation

Submitted to Department of Electrical and Control Engineering

College of Electrical Engineering and Computer Science

National Chiao Tung University

in partial Fulfillment of the Requirements

for the Degree of

Doctor of Philosophy

in

Electrical and Control Engineering

July 2005

Hsinchu, Taiwan, Republic of China

中華民國九十四年七月

博碩士論文授權書

本授權書所授權之論文為本人在_國立交通大學_大學(學院)_電機與控制工程_系所_____組__九十四____學年度第__二__學期取得__博__士學位之論文。

論文名稱：__基於腦波之駕駛員認知反應估測及其在安全駕駛的應用_____

指導教授：__林進燈 博士_____

1. ■同意　　□不同意

本人具有著作財產權之上列論文全文(含摘要)資料，授予行政院國家科學委員會科學技術資料中心(或改制後之機構)，得不限地域、時間與次數以微縮、光碟或數位化等各種方式重製後散布發行或上載網路。

本論文為本人向經濟部智慧財產局申請專利(未申請者本條款請不予理會)的附件之一，申請文號為:_____，註明文號者請將全文資料延後半年再公開。

2. ■同意　　□不同意

本人具有著作財產權之上列論文全文(含摘要)資料，授予教育部指定送繳之圖書館及國立交通大學圖書館，基於推動讀者間「資源共享、互惠合作」之理念，與回饋社會及學術研究之目的，教育部指定送繳之圖書館及國立交通大學圖書館得以紙本收錄、重製與利用；於著作權法合理使用範圍內，不限地域與時間，讀者得進行閱覽或列印。

本論文為本人向經濟部智慧財產局申請專利(未申請者本條款請不予理會)的附件之一，申請文號為:_____，註明文號者請將全文資料延後半年再公開。

3. ■同意　　□不同意

本人具有著作財產權之上列論文全文(含摘要)，授予國立交通大學與台灣聯合大學系統圖書館，基於推動讀者間「資源共享、互惠合作」之理念，與回饋社會及學術研究之目的，國立交通大學圖書館及台灣聯合大學系統圖書館得不限地域、時間與次數，以微縮、光碟或其他各種數位化方式將上列論文重製，並得將數位化之上列論文及論文電子檔以上載網路方式，於著作權法合理使用範圍內，讀者得進行線上檢索、閱覽、下載或列印。

論文全文上載網路公開之範圍及時間 -

本校及台灣聯合大學系統區域網路：94 年 07 月 22 日公開

校外網際網路：94 年 07 月 22 日公開

上述授權內容均無須訂立讓與及授權契約書。依本授權之發行權為非專屬性發行權利。依本授權所為之收錄、重製、發行及學術研發利用均為無償。上述同意與不同意之欄位若未鉤選，本人同意視同授權。

研究生簽名：　吳瑞成　　學號：8612812

（親筆正楷）　　（務必填寫）

日期：民國九十四年　七　月二十二日

1.　本授權書請以黑筆撰寫並影印裝訂於書名頁之次頁。

國家圖書館博碩士論文電子檔案上網授權書

本授權書所授權之論文為本人在_國立交通大學_大學(學院)_電機與控制工程_系所_____組__九十四____學年度第__二__學期取得__博__士學位之論文。

論文名稱：__基於腦波之駕駛員認知反應估測及其在安全駕駛的應用_____

指導教授：__林進燈 博士_____

■同意　　□不同意

本人具有著作財產權之上列論文全文(含摘要)，以非專屬、無償授權國家圖書館，不限地域、時間與次數，以微縮、光碟或其他各種數位化方式將上列論文重製，並得將數位化之上列論文及論文電子檔以上載網路方式，提供讀者基於個人非營利性質之線上檢索、閱覽、下載或列印。

上述授權內容均無須訂立讓與及授權契約書。依本授權之發行權為非專屬性發行權利。依本授權所為之收錄、重製、發行及學術研發利用均為無償。上述同意與不同意之欄位若未鉤選，本人同意視同授權。

研究生簽名：　吳瑞成　　學號：8612812

（親筆正楷）　　（務必填寫）

日期：民國九十四年　七　月二十二日

---

1. 本授權書請以黑筆撰寫，並列印二份，其中一份影印裝訂於附錄三之一(博碩士論文授權書)之次頁；另一份於辦理離校時繳交給系所助理，由圖書館彙總寄交國家圖書館。

推薦函

一、 事由：推薦電機與控制工程系博士班研究生吳瑞成提出論文以參加國立交通大學博士論文口試。

二、 說明：本校電機與控制工程系博士班研究生吳瑞成已完成博士班規定之學科及論文研究訓練。

有關學科部分，吳君已修畢應修學分(請查學籍資料)，通過資格考試；有關論文方面，吳君已完成"基於腦波之駕駛員認知反應估測及其在安全駕駛的應用"研究初稿。論文 "EEG-based Drowsiness Estimation for Safety Driving Using Independent Component Analysis", "Estimating Driving Performance Based on EEG Spectrum Analysis", "A Novel Prosodic-information Synthesizer Based on Recurrent Fuzzy Neural Network for the Chinese TTS System" 及 "Noisy Speech Segmentation/Enhancement with Multiband Analysis and Neural Fuzzy Networks"等四篇已經被 *IEEE Transactions on Circuit and System Part I, EURASIP Journal on Applied Signal Processing*, *IEEE Transactions on Systems, Man, and Cybernetics Part B*, 及 *International Journal of Pattern Recognition and Artificial Intelligence* 等期刊所接受，另有論文 "EEG-based Assessment of Driver Cognitive Responses in a Dynamic Virtual-Reality Driving Environment", "Automatic EEG-based Alertness Estimation System Using Fuzzy Neural Networks", 及"Monitoring Alertness Level with Changes in Driving Performance Based on the EEG Power Spectrum Analysis"已投稿至 IEEE 相關期刊並審查中(請參閱博士論文著作目錄)。

總言之，吳君已具備國立交通大學電機與控制工程系博士班研究生應有之教育及訓練水準，因此推薦吳君參加國立交通大學電機與控制工程系博士論文口試。

此致

國立交通大學電機與控制工程系

電機與控制工程系教授

林 進 燈

中華民國九十四年七月

基於腦波之駕駛員認知反應估測及其在安全駕駛的應用

研究生：吳瑞成　　指導教授：林進燈 博士

國立交通大學電機與控制工程學系（研究所）博士班

摘　　要

在這篇論文裡，我們發展先進的生醫訊號處理技術，結合獨立成份分析演算法、腦波頻譜分析、相關係數分析及模糊類神經網路，在虛擬實境技術所建構的認知駕駛實驗環境中，透過非侵入式記錄的腦波電位分析，來辨識人腦對事件刺激的暫態反應以及估測駕駛者的精神警覺程度。並且應用此分析技術去動態量測駕駛員的精神認知狀態變化，與相對應的認知、辨識、車輛控制能力及駕駛行為的改變，以維持駕駛員的高效能表現，並防止駕駛員在開車時，因過失及失誤所造成的意外事故。

我們首先提出一個新的基於獨立成份分析之時態匹配濾波器，去分析單次事件相關腦電位，過濾人為雜訊的干擾，並改進傳統時域疊加方法的缺點，最後利用模糊類神經網路模型去識別駕駛員看到紅綠燈號誌所產生的相對應腦波暫態反應。實驗結果驗證利用多維腦電位訊號去辨識人的精神認知狀態與對事件刺激所造成的腦波暫態反應是可行的，我們所提出的方法可以提高所量測之腦波暫態反應的訊號品質，以達到較高的辨識率。

我們也提出一個新的基於獨立成份分析之適應性特徵值選擇機制，可以從腦波頻譜中選取最有效的獨立成份及具代表性的頻段作為特徵值，對每一個駕駛員建立個別的模糊類神經網路模型，去探索在疲勞或失神時，腦波的活動特性以及所伴隨的駕駛行為變化。實驗結果顯示，人的腦波頻譜變化與開車行為表現之間的關係非常密切，我們所提出的方法不但可以去除大部分人為雜訊的干擾，並且能夠估測最佳的頭皮位置來放置腦波偵測器，以精確的估測駕駛者的精神警覺程度與實際的開車行為變化。此腦波訊號分析技術未來可以利用可攜式嵌入式系統來實現一個線上精神狀態監控系統，以應用到日常生活中。

EEG-Based Assessment of Driver Cognitive Responses and Its Application to Driving Safety

Student：Ruei-Cheng Wu **Advisor：Dr. Chin-Teng Lin**

Department (Institute) of Electrical and Control Engineering

National Chiao Tung University

Abstract

In this thesis, we develop advanced biomedical signal-processing technologies that combine independent component analysis (ICA), power spectrum analysis, correlation analysis, and fuzzy neural network (FNN) models to assess the event-related transient brain dynamics and the level of alertness of drivers by investigating the neurobiological mechanisms underlying non-invasively recorded electroencephalographic (EEG) signals in the virtual-reality-based cognitive driving tasks. The developed techniques are then applied for dynamically quantifying driver's cognitive responses related to perception, recognition, and vehicle control abilities with concurrent changes in the driving performance to maintain their maximum performance in order to prevent accidents caused by errors and failures for driving safety.

We first propose a novel ICA-based temporal matching filter for analyzing the single-trial event-related brain potentials (ERP) without using conventional trial-averaging results as input features of the FNN classifiers and apply this method to recognize the different transient brain responses stimulated by red/green/amber traffic-light events. Experimental results demonstrate the feasibility for identifying multiple streams of EEG signals related to human cognitive states and responses to task events. Our proposed methods can dramatically increase the quantity and quality of momentary cognitive information and achieve high recognition rates.

We also develop a new ICA-based adaptive feature-selecting mechanism to extract most effective bandpower from EEG power spectrum and build an individual FNN model for each subject to further examine the neural activities correlated with fluctuations in human alertness level accompanying changes in the driving performance in the lane-keeping driving tasks.

Experimental results show a closed relationship between changes in EEG power spectrum and the subject's driving performance. Our proposed models also can effectively remove most non-brain artifacts and locate optimal positions to wire EEG electrodes such that it is possible to accurately estimate/predict the continuous fluctuations in human alertness level indexed by measuring the driving performance quantitatively. The computational methods are well within the capabilities of modern digital signal processing hardware to perform in real time and thus might be used to construct and test on a portable embedded system for an online alertness monitoring system in the future.

致　　謝

『未經一番寒徹骨、焉得梅花撲鼻香』

本篇論文之得以完成，首先要感謝我的指導教授 **林進燈博士**在研究及生活各方面的照顧，教授勤勉不倦的研究態度、實事求是的研究精神以及前瞻精準的研究眼光、給我在研究道路上許多啟發、使我獲益良多。其次、我要感謝 **鍾子平博士**的熱心協助及幫忙，解決了許多研究上遇到的疑惑。另外我要感謝段正仁博士、勝富學長、以及交通大學腦科學中心的學弟妹們：文鴻、玉潔、騰毅與士政、俞傑、欣泓、行偉、弘義、力碩、宗哲在實驗操作上的大力幫忙以及謝謝資訊媒體實驗室的所有研究成員、助理們在日常生活上的照顧，謝謝大家。

最後、我要特別感謝我的父母親、家人及思研小姐在背後的支持及鼓勵，讓我能無憂無慮的順利完成學業。

Contents

Lists of Figures

Lists of Tables

1. Introduction

Many disasters and near-disasters have resulted from loss of alertness, lack of attention, or poor decision-making on the part of ship navigators, airplane pilots, railroad engineers, truck and auto drivers, and plant monitors. Catastrophic errors can be caused by momentary lapses in alertness and attention during periods of relative inactivity. Unfortunately, as sixty years of research in human vigilance and attention has shown, humans are not well-suited to maintaining alertness and attention under monotonous conditions, particularly during the normal sleep phase of their circadian cycle. Yet most operative interfaces today simply assume that an alert and attending operator is always present and available to solve unexpected problems and can make decision and perform essential tasks that cannot be automated. Our society thus becomes more and more vulnerable to circadian alertness issues. This motivates us to develop the advanced biomedical signal-processing techniques and to build a human cognitive-state monitoring system to assist operators working in an interactive monitoring or control environment in maintaining a high sustained cognitive capacity while minimizing performance lapses and errors of interpretation, and to demonstrate the feasibility of detecting and modeling, in near real time via multiple streams of psychophysiological information such as electroencephalogram (EEG) and event-related potential (ERP) that organize operators' cognitive states and responses to task events.

In this chapter, a brief overview of methods to assess brain activities related to human cognitive states is presented, including the study of the transient brain dynamics, the relations of brain dynamics to the changes in the cognitive states of human operators, and problems of monitoring driver's cognitive states related to driving errors, which suggested us the direction of developing advanced biomedical signal processing methodologies and application for diving safety issues.

1.1. Assessment of Brain Activities to Human Cognitive States

The human electroencephalogram (EEG), first studied by Berger in the 1920's, represents macroscopic oscillatory and non-oscillatory brain potentials thought to be generated mostly by synchronous post-synaptic currents in large populations of neurons in the cortex. It is a completely non-invasive measurement of brain function by analyzing the scalp electrical activity generated by brain networks that can be applied repeatedly in patients, normal adults, and children with no risks or limitations. For three generations it has been known that abundant information regarding cognitive states such as alertness and arousal is available in EEG recordings. However, relatively little has been done to capture this information in near-real time until the advent of computers fast enough to adequately process the data and signal processing methods capable of extracting the relevant information. For the past thirty years, the dominant analysis method for human cognitive studies has been the averaged evoked response or event-related potential (ERP). Measures of the EEG spectrum have been widely used only to identify stages of sleep. Now that adequate computing power and signal processing algorithms are available, it is of both practical and theoretical interest to know what information about changes in waking human cognitive capacity and behavior is available in complex EEG signals.

1.1.1. Study of the Transient Brain Dynamics

Several groups have attempted to relate brain potentials recorded non-invasively from the human scalp to speculate a cause and effect relationship between EEG and certain stimuli or tasks. These studies have used the EEG spectrogram or the Event-Related brain Potential (ERP)-liked measuring techniques for comparing the complex EEG data to independent task,

performance or subjective rating measures [1-19]. An early effort in this direction, Pfurtscheller and Araniber first reported a method for quantifying the average transient suppression of alpha band (circa 10-Hz) activity following stimulation [3]. In the last decade, researchers studying Pfurtscheller's event-related desynchronization (ERD, spectral amplitude decreases), and event-related synchronization (ERS, spectral amplitude increases) in a variety of narrow frequency bands (4-40 Hz) have reported on their systematic dependencies on task and cognitive state variables as well as on stimulus parameters [4]. For example, Williamson et al. reported that, given a visually presented arithmetic problem to compute mentally, the resulting subject alpha-band ERD resolved only when the calculation was complete [5].

Typically, psychologists calculated averaged Event-Related Potential (ERP) methods by applying simple measures of peak amplitudes and latencies in ERP averages at single scalp channels and focused on the feasibility studies of brain computer interface (BCI) and biofeedback methods in order to choose characters or move a cursor on a computer screen [6-14]. These response averaging, reducing EEG data sets to one or more averaged ERPs, has been the dominant mode of EEG data analysis in cognitive studies for nearly 40 years. The ERP is accomplished by computing averaging epochs (recording periods) of EEG time-locked to repeated occurrences of sensory, cognitive, or motor events [15-18]. Averaged ERPs evoked by brief unattended visual stimuli consist of a sequence of positive and negative peaks that are generally assumed to reflect activity in individual visual cortical processing regions [19]. In this view, response averaging attempts to remove background EEG activity or unrelated noises, whose time course is presumed to be independent of experimental events, as well as artifactual potentials produced by eye and muscle activity, and reflect only activities which are consistently associated with the stimulus processing in a time-locked way.

1.1.2. Monitoring of Human Cognitive State

During the past 10 years, several scientific researches in electrophysiological analysis had been reported to investigate the feasibility of accurately estimating shifts in an operator's global level of alertness by monitoring the changes in the physiological signals. These methods can be further categorized into two main fields. One focuses on detecting physical changes during drowsiness by image processing techniques, such as average of eye-closure speed, percentage of eye-closure over time, eye tracking as quantization of drowsiness level, driver's head movements, and steering wheel angle [20-28]. These methods can be further classified as being either direct contact by attaching sensors to the driver's body or non-contact types by using optical sensors or video cameras to detect vigilance changes and achieve a satisfactory recognition rate. However, these parameters vary in different environmental situations and driving conditions, it would be necessary to devise different detection logic for different types of vehicles. Recently, Van Ordan and et al. further compared these eye-activity based methods to EEG-based methods for alertness estimates in a compensatory visual tracking task [29]. It showed that although these eye-activity variables are well correlated with the subject performance, those eye-activity based methods require a relatively long moving averaged window aiming to track slow changes in vigilance, whereas the EEG-based method can use a shorter moving averaged window to track second-to-second fluctuations in the subject error in a visual compensatory task [40, 49-52].

The other field focuses on measuring physiological changes of drivers, such as heart rate variability (HRV) and electroencephalogram (EEG), as a means of detecting the human cognitive states [30-34]. It has been known that abundant information in electroencephalogram (EEG) recording can relate with drowsiness, arousal, sleep, and attention [35]. Previous psychophysiological studies show that typical sleep rhythm regulated by the circadian process can be divided into non-rapid-eye-movement (NREM) sleep and

rapid-eye-movement (REM) sleep [36-37]. NREM sleep is further subdivided into stages 1-4. In the first part of falling into sleep (micro-sleep at NREM), increasing amplitudes of slow alpha waves of the EEG signals were observed with positive correlation at occipital sites (O1 and O2) and negative correlation at central sites (C3 or C4) [38-39]. While approaches based on EEG signals have the advantages for making accurate and quantitative judgments of alertness levels, relatively little information has been captured in real time until signal processing methods and computer power are fast enough to extract the relevant information from the EEG [40]. Thus, it is practicable and appealing to know what information about human cognitive state and behavior are available through analyzing complex EEG signals.

1.2. Statement of the Problem

Although EEG-based technologies had been studied and applied in cognitive analysis by many psychologists and brain researchers for nearly 40 years. There are still many problems and limitations existing in analyzing the EEG signals and in practical applications. To achieve a reliable and applicable assessment of human cognitive states by investigating the neurobiological mechanisms underlying non-invasively recorded electroencephalographic (EEG) brain dynamics in the cognitive driving tasks, the following issues should be investigated.

1.2.1. Spatial Resolution and Source Localization

Comparing with other physiological signals, such as heart rate variability (HRV), galvanic skin response (GSR), and functional magnetic resonance imaging (fMRI), the EEG has the advantage of high temporal resolution (up to several KHz) and easy implementation to the subjects. However, previous studies used simple measures of peak amplitudes and latencies in ERP averages at single or fewer scalp channels, the spatial resolution of the EEG

signals distributed on the scalp is difficult to be obtained and is incapable of extracting the relevant information. Thus, the possible source localization, which can be used to wire as few as electrodes, related to the external stimulus or the nidus can not be determined, either.

1.2.2. Single-Trial Analysis

Current ERP-based studies attempt to use response overlap-added averaging method in time domain to reducing EEG data sets to one or more averaged ERPs in order to remove the background EEG activity or unrelated noises. However, previous studies had showed evidences from humans and animals experiments, suggesting that averaging ERPs data from a number of experimental trials only conceals rather than reveals the essential nature of event-related brain dynamics [41-44]. Because of the physics of volume conduction, potentials arising through partial synchronization of neural activity, or from artifacts produced by muscle activity or eye movements, all contribute to the signal recorded from nearly any scalp electrodes. Another disadvantage of the trial-averaging method is that it needs to collect many trials first in order to increase the signal-to-noise ratio and thus, is hard to be used in real-time application.

1.2.3. Inter-trial Time-alignment Problem

For single-trial analysis of ERP signals in time domain, the amplitude and latency of the ERP is an important factor for the classification of ERPs. The time-alignment problem is defined as estimating the time lag of ERP latency due to the time-varying and non-stationary properties of the ERPs in single trials related the same stimulus. There are many psychophysiological factors leading to the time-alignment phenomenon of the single-trial ERP signals for one subject, such as the cognitive state of the subject at that moment, and the different response behavior for each trial of the subject, etc. The time-alignment problem

caused by the different time lags of subject's response in different epoch for the same stimulus will lead to serious problems for identifying the ERPs and decrease the recognition rate.

1.2.4. Artifact Removal

One of the important problem of applying EEG-based method to driving task or other applications is artifact handling due to the non-invasively measuring manner of EEG signals. During the period of collecting the EEG signals, subjects move their hands, torso, head, and eyes, which will create huge muscle movement, eye-blinking artifacts, heart rate, and other line noise. Using low pass filtering method or the trial-averaging method will not remove them but mask them only. The other method uses regressions in the time or frequency domain to derive effective parameters characterizing the spread of EOG noises in the EEG channels [45-46]. However, regressing out EOG activity, which also contains brain signals [47], inevitably involves subtracting a portion of the relevant EEG signals and tends to overcompensate for blink artifacts and may introduce new artifacts into EEG records due to the difference between the spatial EOG-to-EEG transfer functions for blinks and saccades. Regression also cannot be used to remove muscle noise or line noise, either, since these have no reference channels [48].

1.2.5. Cross-Subject's Individual Variability

Details of brain dynamics may be as variable between subjects as details of brain shape and orientation. Thus, measures defined a priori and applied uniformly to data from groups of subjects cannot have the statistical power of measures customized to the relevant features of individual subject brain signals such that it is difficult to build a single model to accurately estimate or predict individual changes in alertness and performance of all the subjects [40, 49-52].

1.2.6. Objective Performance Evaluation

Current brain research uses subjective reports, questionnaires, and the judgments based on the expert's knowledge to determine the subject's cognitive states, such as level of drowsiness, and level of motion sickness, etc. An objective statistic measure is needed to quantify the human performance improvement related to subject's cognitive states and to study the objective criterion for evaluating the overall task performance of system operator(s).

1.2.7. Online Application

In order to apply the developed EEG-based methods for online applications outside the psychophysiology laboratory, the proposed signal processing technologies will have the limitations of less computational cost and use as few as EEG electrodes to be easily implemented on a portable real-time embedded system. Therefore, there is a compromise between computational cost and system accuracy.

1.3. Preventions of Road Traffic Accidents

During the past years, driving safety has received increasing attention in public security. The road traffic injuries constitute a major public health and are predicted to increase if it is not addressed adequately and requires more concerted efforts for effective and sustainable preventions. The major risk factors for road driving safety can be roughly classified in two catalogs. One is the environmental influences, such as the enforcement of traffic rules; defects in road design, layout, and maintenance; inadequate visibility to difficultly detect vehicles and other road users; vehicle factors including braking, handling, and maintenance; insufficient vehicle crash protection for occupants and for those hit by vehicles; and the use of seat-belts and child restraints. Another factors related to driver's behaviors including the violation of

traffic regulations; the detection of targets in the periphery of the eye; the estimation of speed and distance; presence of alcohol, medicinal or recreational drugs; the processing of information by the brain; fatigue/micro-sleep; delay in detecting crash; and other physiological factors associated with age and sex that have a bearing on crash risk.

Although many governments and vehicle manufacturers try to make the use of information and publicity on their own to prevent road traffic accidents including strategies to address rates of speed, alcohol consumption; promotion of using helmets and seat belts, or improvement of design and layout of the road, enhancements of vehicle structures and etc. Yet the knowledge currently exists to take action on a number of fronts to prevent these needless deaths, disabilities, immense loss, and suffering they cause. It is still wide held that the major responsibility of the road crashes still rely on driver's errors. Therefore, preventing such accidents is highly desirable but requires techniques to reduce the number of traffic conditions causing death or injury or to prevent accidents before they happen such as eliminating situations that the driver is in insecure essentials. The key points of preventing accidents caused by driver's errors and failures behind the steering wheel related to the driving safety can be roughly recognized into two aspects: the identification of transient brain dynamic responses and the continuous estimation of driver's alertness level, which support information seeking and attention, decision-making, response selection, and anticipation of expected consequences.

1.3.1. Accidents Related to Driver's Transient Response

The human cognitive states accompanying incorrect/absent motor responses or slow responses in driving tasks on the roads may easily triggers an accident and lead to disastrous consequences as an underlying cause. An impaired driver will not take evasive action prior to a collision, where almost 30% of accidents could be avoided by means of reducing the driver

related reaction time by just 0.5 sec, and thus the reductions in traffic crash losses from reducing crashes attributable to driver impairment far exceed reductions from any other potential countermeasure [53].

1.3.2. Accidents Caused by Driver's Loss of Alertness

Previous studies have showed that drivers' fatigue has been implicated as a causal factor in many accidents because of the marked decline in the drivers' abilities of perception, recognition and vehicle control abilities while sleepy [54-56]. The National Highway Traffic Safety Administration (NHTSA) conservatively estimates that 100,000 police-reported crashes are the direct result of driver fatigue each year [57]. This results in an estimated 1,550 deaths, 71,000 injuries and $12.5 billion in monetary losses. The National Sleep Foundation (NSF) also reported in 2002 [58] that 51% of adult drivers had driven a vehicle while feeling drowsy and 17% had actually fallen asleep. The National Transportation Safety Board found that 58 percent of 107 single-vehicle roadway departure crashes were fatigue-related in 1995, where the truck driver survived and no other vehicle was involved.

Driving under the influences of drowsiness will cause (a) longer reaction time, which will produce effects on crash risk, particularly at high speeds; (b) vigilance reduction including non-responses or delaying responding where performance on attention-demanding tasks declines with drowsiness; (c) deficits in information processing, which will reduce the accuracy and correctness in decision-making tasks.

Therefore, the leading response should be to persuade road users to adopt "error-free" behavior and maintain the human high performance in the context of road traffic safety certainly. Developing accurate and continuous techniques for both identifying driver's transient cognitive responses related to environmental stimuli and continuously detecting, estimating, and predicting driver's alertness level would be highly desirable, particularly if

this measure could be further used to predict changes in driver's performance capacity in order to deliver effective feedbacks to maintain their maximum performance.

1.4. Object and Overview of the Thesis

The objects of this thesis are to develop advanced biomedical signal processing methodologies to quantify the level of the human cognitive state with concurrent changes in the driving performance. To achieve these goals, we develop methodologies that combine independent component analysis (ICA), power spectrum analysis, correlation analysis, and fuzzy neural network (FNN) models for ongoing assessment of the transient event-related brain dynamics and the level of alertness of drivers by investigating the neurobiological mechanisms underlying non-invasively recorded multidimensional electroencephalographic (EEG) brain dynamics in the cognitive driving tasks. We then apply these methods to the field of the driving safety, and focus on two major applications, the visual traffic-light detection task and the continuous lane-keeping task on the highway, since they are most frequently happened events on the road in daily life and will easily lead to huge losses in both health injuries and economics.

Three important parts compose this dissertation. The first part describes the research-oriented methodologies for the analysis of human cognitive responses based on EEG signals to support further applications. The second part describes methods for identification of transient brain cognitive responses of drivers related to Red/Yellow/Amber traffic-light events. The last part focuses on developing methods to monitor alertness level of drivers accompanying changes in driving performances and to explore the relationship between brain activities, and human cognitive states. Each of these parts is described in a separate chapter.

In this chapter, the necessity of developing technologies for driving safety has been described, including statistical reports of road traffic injuries, preventions of traffic accidents

by governments and vehicle-manufactories, and problems of monitoring driver's cognitive states related to driving errors, which suggested the direction of the thesis.

In Chapter 2, we proposed advanced signal processing methodologies for the analysis of brain activities related to cognitive states, including virtual reality technology, EEG measurement system, independent component analysis, temporal matching filter, moving averaged power spectral analysis, correlation analysis, and fuzzy neural network model.

In Chapter 3, we describe the system architectures focusing on identification of event-related brain potentials related to driver's transient cognitive responses on traffic-light stimuli, including details of the traffic-light experimental setup, analysis of EEG data using ICA and temporal matching filter, and classification of EEG pattern related to Red/Yellow/Amber stimuli using fuzzy neural networks. Some discussions and conclusion remarks are also included.

In Chapter 4, we propose models for accurately and continuously monitoring level of driver's alertness accompanying changes in driver's performance in a lane-keeping driving task on the virtual-reality-based highway scene. The EEG-based estimation system combines EEG power spectrum, independent component analysis, correlation analysis for adaptive feature selection, and linear regression models and fuzzy neural network estimators. The relationship among EEG power spectrum, driver's alertness level and driving performance are discussed in detail.

In Chapter 5, contributions of this thesis are summarized with final conclusions. Some further applications using the proposed methodologies are also illustrated.

2. Methodology

In this chapter, a brief overview of the advanced EEG-based biomedical signal processing methodologies for identifying/monitoring driver's cognitive states is presented. We propose quantitative techniques for ongoing assessment of both the transient event-related brain dynamics and the level of alertness of drivers by investigating the non-invasively recorded EEG brain dynamics in two cognitive driving tasks. Fig. 2-1 shows the whole system architecture consisted of four major parts. (1) The virtual reality technology is used to construct an interactive driving environment for performing two cognitive driving tasks, the visual traffic-light stimulated experiment and the driver's alertness estimating experiment on highway. (2) The NeuroScan 40-channel EEG measurement system is used to non-invasively collect multidimensional high-fidelity EEG signals. (3) The advanced signal processing technologies are proposed to remove non-brain artifacts, locate optimal positions to wire EEG electrodes, and extract effective features, including independent component analysis, power spectral analysis, correlation analysis, and adaptive feature selecting mechanism. (4) An individual fuzzy neural network model for each subject is used to classify the transient cognitive responses or to monitor the driving performance related to driver's cognitive states.

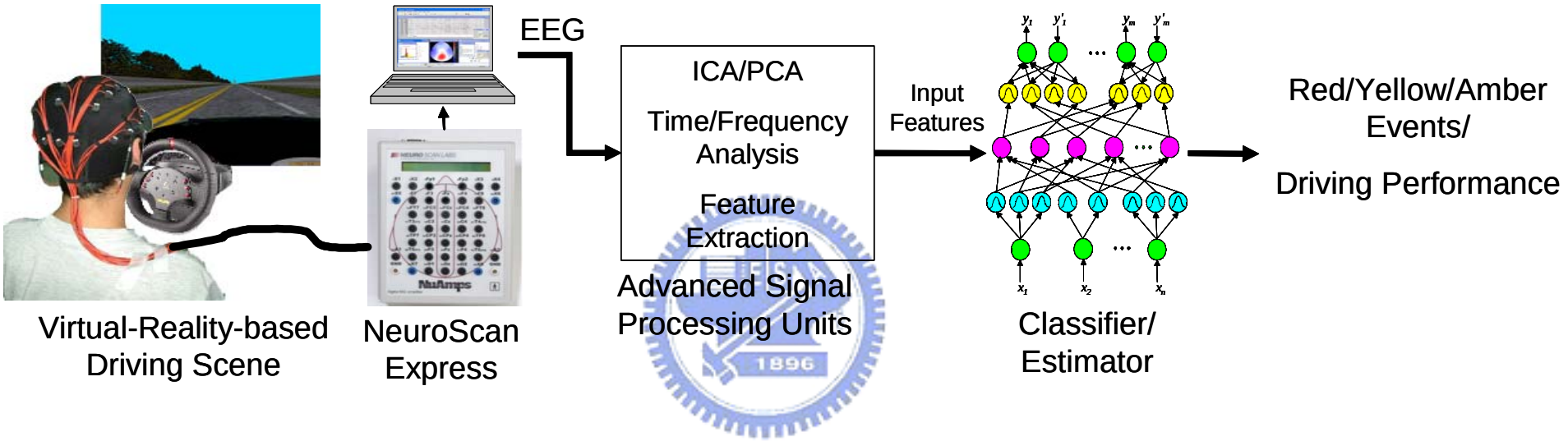

Figure 2-1. The system architecture of the EEG-based driver's cognitive-state monitoring system. It consists of four major parts: (1) Virtual-reality-based driving simulator. (2) The NeuroScan EEG measurement system. (3) Advanced signal-processing unit. (4) Fuzzy-neural-network classifier or estimator.

2.1. Virtual-Reality-based Driving Environment

Public security has become an important issue, especially, the safe manipulation and control of various machines and vehicles such that the authorities can keep emphasizing the strict training of human operators. Currently, such a training process usually relies on the actual machines or vehicles in real sites. This not only has high demands in space, time, and money to perform such a training job, but also leads to another phase of the public security problem. To tackle the above dilemma, the worldwide trend is to use the virtual-reality (VR) technology [59-63] to meet the requirements of public security in training and censoring of human operators. In this way, the operator can feel that he/she is controlling a real machine or vehicle to achieve the goal of real training and censoring.

The VR technology provides a realistic safety environment, which allows subjects to make on-line decisions by directly interacting with a virtual object rather than monotonic auditory and visual stimuli. The VR is also an excellent candidate for brain research on real-time tasks because of its low cost, saving time, less space, and condition control to avoid the risk of operating on the actual machines, and thus extends the applications of possible brain computer interfaces to general populations, not limited to lock-in patients.

In this thesis, we apply the dynamic VR technology to design a well-controlled, virtual driving environment for the cognitive tasks experiments as shown in Fig. 2-2 [61-63]. The high-fidelity interactive 3D scene was developed by the VR development software, WorldToolKit (WTK) library and application programmer's interface (API) [64]. The detailed development diagram of the VR-based scene is shown in Fig. 2-3. It consists of four major components: (1) The textures of the created objects; (2) the corresponding parameters between created objects; (3) the objective dynamic equations of the 3D models; and (4) the control unit to link all the sub-models with the help of WTK library and APIs. To build a realistic driving environment as the test bed for the cognitive tasks, we first create models of

various objects (such as cars, roads, and trees, etc.) for the scene and setup the corresponding positions, attitudes, and other relative parameters between objects. Then, we calculate the parameters of the dynamic equations among these virtual objects and build a complete scene of full functionality with the aid of the high-level C-based API program. Finally, we link the virtual-reality-based driving scene to the EEG measurement/recording system to synchronously provide necessary stimuli and triggering signals for the driving task. Fig. 2-4 and 2-5 show the virtual-city scene for the traffic-light experiment and the highway scene for the lane-keeping experiment, respectively.

Figure 2-2. The virtual-reality-based dynamic driving simulation laboratory.

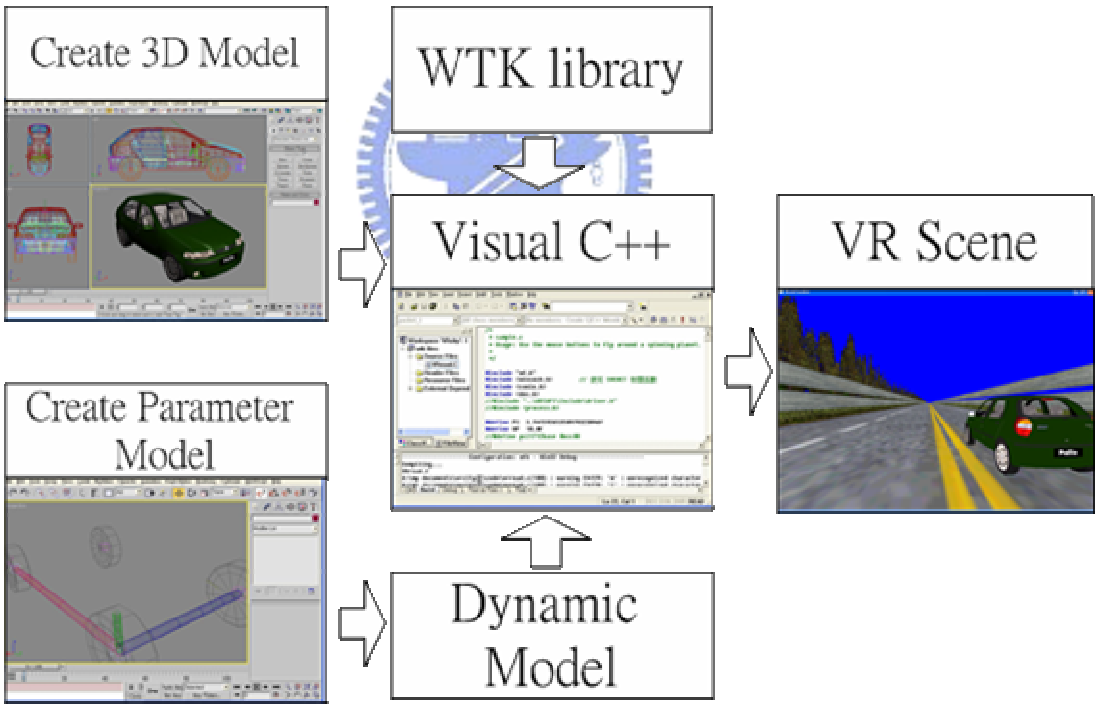

Figure 2-3. Flowchart of the VR-based highway scene development environment. The dynamic models and shapes of the 3D objects in the VR scene are created and linked to the WTK library to form a complete interactive VR simulated scene.

Figure 2-4. Virtual city developed for the VR-based dynamical driving simulator.

Figure 2-5. Virtual-reality-based highway scene

2.2. EEG Measurement System

In this thesis, the EEG/EOG/ECG physiological signals were detected and recorded using the NeuroScan (Scan NuAmps Express System) made by Compumedics Ltd., VIC, Australia. The SCAN NuAmps Express is a fully functional research grade 40-channel digital EEG and ERP recording system. This system allows user to record EEG and conduct spectral analysis, coherence and topographic mapping, where evoked potentials (EP) and event related potentials (ERP) can be recorded, averaged and processed in real-time. Event related spectral analysis, coherence and time frequency measures can be computed. Amplitude and latency measures, peak detection and comparative statistics are provided. Additionally, it also provides a full research grade data processing tool to remove noise and artifacts or decompose complex signals. The whole Scan NuAmps Express System consists of three major components: a NuAmp digital amplifier, a SCAN acquisition and analyzing software, and a multidimensional array of physiological sensors on the scalp based on international 10-20 system as shown in Fig. 2-6.

NuAmps: The NuAmps is a 40-channel monopolar digital amplifier for recording high quality physiological signals. These can be accessed via the high density cap connector or the individual Touch Proof connectors on the face of the amplifier. It was designed as a portable system that obtains power from a laptop computer via USB interface. The power supply of the computer uses the isolation transformer to meet FDA patient safety guidelines for leakage current. The NuAmps is designed to record from Sintered Ag/AgCl electrodes which provide the highest quality and most durable electrical interface. Either individual or cap based electrode systems can be used. NuAmps is a DC amplifier with a maximum sampling rate of 1000 Hz and has an 8 bit stimulus and a 4 bit response input that allows integration of the trigging signals for recording ERPs. The NuAmps also has the facility to support TTL iunput signals from external devices.

SCAN: The SCAN software allows for automation of acquisition and data processing. Real time scalp impedance measurement is included, ensuring fast and simple set up times. All acquired data can be exported for subsequent analysis and a direct import to Matlab software is provided. The SCAN software is capable of computing bipolar derivations and different referencing schemes. Reference and ground channels are included in the count of the 40 channels of NuAmp. In additional to EEG and ERP, other physiological measure can be recorded such as ECG, EMG and EOG.

The SCAN NuAmps Express system requires two computers to be fully operational, one for SCAN and the NuAmps and the other for the virtual reality (VR) system. The connections to the equipment are as follows: The laptop running SCAN connects to the NuAmps via a USB connection. The VR computer connects to the NuAmps via a DB25 pin connector and pigtail converter cable. All of the above cables have an isolation to meet the FDA requirements for leakage current of patient connected devices.

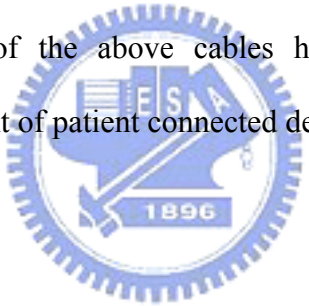

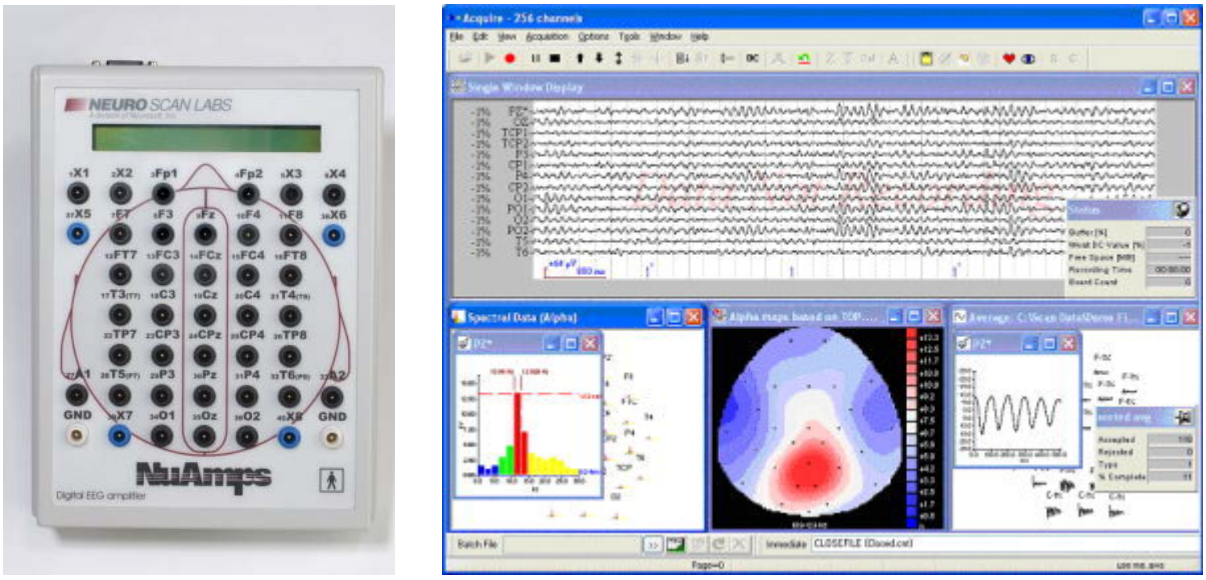

(a) (b)

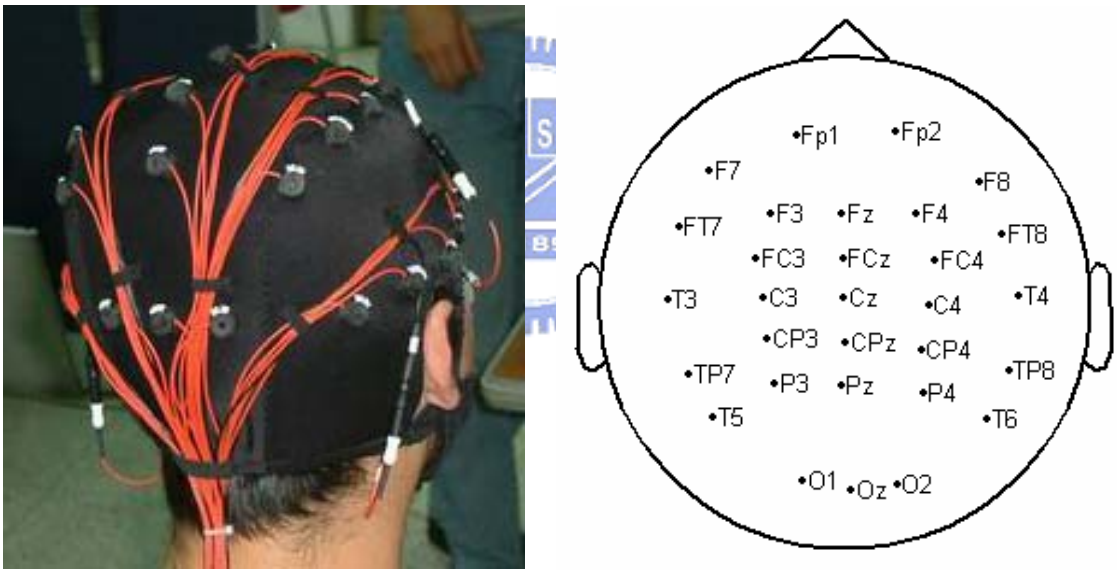

(c) (d)

Figure 2-6. The Scan NuAmp Express System consists of (a) 40-channel NuAmp monopolar digital amplifier, (b) a Scan recording/analyzing software, (c) sintered Ag/AgCl electrodes forming a multidimensional array on the scalp based on (d) international 10-20 system.

2.3. Independent Component Analysis (ICA)

The problem of blind source separation of recorded multi-channel signals into sums of temporally independent sources had been posed some years earlier. In 1994, Comon proposed the first approaches to blind source separation by minimizing the third and fourth-order correlations among the observed variables and achieved limited success in simulations [65]. In 1996, Cardoso, Bell, and Sejnowski generalized this approach, demonstrating a simple neural network algorithm that used joint information maximization or "infomax" as a training criterion [66-67]. By using a compressive nonlinearity to transform the data and then following the entropy gradient of the resulting mixtures, they were able to demonstrate unmixing of ten recorded voice and music sound sources that had been mixed with different weights in ten simulated microphone channels. Their algorithm used only minimal assumptions about the nature of the sources to be separated. Mixing weights (and thus scalp projections) of individual components were assumed to be fixed, and the time courses of the sources mutually independent. In 1996, Makeig and et al further extended the applications of blind decomposition to biomedical time series analysis by applying the infomax ICA algorithm to decomposition of EEG and event-related potential (ERP) data and reported the use of ICA to monitor alertness [49]. This first report demonstrated segregation of eye movements from brain EEG phenomena, and separation of EEG data into constituent components defined by spatial stability and temporal independence. Subsequent technical reports by Ghahremani et al. [68] and Makeig et al. [69] demonstrated successful separation of six simulated EEG sources mixed into six simulated EEG channels using a realistic three-shell head model. Unmixing performance of the ICA algorithm was shown to degrade gracefully in the presence of noise added to simulate sensor noise or additional small EEG sources.

Use of temporal independence as a separation criterion is a novel approach. In contrast,

other EEG decompositions are based on physically modeling the supposed sources [70-71] or on PCA [72]. Makeig et al. evaluated the relative strengths and limitations of the statistical independence criterion using simulations [69]. ICA was successful in separating behaviorally related ERP components in an auditory detection task [73] and several complex visual evoked ERP data sets [43-44, 74-76]. Jung et al. also demonstrated that ICA can also be used to remove artifacts from continuous or event-related (single-trial) EEG data prior to averaging [48, 77-78]. Vigario et al. used a somewhat different ICA algorithm, supported the use of ICA for identifying artifacts in MEG data [79]. Meanwhile, widespread interest in ICA has led to multiple applications to biomedical data as well as to other fields [49, 80]. Most relevant to EEG analysis, McKeown et al. demonstrated the effectiveness of ICA in separating functionally independent components of functional magnetic resonance imaging (fMRI) data [81].

Four main assumptions underlie ICA decomposition of EEG data: (1) Signal conduction times are equal, and summation of currents at the scalp electrodes is linear, both reasonable assumptions for currents carried to the scalp electrodes by volume conduction at EEG frequencies [82]. (2) Spatial projections of components are fixed across time and conditions. (3) Source activations are temporally independent of one another across the input data. (4) Statistical distributions of the component activation values are not Gaussian. (In contrast, PCA assumes that the sources have a Gaussian distribution). The spatial stationarity of the component scalp maps, assumed in ICA, is compatible with the observation made in large numbers of functional imaging reports that performance of particular tasks increases blood flow within small ($\approx cm^3$) discrete brain regions [83]. Since functional hemodynamic imaging experiments typically show metabolic brain increases in defined tasks occur in relatively small cortical areas, EEG sources reflecting task-related information processing may generally assumed to sum activity from compact and spatially stationary generators. However,

spatial stationarity may not apply to some spontaneously generated EEG phenomena such as spreading depression or sleep spindles [84]. To fulfill the temporal independence assumption used by ICA, response components must be activated with temporally independent time courses. For this to occur, the functional degree of independence of different regions of synchronous neural activity, generating the EEG signals, must be expressed in the data. Typically, this means that sufficient numbers of time points need to be used during training.

The joint problems of electroencephalographic (EEG) source segregation, identification, and localization are very difficult since the EEG data collected from any point on the human scalp includes activity generated within a large brain area, and thus, problem of determining brain electrical sources from potential patterns recorded on the scalp surface is mathematically underdetermined. In this thesis, an application of the concept of non-stationary ICA for EEG decomposition is proposed. This is a complex problem, both theoretically and computationally with a tradeoff between the benefits of more complex methods of analysis and their complexity. Normally, more complex methods require more restrictive assumptions to be beneficial. In this thesis, we attempt to completely separate the twin problems of source identification (What) and source localization (Where) by using a generally applicable ICA. Thus, the artifacts including the eye-movement (EOG), eye-blinking, heart-beating (EKG), muscle-movement (EMG), and line noises can be successfully separated from EEG activities. The ICA algorithm was carried out with the "infomax" principle [85-86], where the beauty of the "infomax" approach to blind separation or ICA is the close fit of the "infomax" assumptions to the nature of the EEG data which had been demonstrated in many reports [48, 77-81, 85-86]. The ICA is a statistical "latent variables" model with generative form:

$$\boldsymbol{x}(t) = \boldsymbol{A}\boldsymbol{s}(t), \tag{2.1}$$

where $\boldsymbol{A}$ is a linear transform called a mixing matrix and the s_i are statistically mutually

independent. The ICA model describes how the observed data are generated by a process of mixing the components s_i . The independent components s_i (often abbreviated as ***IC***s) are latent variables, meaning that they cannot be directly observed. Also the mixing matrix ***A*** are assumed to be unknown. All we observed are the random variables x_i, and we must estimate both the mixing matrix and the s_i using the x_i.

Therefore, given time series of the observed data $\boldsymbol{x}(t)=[x_1(t) \quad x_2(t) \quad \cdots \quad x_N(t)]^T$ in *N*-dimension, the ICA is to find a linear mapping ***W*** such that the unmixed signals ***u(t)*** are statically independent.

$$\boldsymbol{u}(t)=\boldsymbol{W}\,\boldsymbol{x}(t) \tag{2.2}$$

Supposed the probability density function of the observations ***x*** can be expressed as:

$$p(\boldsymbol{x})=\left|det(\boldsymbol{W})\right|p(\boldsymbol{u}), \tag{2.3}$$

The learning algorithm can be derived using the maximum likelihood formulation with the log-likelihood function derived as:

$$\boldsymbol{L}(\boldsymbol{u},\boldsymbol{W})=log\left|det(\boldsymbol{W})\right|+\sum_{i=1}^{N} log\ p_i(u_i). \tag{2.4}$$

Thus, an effective learning algorithm using natural gradient to maximize the log-likelihood with respect to ***W*** gives:

$$\Delta\boldsymbol{W}\propto\frac{\partial L(\boldsymbol{u},\boldsymbol{W})}{\partial\boldsymbol{W}}\boldsymbol{W}^T\boldsymbol{W}=\left[\boldsymbol{I}-\varphi(\boldsymbol{u})\boldsymbol{u}^T\right]\boldsymbol{W}, \tag{2.5}$$

where the nonlinearity

$$\varphi(\boldsymbol{u})=-\frac{\frac{\partial p(\boldsymbol{u})}{\partial\boldsymbol{u}}}{p(\boldsymbol{u})}=\left[-\frac{\frac{\partial p(u_1)}{\partial u_1}}{p(u_1)} \quad \cdots \quad -\frac{\frac{\partial p(u_N)}{\partial u_N}}{p(u_N)}\right]^T, \tag{2.6}$$

and $\boldsymbol{W}^T\boldsymbol{W}$ rescales the gradient, simplifies the learning rule and speeds the convergence considerably. It is difficult to know a priori the parametric density function $p(\boldsymbol{u})$, which plays an essential role in the learning process. If we choose to approximate the estimated probability density function with an Edgeworth expansion or Gram-Charlier expansion for generalizing the learning rule to sources with either sub- or super-Gaussian distributions, the nonlinearity $\varphi(\boldsymbol{u})$ can be derived as:

$$\varphi(\mathbf{u}) = \begin{cases} \mathbf{u} - tanh(\mathbf{u}) : \text{for super - Gaussian sources,} \\ \mathbf{u} + tanh(\mathbf{u}) : \text{for sub - Gaussian sources,} \end{cases} \tag{2.7}$$

Then,

$$\Delta W = \begin{cases} \left[\mathbf{I} - \tanh(\mathbf{u})\mathbf{u}^T - \mathbf{u}\mathbf{u}^T\right]\mathbf{W} : \text{super - Gaussian} \\ \left[\mathbf{I} + \tanh(\mathbf{u})\mathbf{u}^T - \mathbf{u}\mathbf{u}^T\right]\mathbf{W} : \text{sub - Gaussian} \end{cases} \tag{2.8}$$

Since there is no general definition for sub- and super-Gaussian sources, if we choose $p(\boldsymbol{u}) = \frac{1}{2}\left(N(1,1) + N(-1,1)\right)$ and $p(\boldsymbol{u}) = N(0,1)sech^2(\boldsymbol{u})$ for sub- and super-Gaussian, respectively, where $N\left(\mu, \sigma^2\right)$ is a normal distribution. The learning rules differ in the sign before the *tanh* function and can be determined using a switching criterion as:

$$\Delta\boldsymbol{W} \propto \left[\boldsymbol{I} - \boldsymbol{K}\,tanh(\boldsymbol{u})\boldsymbol{u}^T - \boldsymbol{u}\boldsymbol{u}^T\right]\boldsymbol{W}, \text{ where } \begin{cases} \kappa_i = 1 : \text{super - gaussian} \\ \kappa_i = -1 : \text{sub - gaussian} \end{cases}, \tag{2.9}$$

where

$$\kappa_i = sign\left(E\left\{sech^2(u_i)\right\}E\left\{u_i^2\right\} - E\left\{tanh(u_i)u_i\right\}\right), \tag{2.10}$$

as the elements of *N*-dimensional diagonal matrix $\boldsymbol{K}$. After ICA training, we can obtain 33 ICA components $\boldsymbol{u}(t)$ decomposed from the measured 33-channel EEG data $\boldsymbol{x}(t)$.

$$\boldsymbol{x}(t)=\begin{bmatrix} x_1(t) \\ x_2(t) \\ \vdots \\ x_{33}(t) \end{bmatrix}=\boldsymbol{W}^{-1}\boldsymbol{u}(t)=\begin{bmatrix} w_{1,1} \\ w_{2,1} \\ \vdots \\ w_{33,1} \end{bmatrix}u_1(t)+\begin{bmatrix} w_{1,2} \\ w_{2,2} \\ \vdots \\ w_{33,2} \end{bmatrix}u_2(t)+\cdots+\begin{bmatrix} w_{1,33} \\ w_{2,33} \\ \vdots \\ w_{33,33} \end{bmatrix}u_{33}(t) \quad (2.11)$$

Fig. 2-7 shows the scalp topographies of ICA mixing matrix $\boldsymbol{W^{-1}}$ corresponding to each ICA component by spreading each $w_{i,j}$ into the plane of the scalp, which provides spatial information about the contribution of each ICA component (brain source) to the EEG channels, e.g., eye activity was projected mainly to frontal sites, and the drowsiness-related potential is on the parietal lobe to occipital lobe, etc. We can observe that the most artifacts and channel noises included in EEG recordings are effectively separated into ICA components 1 and 4 as shown in Fig. 2-7 and the ICA components 5, 11, and 13 may be considered as effective "sources" related to drowsiness in the VR-based driving experiment.

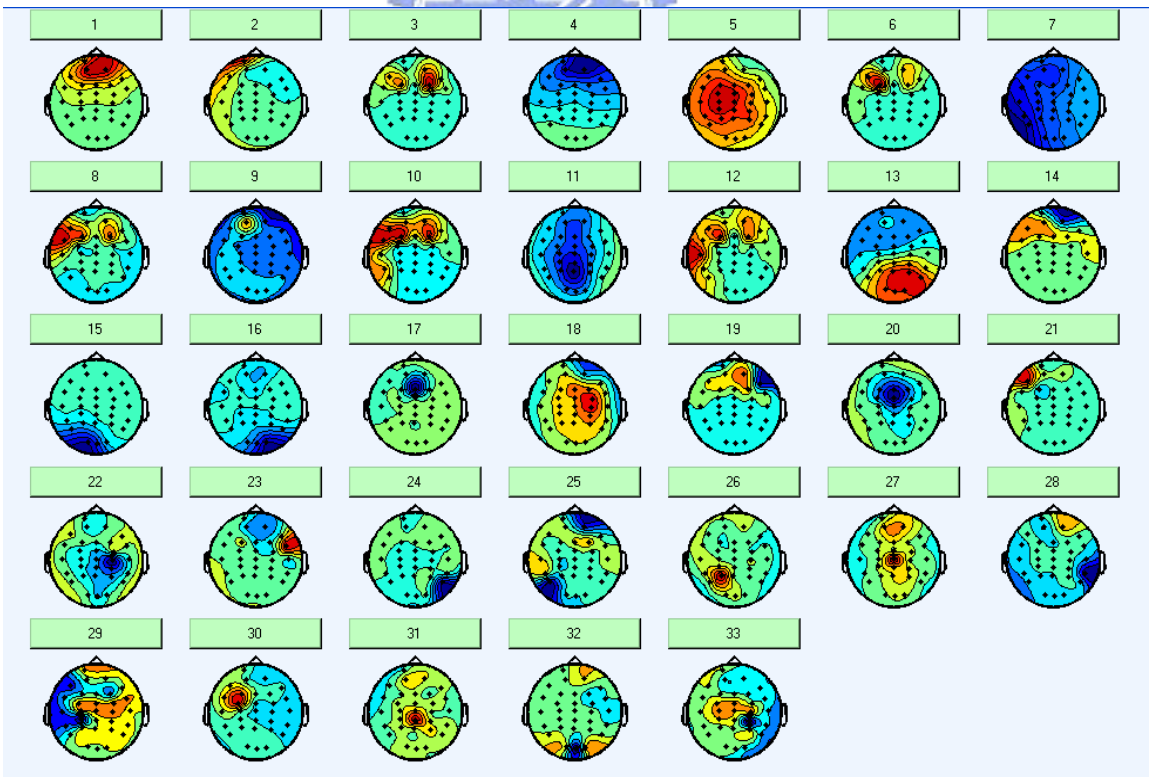

Figure 2-7. Scalp topography of ICA mixing matrix $\boldsymbol{W^{-1}}$ of 33 ICA components trained by EEG data.

2.4. Power Spectral Analysis

Analysis of changes in spectral power and phase can characterize the perturbations in the oscillatory dynamics of ongoing EEG. Applying such measures to the activity time courses of separated independent component sources avoids confounds caused by miscancellation of positive and negative potentials from different sources to the recording electrodes, and by misallocation to the recording electrodes activity that originates in various and commonly distant cortical sources. Fig. 2-8 shows the diagram of moving-average power spectral analysis [87] for one single ICA component, which was decomposed from 33 channels of the EEG signals at sampling rate $\Omega_s = 250$ Hz. The time series of the single ICA component $u_i(t)$ was first divided into several epochs using a 750-point Hanning window with 250-point overlap, i.e., stepping in 2 seconds at sampling rate $\Omega_s = 250$ Hz.

$$p_m(t) = h(t)u_i(t + 500(m-1)), \tag{2-12}$$

where t = 1, 2, …, 750, m is the index of m^{th} epoch, and N-point Hanning window is

$$h(t) = \begin{cases} 0.54 - 0.46\cos(2\pi t/N-1) & 0 \le t \le N-1 \\ 0 & \text{otherwise} \end{cases} \tag{2-13}$$

Windowed 750-point epochs were sub-divided into several 125-point frames using Hanning windows again, with 25-point step size.

$$q_n(t) = h(t)p_m(t + 25(n-1)), \tag{2-14}$$

where t = 1, 2, …, 125, and n is the index of n^{th} frames. Each frame was extended to 256 points by zero-padding for using a 256-point Fast Fourier Transform (FFT) to calculate its power spectrum, where the frequency resolution is near 1 Hz by using a 256-point FFT to the data with 250Hz sampling rate.

$$\upsilon_n(k) = \sum_{t=0}^{N-1} q_n(t) e^{-j\frac{kt}{2\pi N}} \tag{2-15}$$

In this study, there will be many times of wake-sleep cycles in one session of our experiment. Previous studies show that cortical regions produce low amplitude, fast oscillations during waking [88-89]. In contrast, the onset of sleep is marked by high-amplitude, slow cortical oscillations in different frequency bands [90-91]. Therefore, the averaged power spectrum of each epoch was normalized by using logarithmic scaling method in Eq. (2-16) to linearize these expected transient multiplicative effects of subcortical systems involved in wake-sleep regulation of EEG amplitudes [88, 92].

$$\tilde{p}_m(k) = \frac{1}{N_t} \sum_{n=1}^{N_t} 10 log_{10}\left(\upsilon_n(k)^2\right) \tag{2-16}$$

Completing the all epochs of the single ICA component, we obtained the power spectrum time series $\tilde{p}_i(m,k)$, where m is the index of time-stepping, and k is the index of k_{th} frequency index, of i_{th} ICA component $u_i(t)$ for a session consisted of ICA bandpower estimated at 40 frequencies (40 data points presenting from 0.98 to 39.1 Hz) stepping at 2s (500-point, an epoch) time intervals. The same procedure of power spectrum analysis was applied to all 33 ICA components and other 33 EEG channels for comparisons. Finally, a median filtering using a moving averaged 90-s window in Eq. (2-17) was used to further minimize the presence of artifacts in the ICA/EEG signals and to match the time stamp of the driving error index.

$$\boldsymbol{P}_i(n,k) = \frac{1}{M_p} \sum_{m=1}^{M_p} \tilde{p}_i(m+n-1,k) \tag{2-17}$$

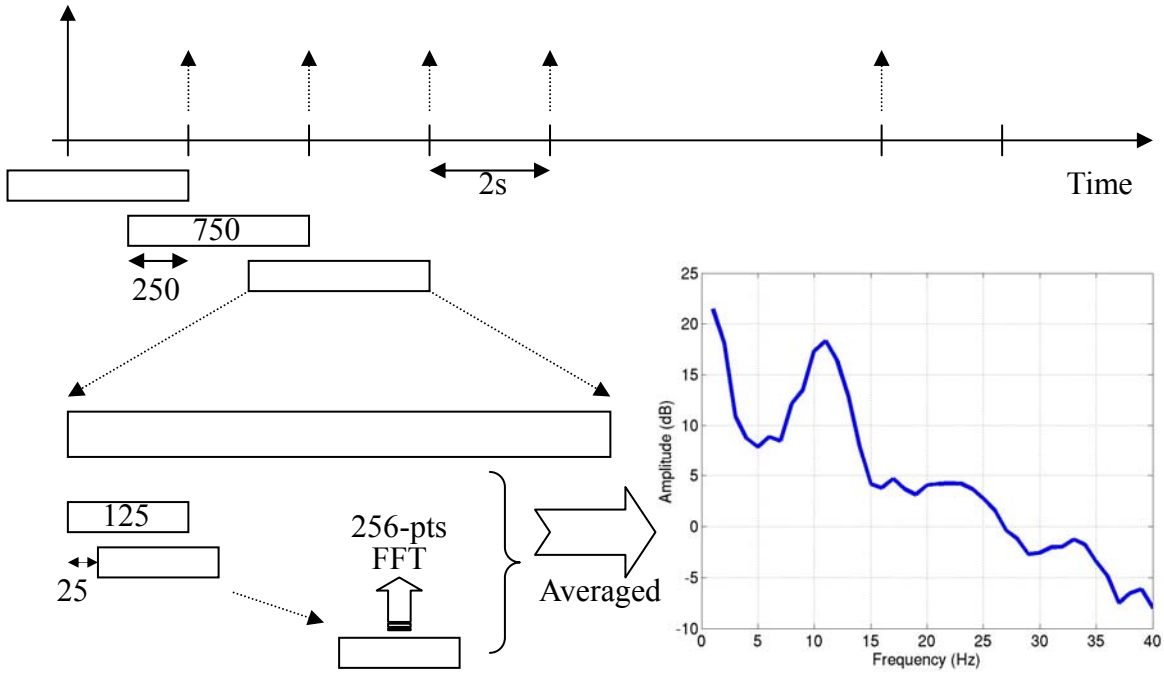

Figure 2-8. Moving-average log power spectral analysis for EEG/ICA signals.

2.5. Correlation Analysis

Supposed the time series of the driving error index stepping in 2 seconds after 90-s moving averaged window was *SDPI(n)*, and the time-frequency series of i_{th} ICA component after 90-s moving averaged window was $\boldsymbol{p}_i(n,k)$, where n is the time stepping size in 2 seconds and k is the frequency index $k = 1, 2, \ldots, 40$. In order to find the relationship between the brain activities and subject's driving performance, and to quantify the level of the subject's drowsiness, we computed the correlation coefficient between the time course of minute-scale fluctuations in driving performance and the concurrent changes in the ICA spectrum of EEG signals by using the Pearson Correlation Coefficient defined as:

$$\boldsymbol{CC}(i,k) = \frac{\sum_n (\boldsymbol{P}_i(n,k) - \overline{P}_i(k))(SDPI(n) - \overline{SDPI})}{\sqrt{\sum_n (\boldsymbol{P}_i(n,k) - \overline{P}_i(k))^2}\sqrt{\sum_n (SDPI(n) - \overline{SDPI})^2}}, \qquad (2\text{-}18)$$

The ***CC(i,k)*** forms a correlation spectrum related to i_{th} ICA component and k_{th} frequency index and is a statistical measure of the linear relationship between two random variables, the driving error index *SDPI(n)*, and ICA power spectrum $\boldsymbol{p}_i(n,k)$, where $\overline{SDPI}$ and $\overline{p}_i(k)$ (related to k_{th} frequency index) are the expected values of *SDPI(n)* and $\boldsymbol{p}_i(n,k)$, respectively. Therefore, the correlation coefficients between the driving performance and the ICA component *i* in the frequency band *k* can be expressed as:

$$\boldsymbol{CC}(i,k)=\begin{bmatrix} c_{1,1} & c_{1,2} & \cdots & c_{1,40} \\ c_{2,1} & c_{2,2} & \cdots & c_{2,40} \\ \vdots & \vdots & \ddots & \vdots \\ c_{33,1} & c_{33,2} & \cdots & c_{33,40} \end{bmatrix} \tag{2-19}$$

Fig. 2-9 (a) and (b) show an example of changes in a single frequency 10 Hz in ICA components 11 and 13 of subject 3 with the minute-scale fluctuation of the driving error index (Fig. 2-9 (c)) in one lane-keeping driving session. Note that the fluctuations in the driving error index change slowly in minute scales, which also can be found in the previous study [40, 51] in an auditory detection task. We can also observe the concurrent changes in the power spectrum in single frequency, e.g. 10 Hz in ICA components 11 and 13 shown in Fig. 2-9 (a) and (b), respectively. We then calculate the correlation coefficient between the time series of the driving error index and the concurrent changes in the power spectrum in single frequency using Eq. (2-18) and obtain a correlation coefficient corresponding to that single frequency. Completing all the frequency (1-40Hz), we get the correlation spectra related to the ICA components 11 and 13 are shown in Fig. 2-9 (d). Fig. 2-10 shows the resulting correlation spectra of subject 3 in 33 ICA components. The horizon axis indexes frequency bands between 1 and 40 Hz and the vertical axis indexes the ICA components. The correlation spectra shows a strong evidence between fluctuations in ICA bandpower of frequency bands within 9 to 25 Hz and driving performance with high positive correlations in ICA components

11 and 13. As driving error increases, so does ICA bandpower.

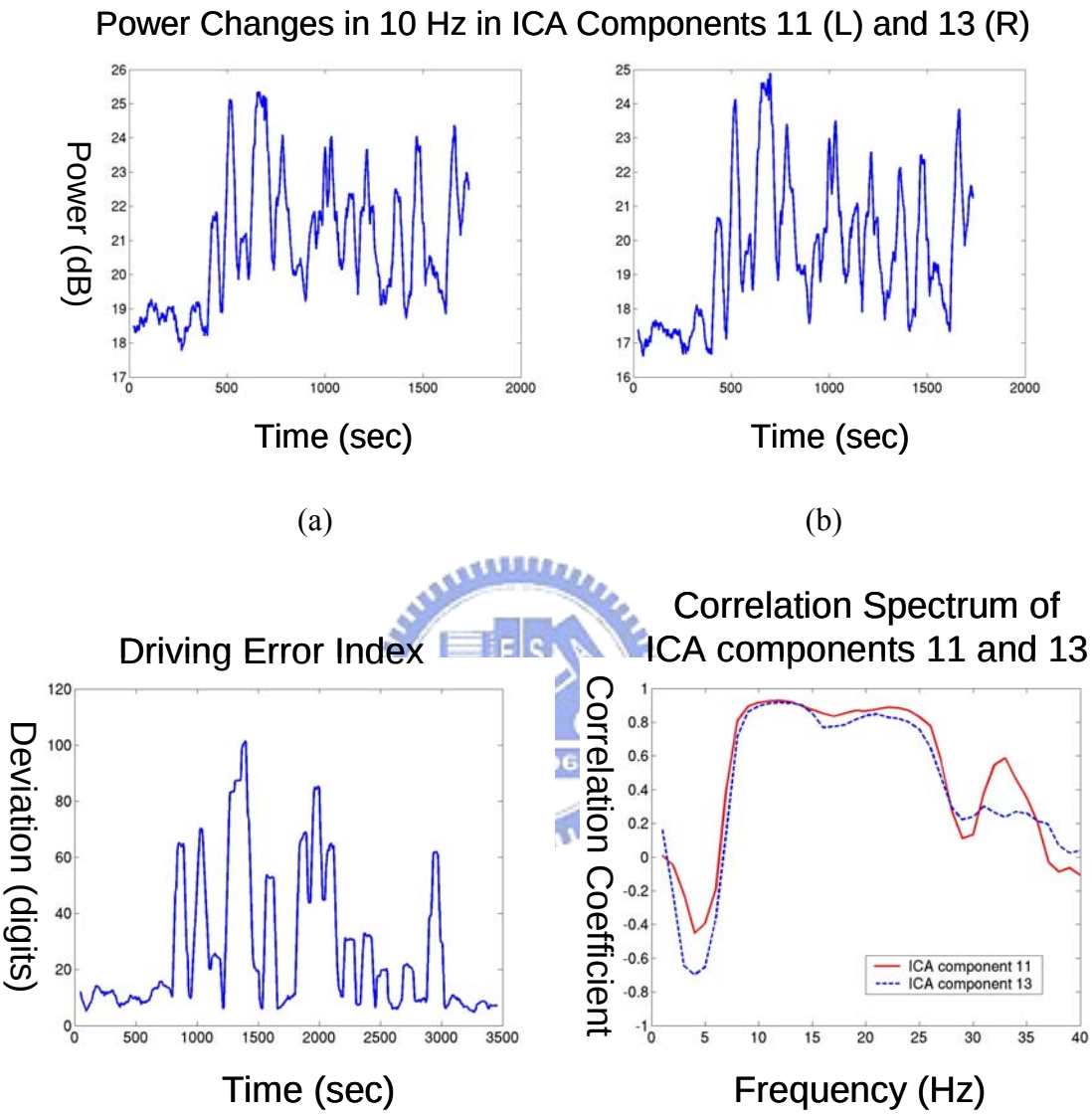

Figure 2-9. Fluctuations in the driving error index and concurrent changes in power spectrum of ICA components and their corresponding correlation spectrum. (a) and (b) shows the changes of power spectrum in 10 Hz with time of the ICA components 11 and 13 of subject 3 after 90-s moving-average spectral analysis. (c) The smoothed 90-s driving error index. (d) Correlation coefficients from 1-40 Hz forming a correlation spectrum of the ICA components 11 and 13.

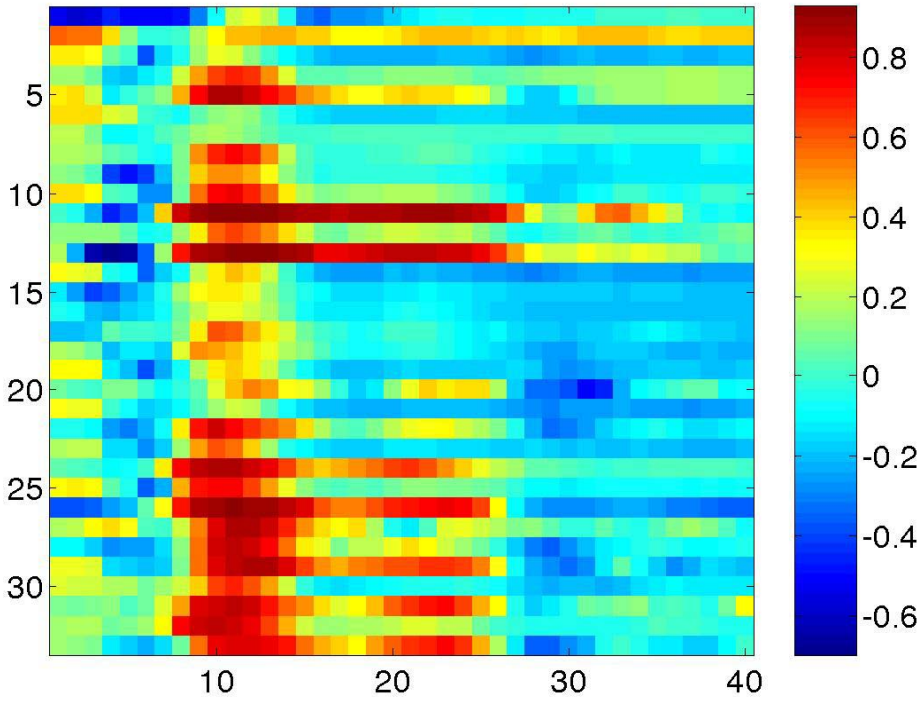

Figure 2-10. Canonical correlation spectral matrix of subject-3. Note that the higher correlation coefficients appear in 9-25 Hz in ICA components 11 and 13, respectively.

2.6. Self-cOnstructing Neuro-Fuzzy Inference Network (SONFIN)

We develop a Self-cOnstructing Neural Fuzzy Inference Network called SONFIN shown in Fig. 2-11, which is a general connectionist model of a fuzzy logic system. The SONFIN can always find its optimal structure and parameters automatically. Both the structure and parameter identification schemes are done simultaneously during on-line learning without any assignment of fuzzy rules in advance. The SONFIN can always construct itself with an economic network size, and the learning speed as well as the modeling ability is well appreciated. Comparing with other neural networks [93-94] in different areas including

control, communication, and signal processing, the on-line learning capability of the SONFIN has been demonstrated. This 6-layered network realizes a fuzzy model of the following form:

$$\text{Rule } i: \quad \text{IF } x_1 \text{ is } A_{i1} \text{ and } \ldots \text{ and } x_n \text{ is } A_{in}$$
$$\text{THEN } y \text{ is } m_{0i} + a_{ji}x_j + \ldots, \tag{2-20}$$

where A_{ij} is a fuzzy set, m_{0i} is the center of a symmetric membership function on y, and a_{ji} is a consequent parameter. Unlike the traditional TSK model where all the input variables are used in the output linear equation, only the significant ones are used in the SONFIN; i.e., some a_{ji}s in the above fuzzy rules are zero.

Each node in Layer 1, which corresponds to one input variable, only transmits input values to the next layer directly. Each node in Layer 2 corresponds to one linguistic label (small, large, etc.) of one of the input variables in Layer 1. A node in Layer 3 represents one fuzzy logic rule and performs precondition matching of a rule. The number of nodes in Layer 4 is equal to that in Layer 3, and the result (firing strength) calculated in Layer 3 is normalized in this layer. Layer 5 is called the consequent layer. Two types of nodes are used in this layer, and they are denoted as blank and shaded circles in Fig. 2-11, respectively. The node denoted by a blank circle (blank node) is the essential node representing a fuzzy set of the output variable. The shaded node is generated only when necessary. One of the inputs to a shaded node is the output delivered from Layer 4, and the other possible inputs (terms) are the selected significant input variables from Layer 1. Combining these two types of nodes in Layer 5, we obtain the whole function performed by this layer as the linear equation on the THEN part of the fuzzy logic rule in Eq. (2-20). Each node in Layer 6 corresponds to one output variable. The node integrates all the actions recommended by Layer 5 and acts as a defuzzifier to produce the final inferred output.

Two types of learning, structure and parameter learning are used concurrently for constructing the SONFIN. The structure learning includes both the precondition and

consequent structure identification of a fuzzy if-then rule. Here the precondition structure identification corresponds to the input-space partitioning and can be formulated as a combinational optimization problem with the following two objectives: to minimize the number of rules generated and to minimize the number of fuzzy sets on the universe of discourse of each input variable. As to the consequent structure identification, the main task is to decide when to generate a new membership function for the output variable and which significant terms (input variables) should be added to the consequent part (a linear equation) when necessary. For the parameter learning based upon supervised learning algorithms, the parameters of the linear equations in the consequent parts are adjusted by either LMS or RLS algorithms and the parameters in the precondition part are adjusted by the back-propagation algorithm to minimize a given cost function.

The SONFIN can be used for normal operation at any time during the learning process without repeated training on the input-output patterns when on-line operation is performed. There are no rules (i.e., no nodes in the network except the input-output nodes) in the SONFIN initially. They are created dynamically as learning proceeds upon receiving on-line incoming training data by performing the following learning processes simultaneously: 1) input/output space partitioning; 2) construction of fuzzy rules; 3) optimal consequent structure identification; 4) parameter identification. In the above, learning processes 1), 2), and 3) belong to the structure learning phase and 4) belongs to the parameter learning phase.

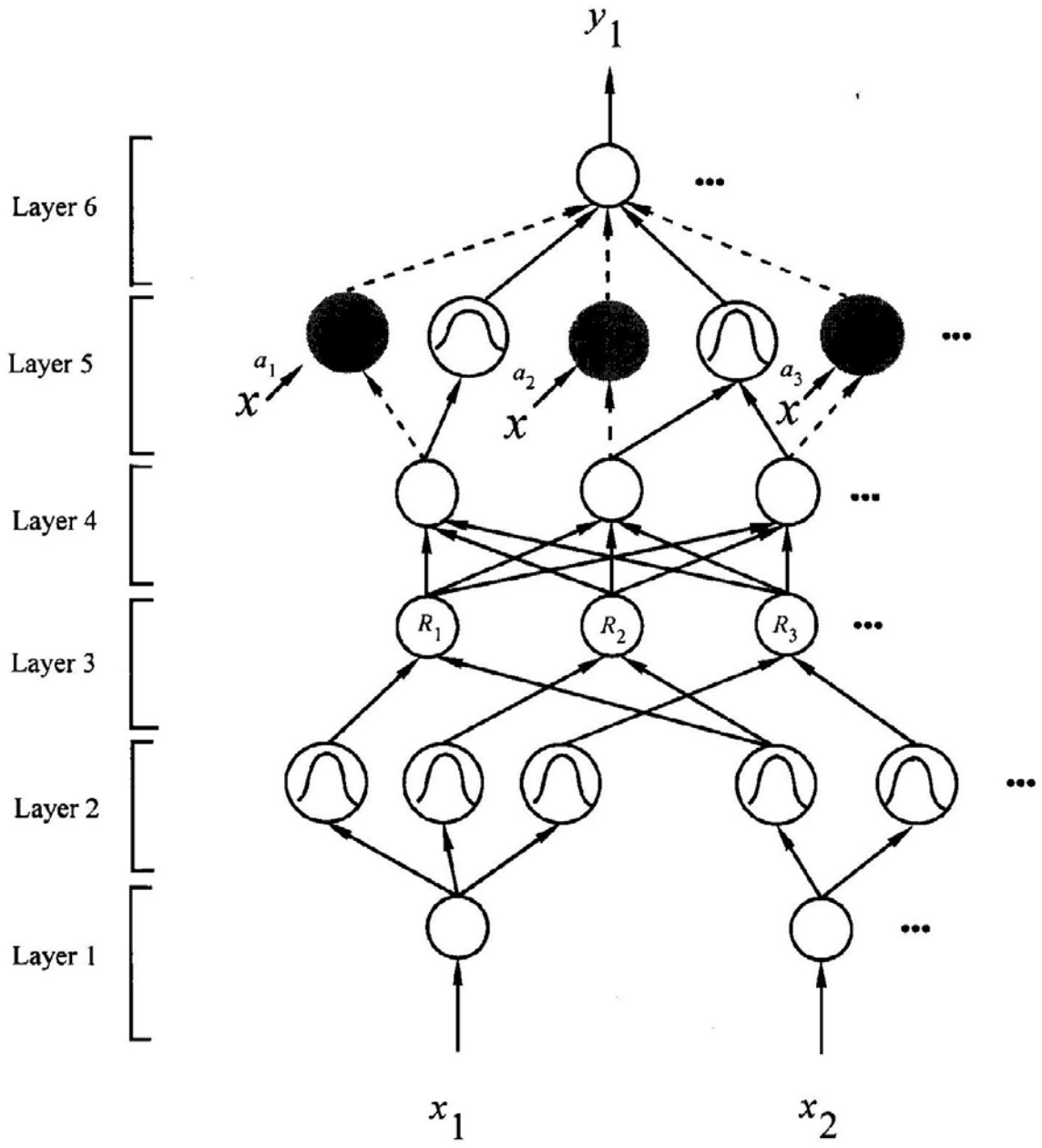

Figure 2-11. The network structure of SONFIN.

3. Classifications of the Transient Brain Dynamics in Single Trials

Accidents caused by errors and failures in human performance among these fatalities have a high rate causing death, especially when driving through the crossroad. A key problem of causing failures is the inability to dynamically quantify cognitive changes in the human capacity to perform such a work. In recent studies [40, 95-102], many researchers had proposed to develop quantitative techniques for ongoing assessment of cognitive effort, engagement and workload, by investigating the neurobiological mechanisms underlying electroencephalographic (EEG) brain dynamics events. A way to determine the relationship between different stimuli and human cognitive responses accompanying correct, incorrect and absent motor responses is the use of event-related brain potential (ERP) signals. An ERP signal can be observed with some latency (e.g., P300) as the stimulus event is given or removed to a subject. We can observe ERP signals in many different stimuli such as audio, vision, pain, electric shock, emotion changes, etc. However, current applications of EEG-based brain research work have limitations due to the signal processing methods are incapable of extracting the relevant information caused by many artificial sources for EEG signals, such as eye movements, eye blinks, cardiac signals, muscle noise, and line noise. Thus, the recent brain computer interface (BCI) works [6-14] have focused on the feasibility studies of on-line averaging and biofeedback methods in order to choose characters or move a cursor on a computer screen.

In this chapter, we develop methods for analyzing single-trial electrical recordings from the human scalp and make it possible to optimally combine multidimensional information obtained from an array of scalp electrodes and to model the dynamics of the underlying brain

networks. This method dramatically increases the amount of transient dynamic cognitive state information that support information seeking and attention, decision-making, response selection, and anticipation of expected consequences. We also design a detailed experimental procedure and a complete analyzing method to detect, acquire, and analyze relationship of human cognitive responses to different events by the use of ERP signals in the traffic-light simulation experiments, which can be applied to on-line vehicle driving-safety system. First, we construct a Red/Green/Amber traffic-light scene based on the interactive virtual reality (VR) technology. We also use the Independent Component Analysis (ICA) to remove a wide variety of artifacts based on blind source separation and to extract the representative features. Then, we design a novel temporal filter to solve the time-alignment problem between single trials and thus increasing the recognition rate of the ERP events. The Principle Component Analysis (PCA) is further used to reduce the feature dimension for realistic applications. Finally, we develop a Self-cOnstructing Neural Fuzzy Inference Network (SONFIN) to classify the recorded ERP signals. This results and know-how can also be generalized to develop computational approaches to analyze neural activity associated with human cognition under kinesthetic/visual/auditory stimuli in EEG experiments and to translate or interpret EEG patterns appropriate for artificial devices as control signals of driving-safety system.

3.1. Virtual-Reality-Based Traffic-Light Experiment

In this thesis, we focus on the detecting and analyzing of the responses of brain activities to the traffic-light events (Red-Green-Amber) in a stoplight detection task since they are the most frequently happened events when driving on the roads and have a high fatality rate when drivers ignore and run the stoplight. A virtual-city scene shown in Fig. 2-4 was first developed based on the virtual reality (VR) technology, which allows subjects to make on-line decisions in a dynamic environment involving interaction with virtual objects to look at on-line cue recognition. For convenient analysis and avoiding additional visual-cue noise, the traffic-light driving simulation in the virtual city is simplified to have three kinds of traffic-light stimuli, the red, green, and amber lights, which are displayed at center on a color XVGA 15” monitor (304.1-mm wide and 228.1-mm high). The VR-based traffic light simulative sequences contain 150 events for each session as shown in Fig. 3-1, where the event allotment ratios are 30%, 60%, and 10% for red, green, and amber traffic lights, respectively. Therefore, there are totally 45 red-light events, 90 green-light events, and 15 amber-light events in a driving session. Previous study had showed that the stimulus needs to be presented both rarely and task relevantly in order to evoke event-related potentials [103-104]. A similar response occurs in a VR driving world, such that each single stimulus was designed to appear in random intervals between 1.7, 2.1, and 2.3 seconds and lasts for 300 ms. The onset time of the traffic-light stimuli and the subject’s response time to the target is triggered by the VR program and recorded synchronously with continuous EEG signals in the EEG measurement system.

3.2. Subject's Protocols

A total of ten subjects (ages from 20 to 40 years) participated in the VR-based traffic-light driving experiments where EEG signals were simultaneously recorded. Each subject participated in six simulated work sessions on the same time in a day. For each session, the subject started with a 5~10 minutes training session to practice the operation in this experiment. Subjects reported that this amount of training was sufficient to train participants to asymptote on the task. Participants were then fitted with an EEG electrode cap to record the physiological EEG signals. After practicing, the subject started a 10-min visual traffic-light detection tasks (10~15 minutes break between sessions) and was asked to decelerate/stop the car when he/she detected a red light, to accelerate the car when he/she saw a amber light, and do nothing (keep constant speed) when he/she saw the green light.

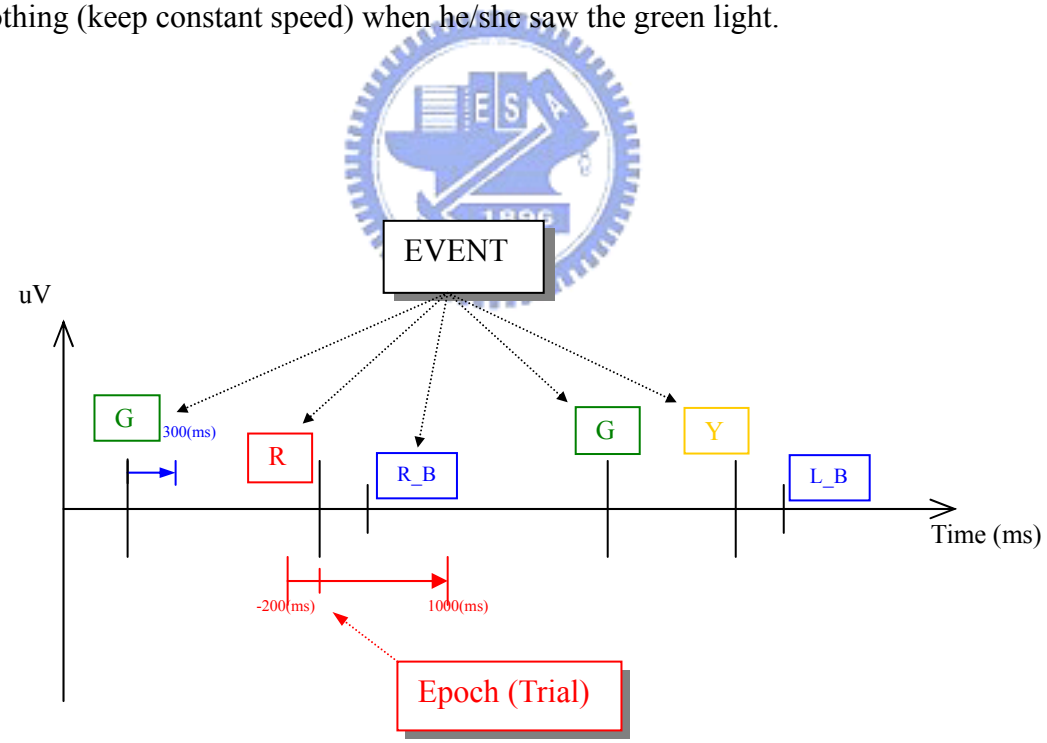

Figure 3-1. Traffic-light stimulus sequences, where G, R, Y representing the Green-light, Red-light, and Amber-light events, respectively, and R_B is the subject's response to the Red-light (e.g., braking the car), and L_B is the subject's response to the Amber-light (e.g., speeding up the car).

3.3. EEG Data Collection

During each visual traffic-light detection session, the 31-channel EEG and 4-channel EOG using sintered Ag/AgCl electrodes with an unipolar reference at right earlobe were simultaneously recorded by the Scan NuAmps Express system (Compumedics Ltd., VIC, Australia). All the EEG/EOG channels were located based on a modified International 10-20 system based on the relationship between the location of an electrode and the underlying area of cerebral cortex. Before data acquisition, the contact impedance between EEG electrodes and scalp was calibrated to be less than 5kΩ. The EEG data were recorded with 16-bit quantization level at a sampling rate 1 KHz and down-sampled to 500 Hz for the simplicity of data processing. Then EEG data were preprocessed using a simple low-pass filter with a cut-off frequency of 50 Hz to remove the line noise (60 Hz and its harmonics) and other high-frequency noise for further analysis. Finally, we successfully collected more than 700 successful ERP events of one subject in a driving experiment. Fig. 3-2 shows an example of the collected time series of EEG signals of subject 1. The red/green/amber traffic-light stimuli were marked as red, green, and yellow lines, respectively. The subject's correctly responded target responses were also observed followed the target stimuli, i.e. a blue line was observed about 300-ms fallen behind the red-light stimulus at 25.7 second, and a cyan line was also observed about 350-ms fallen behind the amber-light stimulus at 23.2 second. To further analyzing the relationship between the visual traffic-light stimuli and the subject's corresponding response, the synchronously measured continuous EEG signals are separated into several epochs/trials where an epoch or a trial contains the sampled EEG data from –200 ms to 1000 ms with a light stimulus given at 0 ms and were connected together as shown in Fig. 3-3 for the analysis of traditional time-domain overlap-added averaged methods or ICA algorithm. The extracted single-trial epochs for the red light stimuli at Pz channel and their time-domain overlap-added average (black line) were shown in Fig. 3-4 (a). Note that the ERP,

P300, was clearly observed. Fig. 3-4 (b) shows the single-trial ERP-image plots of correctly responded target response data at Pz channel (occipital site) from a red-light visual stimulus. The subject's response time (black line) is very time-locked to the P300 ERP corresponding to red-light stimulus. Fig. 3-5 shows the time-domain overlap-added averaged ERP signals for three kinds of traffic-light stimuli in Pz channel. We can observe that the ERPs related to different traffic-lights have apparent differences. Although using the time-domain overlap-added averaged method can successfully observe the appealing differences between ERPs related to different stimuli, it costs much time to collect enough epochs (at least 30 trials) before performing such time-domain overlap-added averaged algorithm and can not be used for online applications. Therefore, in this thesis, we introduce a new single-trial analyzing method based on ICA algorithm to deal with the prior-average problem of time-domain overlap-added averaged method without loss any information of the original ERP signals.

Fig. 3-6 shows the scalp topography of the time series of averaged epochs for one stimulus (red light) of subject 1. The results demonstrated that the active brain responses to significant events or external stimuli involve synchronized oscillations in local field potentials in a number of brain regions as reported in previous studies [15-16]. These brain dynamic events appear to begin in the frontal cortex, implying they carry or channel top-down information about intention, including attentional focus, to sensorimotor brain areas [18] triggering other dynamic events that carry or channel bottom-up information from sensory to response-selection areas [83]. The analyzing results in Figs. 3-2 to 3-6 calibrate the successful design of the visual traffic-light detection tasks.

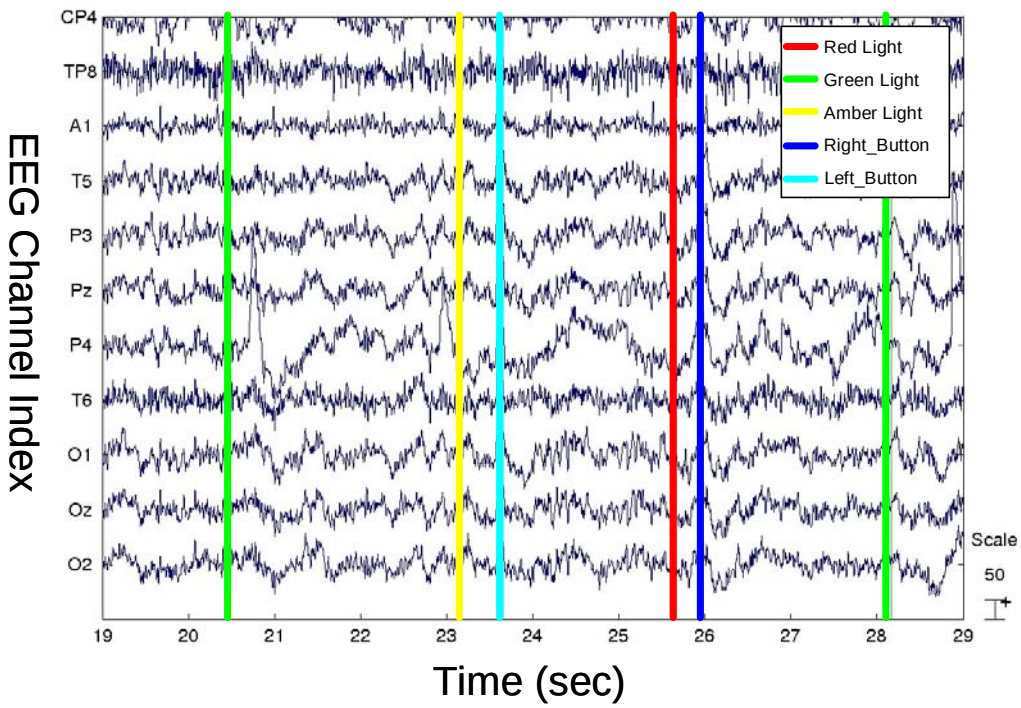

Figure 3-2. An example of the recorded raw data of EEG signals with synchronous onset times of three kinds of the traffic-light stimuli and two kinds of subject's responses. The onset time of the red/green/amber traffic lights are presented as red, green, and yellow lines, and the subject's responses, pressing a right button for a red light and a left button for an amber light, are presented as blue and cyan lines, respectively.

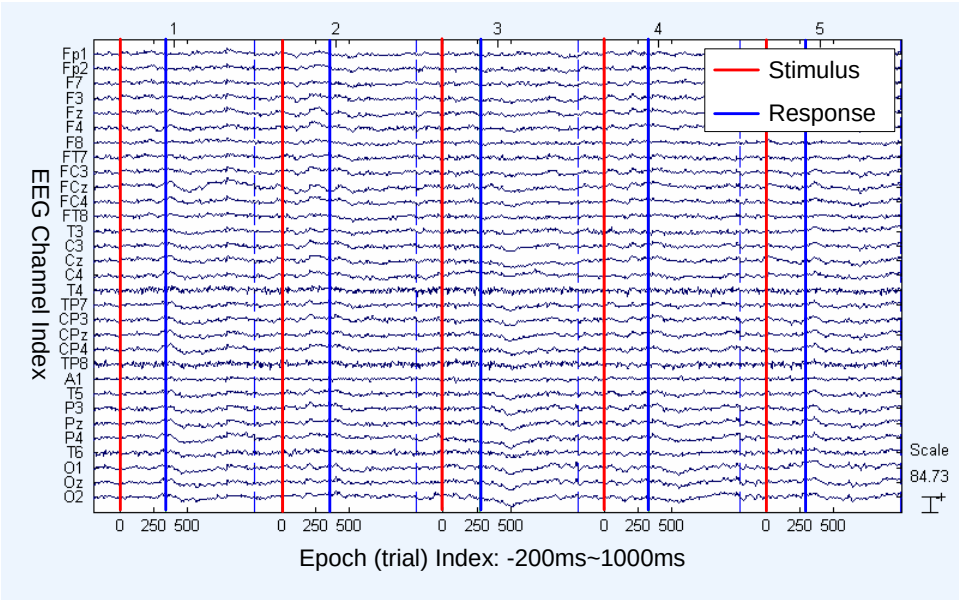

Figure 3-3. Extracted epochs (dashed intervals) for one stimulus (red right) and subject's response (right button).

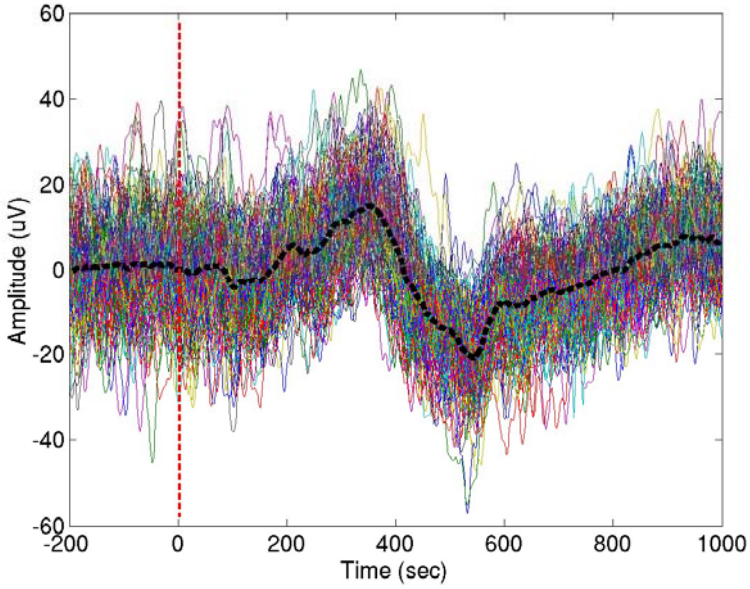

(a)

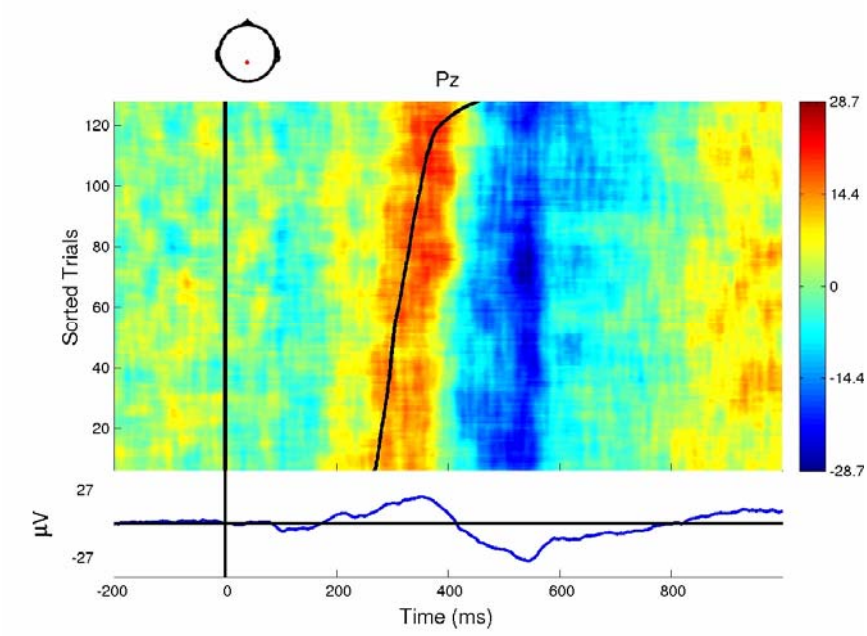

(b)

Figure 3-4. (a) Observed epochs (trials) for the red light stimuli at Pz channels and their time-domain overlap-added average (black line). Note that the ERPs, P300, was clearly observed. (b) Single-trial ERP-image plots of correctly responded target response data at Pz channel (occipital site) from a red-light visual stimulus. The subject's response time (black line) is very time-locked to the P300 ERP corresponding to Red-light stimulus.

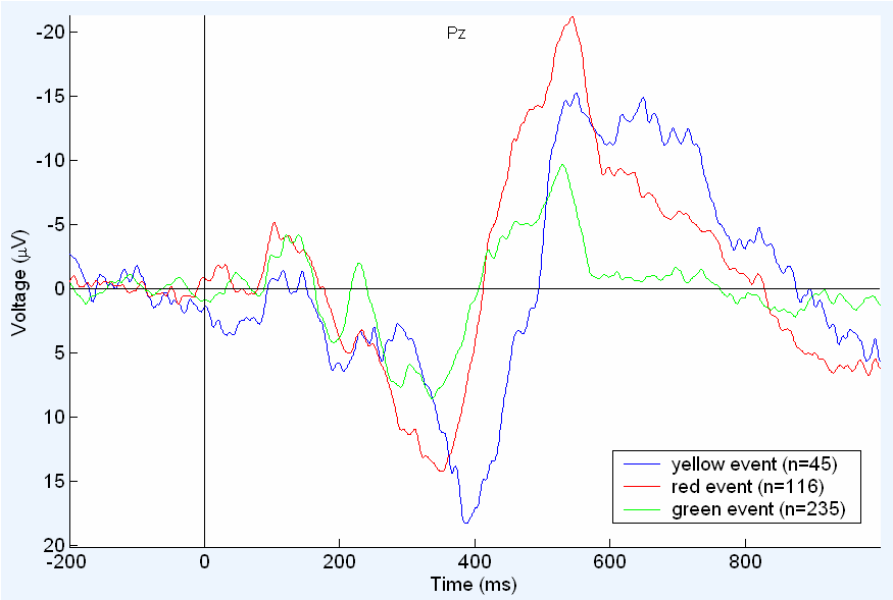

Figure 3-5. Time-domain overlap-added averaged ERP signals for three kinds of traffic-light stimuli in Pz channel.

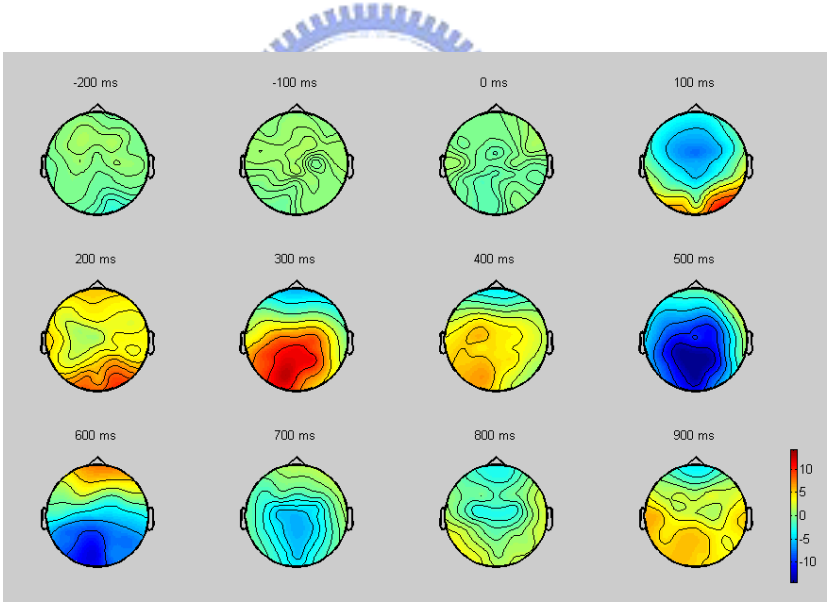

Figure 3-6. Scalp topography of the time series of an averaged epoch for one stimulus (red light). These results show that active brain responses to significant events or external stimuli involve synchronized oscillations in local field potentials in a number of brain regions [28-29]. These brain dynamic events appear to begin in the frontal cortex, implying they carry or channel top-down information about intention, including attentional focus, to sensorimotor brain areas triggering other dynamic events that carry or channel bottom-up information from sensory to response-selection areas.

3.4. Data Analysis

Fig. 3-7 shows the system flowchart for processing the ERP signals. After collecting high-fidelity EEG signals, a low-pass filter is first used to remove the line noise and higher frequency (>50Hz) noise. A first calibration based on time-domain overlap-added averaged ERP and ERP image is perform to demonstrate the validity of the collected EEG signals. In order to remove a wide variety of artifacts and for the applications of on-line use, unlike traditional time-domain overlap-added averaged methods for processing ERP data, the measured ERP signals are further analyzed using ICA algorithm (described in Chapter 2-3) in single trials. The ICA is also used to select possible ERP features related to the traffic-light stimuli based on the time sequences of the ERPs and the corresponding scalp distribution of the ICA components. After extraction of the single-trial ERP signal, we design a novel temporal matching filter to solve the time-alignment problem caused by the variations of subject's response in each single trial. The PCA algorithm is then applied to the filtered ERP data to reduce dimension and select the representative components. Finally, we develop a fuzzy neural network (FNN) model (Chapter 2-6) compared to Learning Vector Quantization method (LVQ) and Back-propagation Neural Network model (BPNN) to on-line classify the ERP data corresponding to different stimuli. The classified results can be used as control and feedback commands in vehicle safety-driving systems.

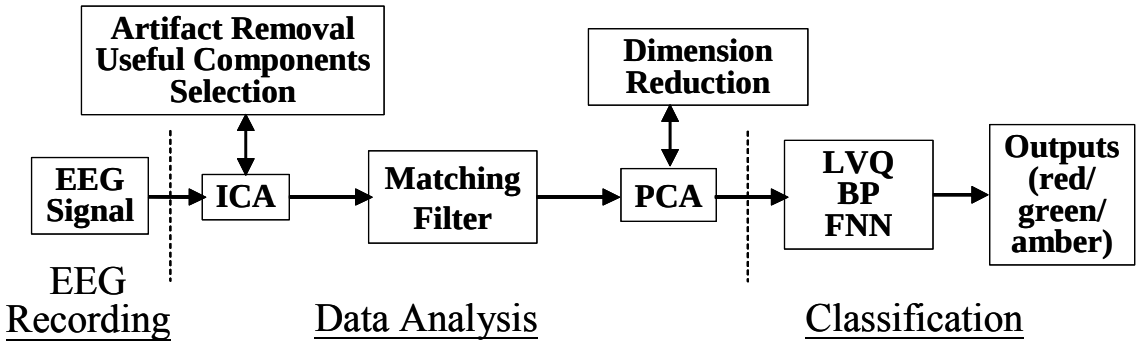

Figure 3-7. Flowchart of ERP data analysis in the visual traffic-light detection experiment.

3.4.1. ICA Decompositions of the ERP Data

The brief schematic depiction of the decomposition by ICA is shown in Fig. 3-8. In our experiment, we assume that the multi-channel EEG recordings are mixtures of underlying brain sources and artificial signals. As discussion in Chapter 2-3, we suppose that the number of sources is the same as the number of sensors by assuming that the source numbers contributing to the scalp EEG are statistically independent; that is, if there are N sensors, the ICA algorithm can separate N source components. The conduction of the EEG sensors is assumed to be instantaneous and linear such that the measured mixing signals are linear and the propagation delays are negligible. We also assume that the signal source of muscle activity, eye, and, cardiac signals are not time locked to the sources of EEG activity which is regarded as reflecting synaptic activity of cortical neurons. Therefore, the time courses of the sources are assumed to be independent. The important fact used to distinguish a source, s_i, from mixtures, x_i, is that the activity of each source is statistically independent of the other sources, i.e., the mutual information between any two sources, s_i and s_j, is zero. The task of ICA algorithm is to recover a version, of the original sources S by finding a square matrix W that inverts the mixing process linearly and save the identical scale and permutation. For EEG analysis, the rows of the input matrix X are the EEG signals recorded at different electrodes, the rows of the output data matrix $u = WX$ are time courses of activation of the ICA components, and the columns of the inverse matrix W^{-1} give the projection strengths of the respective components onto the scalp sensors. The scalp topographies of the components provide information about the location of the sources (e.g., eye activity should project mainly to frontal sites, and the visual event-related potential is on the center to posterior area, etc.). "Corrected" EEG signals can then be derived as $X = W^{-1}u$, where u is the matrix of activation waveforms u.

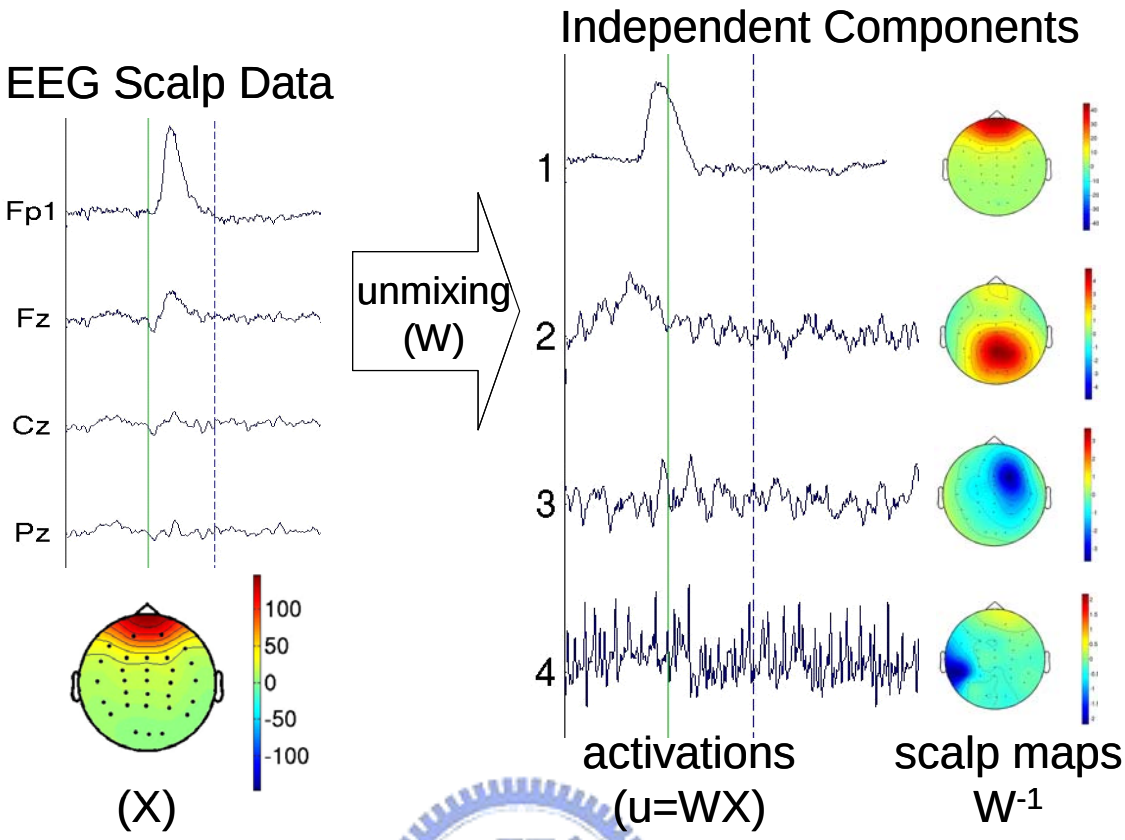

Figure 3-8. Schematic depiction of ICA decomposition of EEG signals.

3.4.2. Temporal Matching Filter

For single-trial analysis of ERP signals in time domain, the amplitude and latency of ERP (P300) is an important parameter for the ERP classification. Due to the time varying and non-stationary property of P300 in each single trial of the same stimulus, one frequent happened problem concerning classification is the time-alignment problem defined as the time varying of the latency in P300. There are many psychophysiological factors leading to the time-alignment phenomenon of the single-trial ERP signals for one subject, such as the cognitive state of the subject at that moment, the different response behavior for each trial of the subject, etc. The time-alignment problem caused by the different time lags of subject's response for the same kind of stimuli in different epoch will lead to serious problems when extracting representative features for the same group of ERP data (i.e., the single trial ERP

signals caused by the same stimulus could be classified into different principles in PCA due to the time alignment problem.) and decrease the recognition rate. To solve such a problem, we process the single-trial EPR signals with short-term techniques using maximum magnitude of cross-correlation function and propose a novel temporal matching filter. Fig. 3-9 shows the concept diagram of this matching filter. After collecting high-fidelity ERP signals, the temporal matching filter is selected by averaging the first N single trials as the standard pattern of P300 for each subject. Then we calculate the cross-correlation value between the matching filter and subsequent single trial, and find out the maximum magnitude of cross-correlation function. Finally, the original single-trial sequence is shifted to a new time sequence according to the maximum cross-correlation value. Detailed algorithms are listed below:

1. Given the input single-trial source component u_i (i is the trial index), we calculate the average of the first N trials by $\bar{u} = \sum_{i=1}^{N} u_i$ as the standard pattern of the matching filter.
2. Find the maximum cross-correlation coefficients between the standard pattern $\bar{u}$ and subsequent single trials by calculating $k_i = \arg\max_j u_{xcorr}(k)$, where $u_{xcorr}(k) = \sum_{j=1}^{M} \bar{u}(j) u_i(j+k)$.
3. Rearrange the time series of each single-trial by $u_i'(j) = u_i(j+k_i)$ as a new input sampled trial.

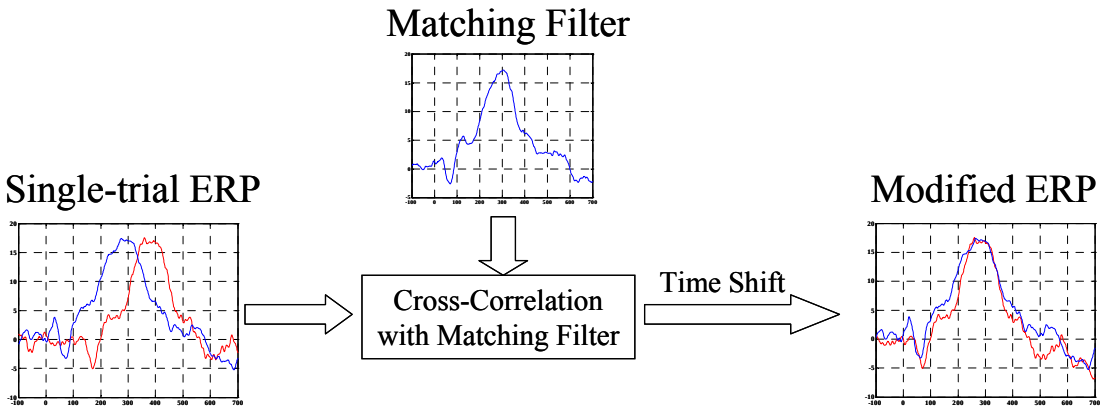

Figure 3-9. The use of Matching Filter for temporal alignment of the single-trial ERP.

3.4.3. Principle Component Analysis (PCA)

Given the observed zero-mean data matrix $X(t)=[x_1(t) \quad x_2(t) \quad \cdots \quad x_N(t)]^T$, the principle component analysis (PCA) is to find an orthogonal $N\times N$ matrix $P=[p_1 \quad p_2 \quad \cdots \quad p_N]$, p_i is a N×1 vector, that determines a transformation of variable, $X(t)=PY(t)$, such that the new variables $Y(t)=[y_1(t) \quad y_2(t) \quad \ldots \quad y_N(t)]$ are uncorrelated and arranged in order of decreasing variances.

Let $S_X = XX^T/(N-1)$ be the covariance matrix of *X(t)* and let *D* be a diagonal matrix with the eigenvalues $\lambda_1,\ldots,\lambda_N$ of S_X, where $\lambda_1 \geq \lambda_2 \geq \ldots \geq \lambda_N \geq 0$. The desired orthogonal matrix *P* is one that makes S_X diagonal by performing $D=P^T S_X P$ where *P*'s columns are the corresponding unit eigenvectors $p_1,\ldots,p_N$ of S_X. The unit eigenvectors $p_1,\ldots,p_N$ are then called the *principle components* of the data. The k_{th} principle component p_k determines the new variable $y_k(t)$ in the following way: Let the entries in p_k express as $p_k=[p_{1,k} \quad p_{2,k} \quad \cdots \quad p_{N,k}]^T$. The equation $X(t)=PY(t)$ shows that $y_k(t)=p_k^T X(t)=p_{1,k}x_1(t)+p_{2,k}x_2(t)+\ldots+p_{N,k}x_N(t)$. Thus, $y_k(t)$ is a linear combination of the original variables, $x_1(t),\ldots,x_N(t)$, using the entries in the eigenvector p_k as

weights. Using a cutoff on the first K_{th} principle components, the observed data matrix may thus be reduced in its dimensionality from N to K without much loss of information [93].

3.4.4. Learning Vector Quantization (LVQ)

The Learning Vector Quantization is a supervised competitive learning algorithm from vector quantization (VQ) and Self-Organizing Map (SOM) algorithm by Kohonen [105-106], which has the network to "discover" structure in the data by finding how the data are clustered. The goal of LVQ algorithm is to approximate the distribution of a class using a reduced number of codebook vectors where the algorithm seeks to minimize classification errors. The algorithm is associated with the neural network class of learning algorithms, though works significantly differently compared to conventional feed-forward networks like Back-propagation. The neural network for learning vector quantization consists of two layers: an input layer and an output layer. It represents a set of reference vectors, the coordinates of which are the weights of the connections leading from the input neurons to an output neuron. Hence, one may also say that each output neuron corresponds to one reference vector. The learning method of learning vector quantization is often called competition learning, because it works as follows [107]: For each training pattern the reference vector that is closest to it is determined. The corresponding output neuron is also called the winner neuron. The weights of the connections to this neuron - and this neuron only: the winner takes all - are then adapted. The direction of the adaptation depends on whether the class of the training pattern and the class assigned to the reference vector coincide or not. If they coincide, the reference vector is moved closer to the training pattern; otherwise it is moved farther away. This movement of the reference vector is controlled by a parameter called the learning rate. It states as a fraction of the distance to the training pattern how far the reference vector is moved. Usually the learning rate is decreased in the course of time, so that initial changes are larger than changes

made in later epochs of the training process. Learning may be terminated when the positions of the reference vectors do hardly change anymore.

3.4.5. Back-propagation Neural Network Model (BPNN)

Another algorithm which has hugely contributed to neural network fame is the back-propagation algorithm [93, 108]. The principal advantages of back-propagation are simplicity and reasonable speed. Back-propagation is well suited to pattern recognition/classification problems. In essence, the back-propagation network is a perceptron with multiple layers, a different threshold function in the artificial neuron, and a more robust and capable learning rule. Back-propagation can train multilayer feed-forward networks with differentiable transfer functions to perform function approximation, pattern association, and pattern classification. The term back-propagation refers to the process by which derivatives of network error, with respect to network weights and biases, can be computed. This process can be used with a number of different optimization strategies. The architecture of a multilayer network is not completely constrained by the problem to be solved. The number of inputs to the network is constrained by the problem, and the number of neurons in the output layer is constrained by the number of outputs required by the problem. However, the number of layers between network inputs and the output layer and the sizes of the layers are up to the designer. The two-layer sigmoid/linear network can represent any functional relationship between inputs and outputs if the sigmoid layer has enough neurons.

3.5. Results and Discussions

In this thesis, we propose a novel ICA-based temporal matching filter for analyzing the single-trial event-related brain potentials (ERP) without first averaging over trials as input features of the FNN classifiers and apply this method to recognize the different transient brain

responses stimulated by red/green/amber traffic-light events. After collecting 31-channel EEG signal, the time-domain overlap-added averaged method was used to calibrate the correctness of the extracted ERP signals for three kinds of stimuli in Pz channel are shown in Fig. 3-2 to Fig. 3-6. We can find that the averaged ERP signal in this traffic-light experiment is similar to the general visual ERP signal, where the event related potentials, P300 were clearly observed. Scalp topography of the time series of an averaged epoch for one stimulus (red light) show that active brain responses to significant events or external stimuli appear to begin in the frontal cortex including attentional focus to sensorimotor brain areas and from sensory to response-selection areas as shown in Fig. 3-6. The averaged EEG responses of three events in Fig. 3-5 are very different and can be used as the features in single trials for further classification. More detailed results are discussed below including artifact removal using ICA, effect with/without matching filter, and comparisons of linear and nonlinear classifiers.

3.5.1. Artifact Removal Using ICA

The measured ERP signals are first analyzed using ICA algorithm trained in single trials as described in Eq. (2-9) in Chapter 2. For EEG analysis, the rows of the input matrix X are the cascade-connection ERP signals recorded at different electrodes, the rows of the output data matrix $u=WX$ are time courses of activation of the ICA components, and the columns of the inverse matrix, W^{-1}, give the projection strengths of the respective components onto the scalp sensors. The scalp topographies of the components provide evidence for their biological origin (e.g., eye activity should project mainly to frontal sites). In general, corrected EEG signals can then be derived as $\hat{X} = W^{-1}\hat{u}$, where $\hat{u}$ is the matrix of activation waveforms u, with rows representing artifactual sources set to zero. After training, we can obtain 31 ICA components from 31-channels EEG data. Fig. 3-10 (a) shows the averaged ERP signals for 31 channels, where each line presents one-channel averaged ERP signal (from -200 ms to

1000ms, with stimulus given at 0 ms). The amplitude of artifacts (EOG, etc.) is larger than ERP (P300) and its position on scalp is apparently observed. The detailed influence can be further observed in Pz channel in single trials shown in Fig. 3-10 (b). The horizontal axis is time scale from –200 ms to 800 ms, the vertical axis is trial index, and the amplitude of each single trial is shown in color bar. The artifact can be observed almost in each single trial and the ERP, P300, related to visual traffic-light stimuli is destroyed by the artifact noise. The topographic maps of the obtained 31 ICA components after training are shown in Fig. 3-11, where the orders of the ICA components were sorted by the variances of time courses of the activations of ICA components. That is, the former ICA components are more effective to the ERP signals, and vice versa. The major artifact, i.e., eye-blinking, is separated in ICA components 1 and 7, visual evoked ERPs are separated into component 4. We can observe that most artifacts and representative visual ERP signals (P300) are effectively separated into ICA components 1 and 4 after ICA processing shown in Fig. 3-12. The artifact (EOG) is obviously observed by spatial position on scalp and amplitude in time scale. The separated noise-free ERPs (P300) in single trials are easily observed in ICA component 4. The same phenomenon could also be observed at other channels. Therefore, component 4 can be regarded as the major source of visual ERP signals to analyze human‘s perception of traffic-light events. Comparing ERP signals at the original Pz channel (Fig. 3-12, left block) and the re-projection from ICA component 4 to Pz channel, we can also find out that the ERP signal obtained from the analysis of ICA algorithm in single trial is more clear and noise-free than the original one. This experimental result encourages us to design an on-line application in single-trial assessment of drivers' cognitive states for the vehicle safety-driving system.

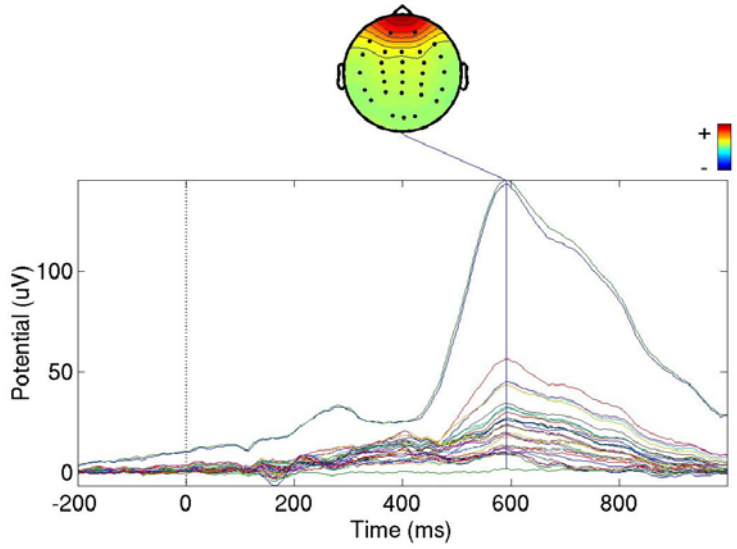

(a)

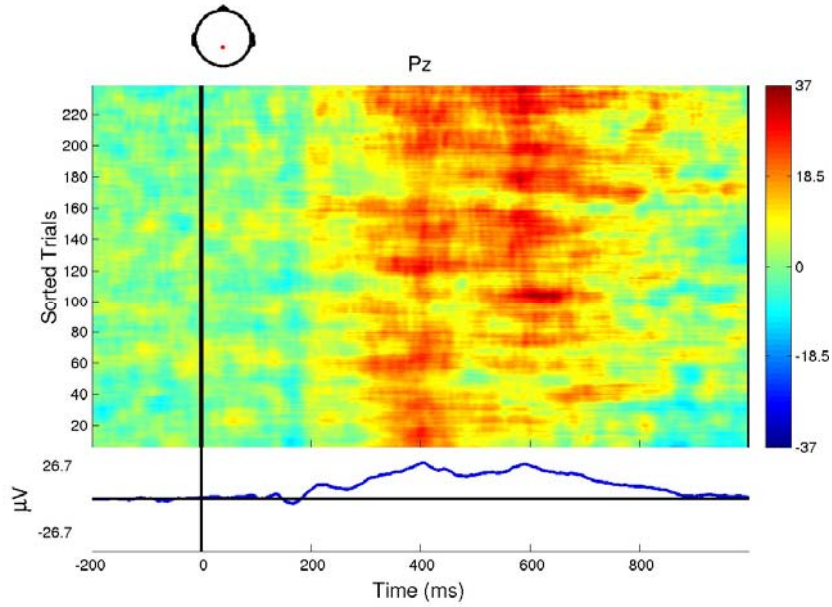

(b)

Figure 3-10. (a) The absolute values of the averaged ERP signals for 31 channels, where each line presents one-channel averaged ERP signal (from -200 ms to 1000ms, with stimulus given at 0 ms). The amplitude of artifacts (EOG, etc.) is larger than ERP (P300) and its position is apparently observed at frontal sites on scalp. (b) The ERP image in single trials observed in Pz channel. Note that the eye-blinking artifact is propagated to the occipital site (Pz) and seriously influenced the collected ERP signals related to visual stimuli.

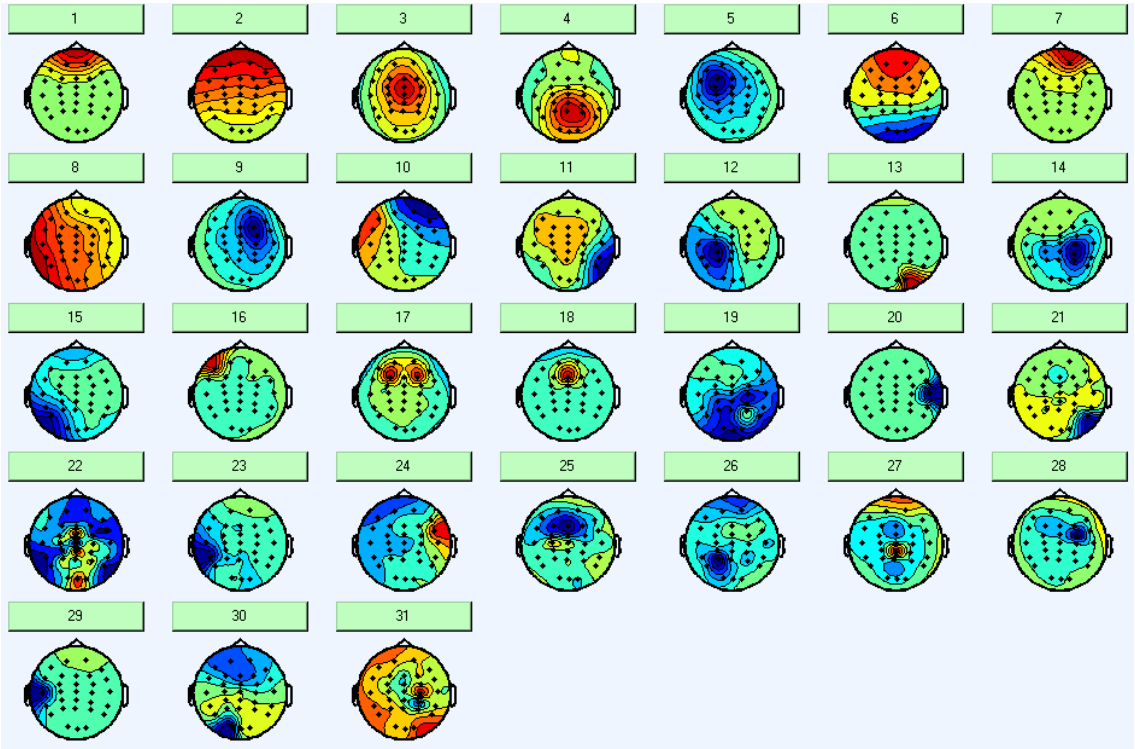

Figure 3-11. The scalp topography of the ICA mixing matrix W^{-1}, where the orders of the ICA components were sorted by the variances of the activations of ICA components. The major artifact, i.e., eye-blinking, is separated in ICA components 1 and 7, visual evoked ERPs are separated into component 4.

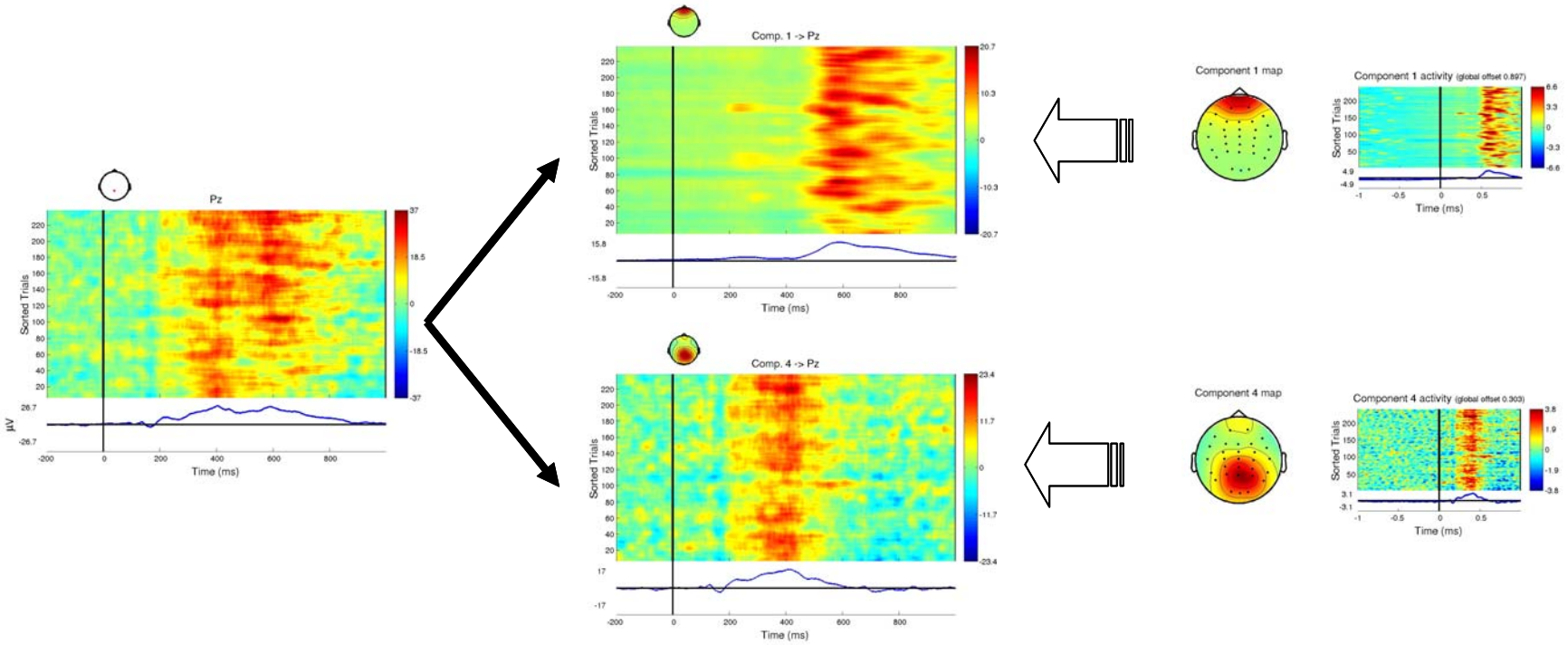

Figure 3-12. Diagram of artifact removal based on ICA algorithm. The left block shows the "polluted" ERPs at Pz channels. The visual evoked ERPs (P300) and the eye-blinking artifacts can successfully be separated into two major parts, P300 at middle-down block and artifacts at middle-top block, which were re-projected back from ICA components 4 and 1.

3.5.2. Effects With/Without Temporal Matching Filter

The single-trial ERP signals in time-domain analysis are first filtered by a temporal matching filter (discussed in Chapter 3.4.2) before fed into PCA algorithm. After passing through the temporal matching filter (as shown in Fig. 3-9) and using PCA to reduce the feature dimensions, the selected first 50 PCA components (ERP data ranged from 0 ms to 800 ms) were then trained by LVQ and SONFIN to learn the relationship of ERP responses between different traffic-light stimulus. Fig. 3-13 (a) and (b) showed the classification results using LVQ and SONFIN, respectively. We can obviously observe that the recognition rate gets a significant increase up to 10 % with temporal matching filter both in LVQ and SONFIN. We also demonstrate that the recognition rate by our proposed SONFIN is 10% better than that by LVQ.

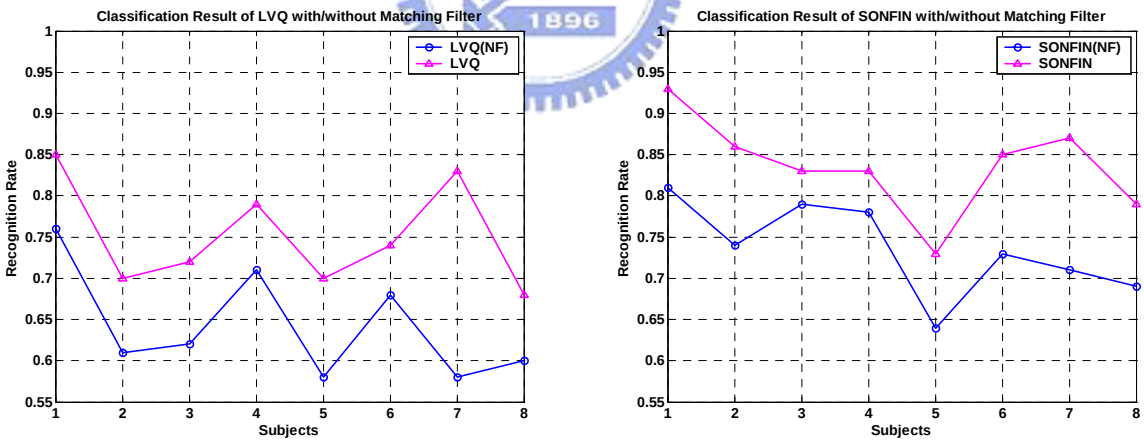

(a) LVQ (b) SONFIN

Figure 3-13. Comparisons of classification results with/without (NF) temporal matching filter using (a) LVQ and (b) SONFIN classifiers, respectively.

3.5.3. Performance Comparisons of LVQ, BP, and SONFIN Classifiers

There are totally 10 subjects participating in our traffic light simulation experiments. The collected ERP data were divided into two parts for training and testing purposes. We removed the subjects with the highest and lowest recognition rates. Table 3-1 and Fig. 3-14 show the testing recognition results of remaining eight subjects by three classifiers (LVQ, BP, and SONFIN). We can observe that the recognition rate using SONFIN is always higher than those using BP and LVQ. The result is reasonable because the SONFIN has the advantages of combining the fuzzy reasoning, discriminative power, learning abilities, and flexibility of neural networks. Table 3-1 also reveals that the nonlinear classifier (BP) always has higher classification rates than the linear one (LVQ).

Table 3-1. Classification rates of three linear/nonlinear classifiers with/without temporal matching filters for 8 subjects in the VR-based traffic-light motion simulation experiments.

	Without Temporal Matching Filter			With Temporal Matching Filter		
	LVQ	BP	SONFIN	LVQ	BP	SONFIN
S1	0.76	0.77	0.81	0.85	0.91	0.93
S2	0.61	0.69	0.74	0.70	0.76	0.86
S3	0.62	0.76	0.79	0.72	0.77	0.83
S4	0.71	0.70	0.78	0.79	0.78	0.83
S5	0.58	0.62	0.64	0.70	0.71	0.73
S6	0.68	0.70	0.73	0.74	0.81	0.85
S7	0.58	0.68	0.71	0.83	0.85	0.87
S8	0.60	0.66	0.69	0.68	0.73	0.79
Average	0.64±0.07	0.70±0.06	0.74±0.06	0.75±0.06	0.79±0.07	0.84±0.06

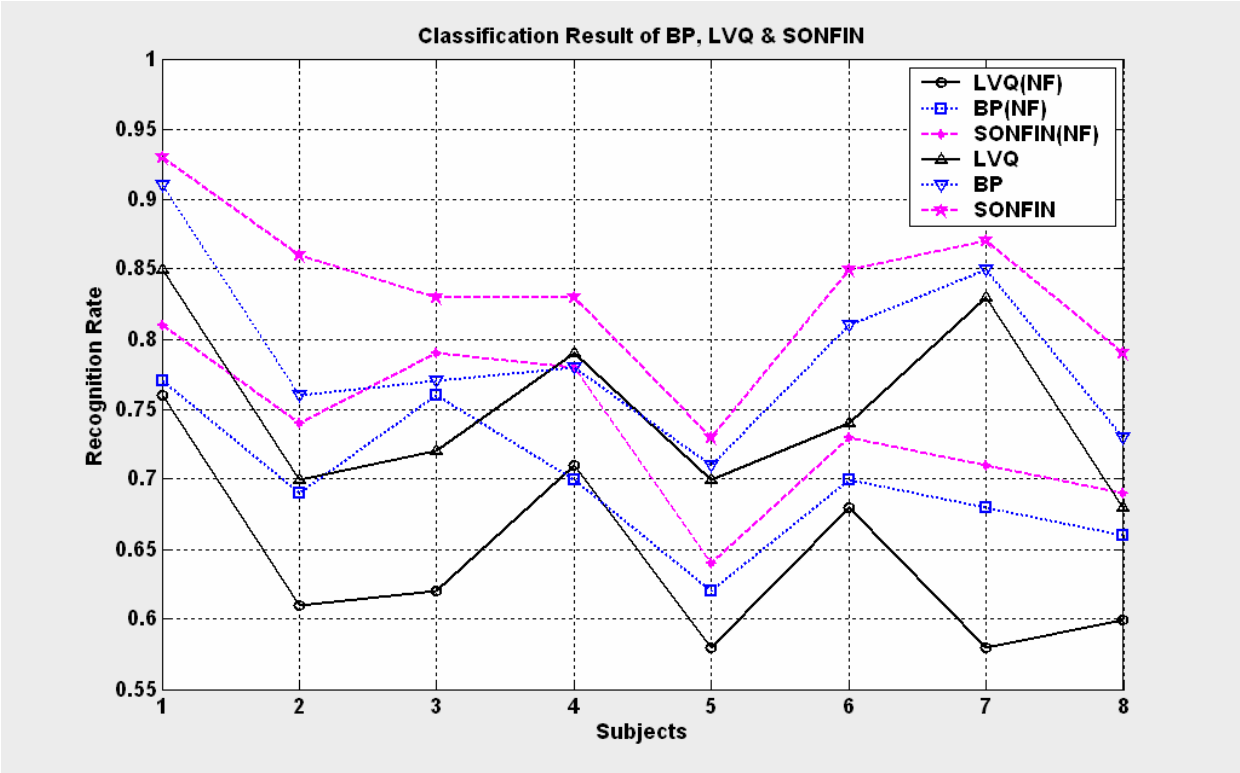

Figure 3-14. Classification results of traffic-light-stimulated ERP with/without (NF) temporal matching filter using LVQ, BP, and SONFIN classifiers, respectively.

3.6. Conclusion Remarks

In this chapter, we developed a quantitative analysis technique for ongoing assessment of drivers' cognitive responses by investigating the neurobiological information underlying EEG brain dynamics in traffic-light motion simulation experiments. It consists of a virtual-reality (VR) motion-simulation driving platform and an EEG signal detection and analysis system. The use of dynamic VR technology not only provides dynamic motion (i.e., kinesthetic or so-called proprioceptive) stimuli in addition to conventional audio/visual ones, but also extends the applications of possible safety-driving prototypes to general population (not limited to lock-in patients) by allowing subjects to interact directly with virtual objects. We proposed a detailed experimental design and data-processing procedures for measuring and analyzing ERP signals. The experimental results show that the proposed signal processing

procedures can analyze ERP signals in single trials correctly without using traditional time-domain overlap-added method. After applying ICA algorithm, we obtained a correct, clear, and noise-free ERP signals in single trials. We also designed a new temporal matching filter to solve the time alignment problem and increase the recognition rate up to 10 %. After using PCA to reduce the feature dimensions and save computation cost, we classified these ERP features using LVQ, BP or SONFIN classifiers. Classification results show that the proposed SONFIN can achieve a high recognition rate about 85% on average. These high-accuracy classification results can be further transformed as the control/monitoring signals of on-line brain computer interfaces in the safety-driving systems.

4. Estimating Driving Performance Based on EEG/ICA Power Spectrum

Accidents caused by driver's drowsiness behind the steering wheel have a high fatality rate because of the marked decline in the driver's abilities of perception, recognition and vehicle control abilities while sleepy. Preventing such accidents caused by drowsiness is highly desirable but requires techniques for continuously detecting, estimating, and predicting the level of alertness of drivers and delivering effective feedbacks to maintain their maximum performance. A well-designed active safety system might effectively avoid accidents caused by drowsiness at the wheel in advance by way of accurate and non-intrusive monitoring driver's alertness level, particularly if this measure could be further used to predict changes in driver's performance capacity. Although many researches have proposed EEG-based methods on the detection of driver's vigilance, there are still many difficulties in developing such a system such as lacks of significant index for detecting drowsiness objectively, the contamination of EEG activities by the complicated noise interferences in a dynamic driving environment, and the large individual variability in EEG dynamics accompanying loss of alertness such that we could not accurately estimate or predict individual changes in alertness and performance.

In this chapter, the scope of current study is to develop the biomedical signal processing technologies to examine neural activity correlated with fatigue/drowsiness, which can be used to online monitor/estimate driver's cognitive state (alertness) combined further with a bio-feedback system to maintain driver's high performance. Our research investigates the feasibility of using multi-channel EEG data to estimate and predict non-invasively the continuous fluctuations in human global level alertness indirectly by measuring the driving

performance expressed as deviation between the center of the vehicle and the center of the cruising lane, in a very realistic driving task. We first use the virtual-reality (VR) technology to construct an interactive freeway driving environment for lane-keeping experiment to indirectly quantify driver's drowsiness level by continuously measuring fluctuations in driving errors and concurrent changes of the EEG power spectrum. The VR allows subjects to interact directly with a virtual environment rather than monotonic auditory and visual stimuli, and is an excellent strategy for brain research on interactive and realistic tasks because of its low cost and avoiding risk of operating on the actual machines. After collecting the multi-stream brain potentials, four computational approaches were proposed to extract effective features as well as linear regression model or a Self-cOnstructing Neuro-Fuzzy Inference Network (SONFIN) model [94] to estimate and predict the individual driver's driving performance. The first approach focuses on using the principal components from the power spectrum of only 2-channel EEG signals as input features of the estimators (*as suggested in Section* 4.6.1). The following three approaches introduce a new generally applicable Independent Component Analysis algorithm [85-86] to isolate and remove a wide variety of EEG artifacts and to locate optimal positions to wire EEG electrodes. The ICA method is based on spatial filtering and does not rely on having a "clean" reference channel. It effectively decomposes multiple-channel EEG data into spatially-fixed and temporally independent components. Clean EEG signals can then be derived by eliminating the contributions of artifactual sources with their time courses are generally temporally independent from and differently distributed than sources of EEG activity. Optimal EEG electrodes can also be obtained by examining the center position from the scalp topography of the ICA mixing matrix. Therefore the second approach takes the advantage of the ICA algorithm in the training process and uses a few frequency bandpower of only 2-channel EEG data as inputs features in the testing application, whereas the third approach uses the

bandpower of 2 most important ICA components as input features in order to achieve higher predicting accuracy. In the last approach, we propose a novel adaptive feature extracting mechanism to solve the reliable and sorting problem [109-111] of ICA components for realizing an on-line monitoring system based on the correlation analysis between the time-frequency power spectra of ICA components and the driving error index for selecting effective frequency bands in ICA components as features of estimators. We then take advantages of fuzzy reasoning and the discriminative power, learning abilities, and flexibility of neural networks as a good candidate to complement the traditional methods by building a Self-cOnstructing Neuro-Fuzzy Inference Network (SONFIN) model to online estimate and predict the individual driver's driving performance.

4.1. Virtual-Reality (VR)-based Lane-Keeping Driving Experiment

We build a VR-based high-fidelity 3D interactive highway scene as shown in Fig. 4-1 by using the emulation software, WorldToolKit (WTK) library and application programmer's interface (API). The detailed development diagram of the VR-based scene is shown in Fig. 2-3. The VR-based four-lane highway scene as shown in Fig. 2-5 is projected on a 120°-surround screen (304.1-cm wide and 228.1-cm high), which is 350 cm away from the driving cabin. The four lanes from left to right are separated by a median stripe. The distance from the left side to the right side of the road is equally divided into 256 points (digitized into values 0-255), where the width of each lane and the car is 60 units and 32 units, respectively. The refresh rate of highway scene was set properly to emulate a car driving at a fixed speed of 100 km/hr on the highway. The car is randomly drifted (triggered from the WTK program and the on-set time is recorded) away from the center of the cruising lane to mimic the

consequences of a non-ideal road surface. The subject's performance is defined as the deviations between the center of the vehicle and the center of the cruising (3rd) lane and it was continuously and simultaneously measured by the WTK program and recorded in the physiological measurement system accompanying with EEG/EOG/ECG physiological signals.

Figure 4-1. The dynamic driving simulation laboratory consists of the virtual-reality-based 360^{o}-surrounding screen and a six-degree-of-freedom motion platform.

4.2. Subject's Protocol

The circumstances in which drowsiness-related accidents usually happen should be taken into account. It has been known that the drowsiest time often occurs from late midnight to early morning, and mid-afternoon hours. Young drivers have no increased risk during the afternoon. Drivers over 45 years old on the other hand have fewer night time crashes, with a peak at 7 a.m., and are more likely to have such crashes during the mid-afternoon [20, 55-56]. During these periods, alertness may easily diminish within one-hour monotonous working. In

this chapter, we design a drowsiness monitoring experiment at the early afternoon hours after lunch for doing the highway-driving simulation. All the subjects were instructed to keep the car at the center of the cruising lane by controlling the steering wheel. For each session, the subject started with a 15 ~ 45-minute calibration procedure and then was asked to drive the car continuously for 45 minutes. The EEG/EOG/ECG data and the driving performance were measured and recorded simultaneously. Participants then returned on different days to complete the second 45-min driving session or the third session if necessary. We had collected successfully EEG data of 16 subjects (ages from 20 to 35 years) participated in the proposed VR-based driving task. We select participants who had two or more micro-sleeps checked by video recordings in both driving sessions for further analysis. Based on these criteria, five subjects (10 sessions) were selected for further modeling and cross-session testing.

4.3. Data Acquisition

The acquisition of the physiological data uses 33 sintered Ag/AgCl EEG/EOG electrodes with an unipolar reference at right earlobe and 2 ECG channels in bipolar connection placed on the chest. All the EEG/EOG channels were located based on a modified International 10-20 system based on the relationship between the location of an electrode and the underlying area of cerebral cortex. Before data acquisition, the contact impedance between EEG electrodes and scalp was calibrated to be less than 5kΩ. We use the Scan NuAmps Express system (Compumedics Ltd., VIC, Australia) to simultaneously record the EEG/EOG/ECG data and the deviation between the center of the vehicle and the center of the cruising lane triggered by the WTK program. The EEG data were recorded with 16-bit quantization level at a sampling rate of 500 Hz and the recording are down-sampled to 250 Hz for the simplicity of data processing. Then EEG data were preprocessed using a simple low-pass filter with a cut-off frequency of 50 Hz to remove the line noise (60 Hz and its

harmonics) and other high-frequency noise for further analysis.

4.4. Drowsiness Measurement

To quantify the level of the subject's alertness and find the relationship between the EEG signals and subject's cognitive state, we measure the driving error *e(t)* defined as the deviation from the left railing to the center of the vehicle on freeway. Previous study [112] and our pilot study demonstrate when the subject starts to fall into micro-sleep or asleep during the lane-keeping task, the car will drift away from the center of the cruising lane rapidly and hit the railing of the freeway easily in a few seconds. Thus, the *e(t)* is a good performance index to indirectly measure the driver's drowsiness level. The recorded *e(t)* time series was first normalized by subtracting the center position of the cruising lane, e_h, using Eq. (4-1), where e_h is the value having the maximum frequency in the histogram distribution of *e(t)* depending on each subject's driving habit as shown in Fig. 4-2 (a). Thus, the subject's driving error index (*SDPI*) in Eq. (4-2) to smooth $\tilde{e}(t)$ using a causal 90-s square moving-average filter advancing at 2-sec steps as shown in Fig. 4-2 (b) to eliminate variance at cycle lengths shorter than 1-2 minutes since the fluctuates of drowsiness level with cycle lengths were longer than 4 minutes [51, 67]. Experimental results shows when the subject is drowsy (checked from video recordings and subject's reports), the driving error index increases, and vice versa.

$$\tilde{e}(t) = \left| e(t) - e_h \right|, \text{ where } \left| x \right| = \begin{cases} x & x \geq 0 \\ -x & x < 0 \end{cases} \tag{4-1}$$

and

$$SDPI(t) = \frac{1}{M_e} \sum_{i=1+2(t-1)\Omega_s}^{M_e+2(t-1)\Omega_s} \tilde{e}\left[M_e + 2(t-1)\Omega_s - i \right], \tag{4-2}$$

where $M_e = 90 \times \Omega_s$, $n=1, 2, \ldots, N$, is the 90-s moving-average windows.

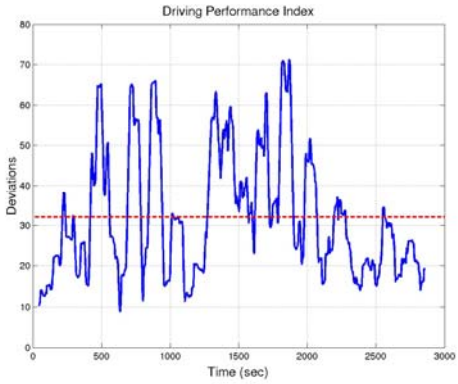

(a) (b)

Figure 4-2. (a) The VR-based freeway scene. (b) Example of the driving performance index. Note that the red dashed line means the "dangerous" boundary. When the driving performance is larger than 32 (red line), the target car entirely crossed the lane line to other traffic lane and will easily lead to accidents.

4.5. Data Analysis

After collecting 33-channel EEG signals and driving deviations in a 45-min simulated driving session, we proposed four strategies to extract effective features in order to find the relationship between driver's alertness level from EEG power spectrum and concurrent changes in driving performance based on ICA, power spectrum analysis, correlation analysis, and the linear regression model or the FNN estimator. The developments of these four approaches were based on a compromise between computational cost and estimation accuracy for an online real-time application. More descriptions are given in the following session.

4.5.1. Estimating Driving Performance Using 2-Channel EEG Power Spectrum

In this strategy, we use a least-square linear regression model [113] to estimate/predict the subject's driving performance based on the information available in log power spectrum of 2-channel EEG signals. The training flowchart of data analysis for estimating the level of

alertness based on the EEG power spectrum was shown in Fig. 4-3. For each subject, after collecting 33-channel EEG signals and driving deviations in a 45-min simulated training session, the EEG data were first preprocessed using a simple low-pass filter with a cut-off frequency of 50 Hz to remove the line noise and other high-frequency noise. Then, we calculate the moving-average log power spectrum of all 33-channel EEG data using Eqs. (2-12) to (2-17) as described in Chapter 2.4. The correlation coefficients between the smoothed subjects' driving error index and the log power spectra of all 33-channel EEG signals at each frequency band are further evaluated to form a correlation spectrum. The log power spectra of 2-channel EEG signals with the highest correlation coefficients are further selected as the effective features (*as suggested in Section* 4.6.1). We then applied Karhunen-Loeve Principal Component Analysis (PCA) to decompose the selected log power spectra of 2-channel EEG signals and extract the directions of largest variance for each session. The PCA is a linear transformation, which can find the principal coordinate axes of samples such that along the new axes, the sample variances are extremes (maxima and minima), and uncorrelated. Using a cutoff on the spread along each axis, a sample may thus be reduced in its dimensionality [114]. The principal axes and the variance along each of them are given by the eigenvectors and associated eigenvalues of the dispersion matrix. In our study, projections (PCA components) of the EEG log spectral data on the subspace formed by the eigenvectors corresponding to the largest 50 eigenvalues were then used as inputs to train the individual linear regression models for each subject. The parameters of the 50-orders linear regression model were trained iteratively by minimizing the least-square-error cost function between the actual driving error index and the estimated output of the linear regression model. After training, the parameters of the PCA model (eigenvectors) were used to project features in the testing sessions so that all data were processed in the same way for the same subject before feeding to the estimation models. The parameters of the linear regression model were

also held to estimate the time courses of the actual driving error index in the testing session. Each model was trained using the features only extracted on the training session and tested on a separate testing session from the same subject for each of the five selected subjects.

In the testing session, the subject was wired with the selected 2-channel EEG electrodes, which is determined from the training process. The collected 2-channel EEG data were first preprocessed using the same low-pass filter. After moving-average power spectral analysis, for each 45-min driving session stepping at 2-sec time intervals and frequency range from 1 to 40 Hz, we obtained the selected time series of the log power spectrum for 2-channel EEG data consisting of 1350-point EEG power estimations. Then the 80 frequency bandpower (2*40Hz) were passed through the PCA model. The first 50 entries of the output time series of the PCA components were fed into the linear regression model to estimate the actual driving errors.

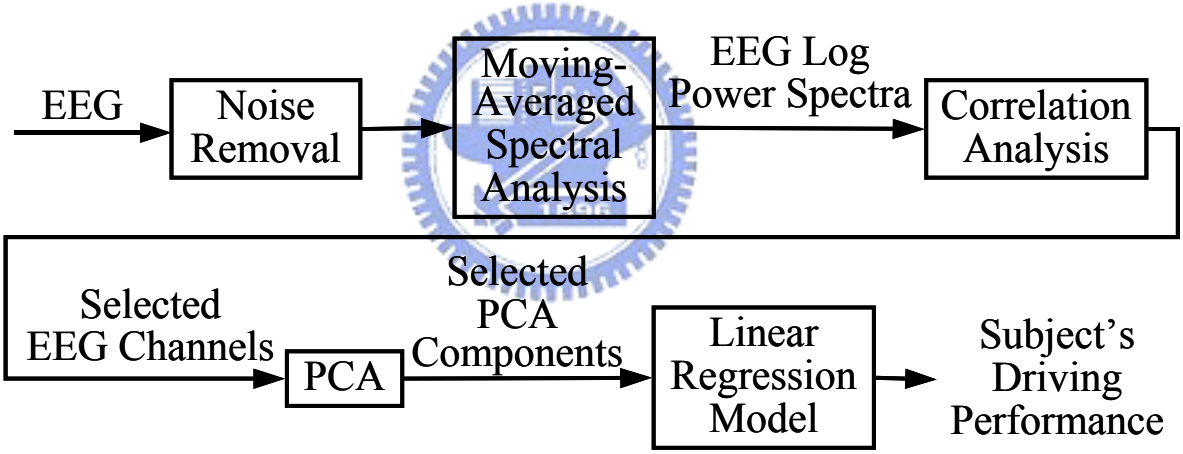

Figure 4-3. Flowchart of the training process for estimating subject's driving errors. (1). A low-pass filter was used to remove the line noise and higher frequency (>50Hz) noise. (2). Moving-averaged spectral analysis was used to calculate the EEG log power spectrum of each channel advancing at 2-sec steps. (3). Two EEG channels with higher correlation coefficients between subject's driving performance and EEG log power spectrum were further selected. (4). Principal Component Analysis was trained and used to decompose selected features and extract the representative PCA-components as the input vectors for the linear regression models. (5). The linear regression models were trained in one training session and used to continuously estimate and predict the individual subject's driving performance in the testing session.

4.5.2. Driving Performance Estimation Using Critical Bandpower of Optimal 2-channel EEG Signals based on Independent Component Analysis

In this strategy, we proposed the ICA-based method for estimating the subject's driving performance using the critical bandpower of optimal 2-channel EEG signals centered at the effective ICA components. Fig. 4-4 shows the flowchart of the proposed signal processing procedure. In the training process, the collected 33-channel EEG signals was first applied to train the ICA model. By applying ICA algorithm to the EEG recorded from the scalp surface, we attempt to achieve the twin goals: removing artifacts and possible source separation based on stabilities of ICA spatial weighting matrices and temporal independence between artifacts and EEG signals. The effectiveness for removing eye blinking and other artifacts by using ICA had been demonstrated in the many studies as described in Chapter 2.3. Thus, some "artifact" sources in the ICA components were removed and the remaining ICA components were projected back to the EEG channels to get the "corrected" EEG signals. Then, we calculate the moving-average log power spectra of both the ICA components and "corrected" EEG channels. The correlation coefficients between the smoothed time series of subject's driving error index and the power spectra of the ICA components at each frequency band are further evaluated to form a correlation spectrum. The 2 ICA components having the highest correlation coefficients in some critical bands were determined and marked as "drowsiness" sources. Then, we selected the corresponding 2 EEG channels with the marked critical bands at the centered positions of the "drowsiness" sources based the scalp topography of ICA mixing matrix. Finally, the selected critical bands in 2 EEG channels were used as the input features to train the linear regression models. Once a linear regression model has been developed for each driver, this method uses only selected critical bandpower of 2-channel EEG signals of the individual subject, and does not require further collection or analysis of

operator performance in the testing session.

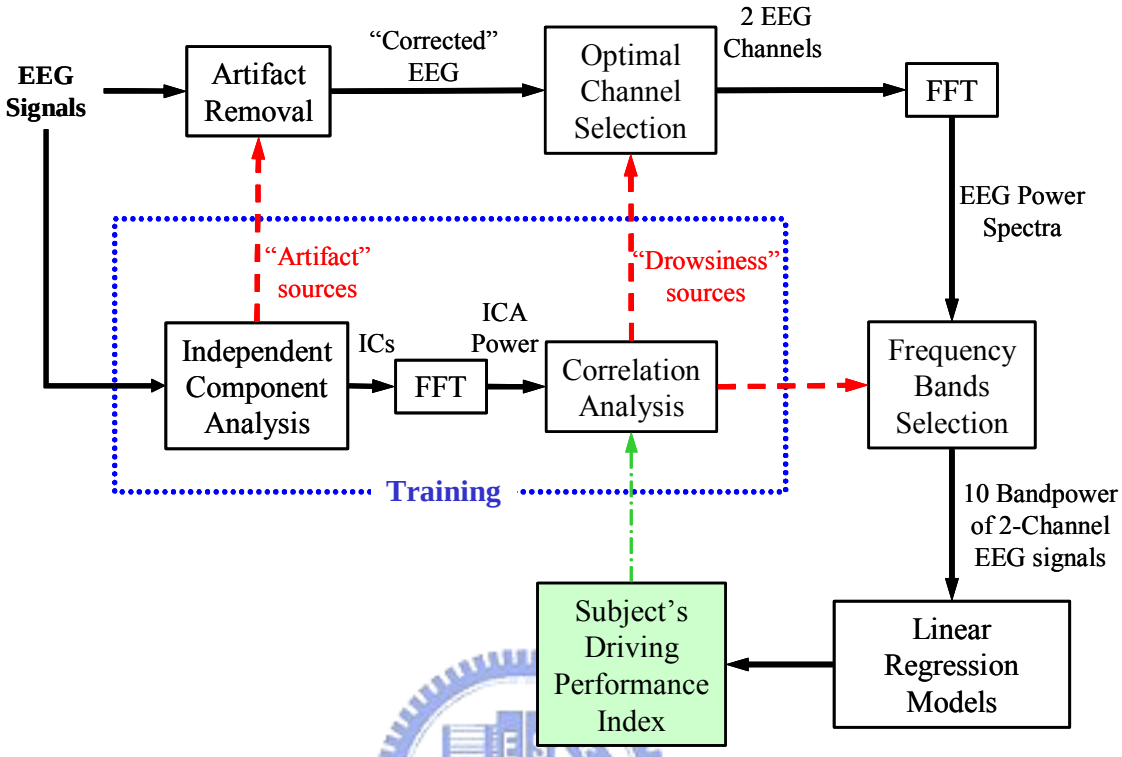

Figure 4-4. Signal Flowchart of the drowsiness estimation system based on the bandpower of the 2-channel EEG signal centered in the effective ICA components.

4.5.3. Estimating Driving Performance Using 2 Optimal ICA Components

Fig. 4-5 shows the signal flowchart for estimating driver's performance using effective bandpower of 2 ICA components. In the training session, after collecting 33-channel EEG signals and driving deviations in a 45-min simulated driving session, the ICA algorithm is first trained to remove a wide variety of artifacts. Then, we calculate the moving-average log subband power spectra of all 33 ICA components. The correlation coefficients between the smoothed subject's driving performance and the subband power spectra of all ICA components at each frequency band are further evaluated to form a correlation spectrum. The normalized log subband power spectra of 2 ICA components with the highest correlation coefficients in some critical bands are further selected manually as the input features of the

linear regression model to estimate the individual subject's driving performance. In order to achieve maximum estimating accuracy, the ICA mixing matrix and the manually selected critical bandpower were reserved in the testing session.

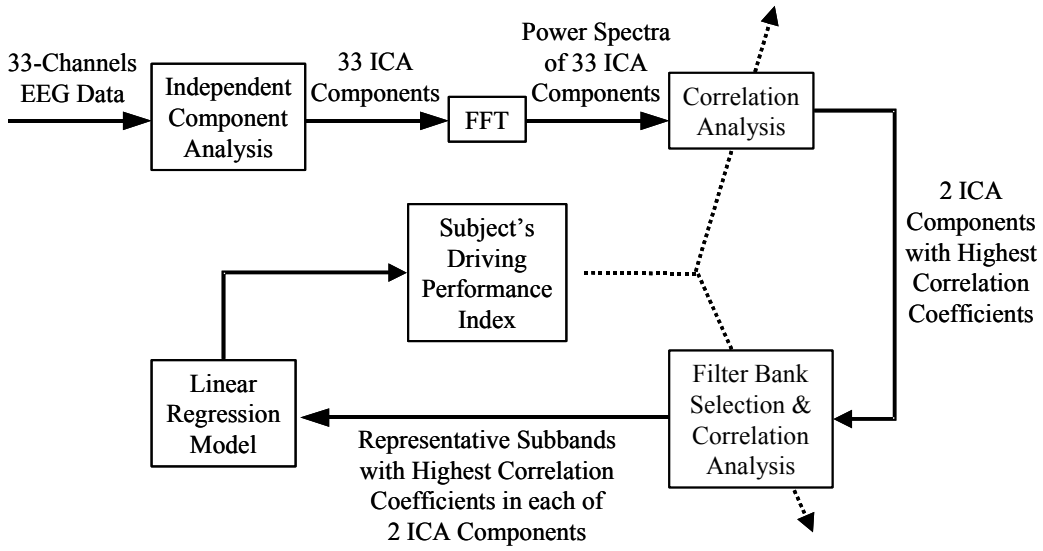

Figure 4-5. Signal Flowchart of drowsiness estimation system based on the bandpower of optimal 2-ICA components with highest correlation coefficients between time series of subject's driving error index and the power spectra of the ICA components.

4.5.4. ICA-based Automatic Feature Extraction for Driving Performance Estimation

In this strategy, we proposed a novel adaptive feature selection mechanism (AFSM) for the automatic ICA-based alertness estimation system using fuzzy neural networks for online applications. The block diagram of data analysis is given in Fig. 4-6. After collecting 33-channel EEG signals ***x(t)*** and driving error index (*SDPI*) in a 45-min simulated driving session, the ICA algorithm is first trained to distinguish the EEG signals from artifact noise, i.e., removing a wide variety of artifacts. Then, we calculate the normalized moving-average log bandpower spectra of all 33 ICA components. The correlation coefficients between *SDPI* and the bandpower spectra of all ICA components at each frequency band are further

evaluated to form a correlation spectrum. We use the AFSM to select the log bandpower spectra of the ICA components with the highest correlation coefficients in some critical bands as the input features of the linear regression model and SONFIN to estimate the individual subject's driving performance. Detailed description of the proposed AFSM are given as follows:

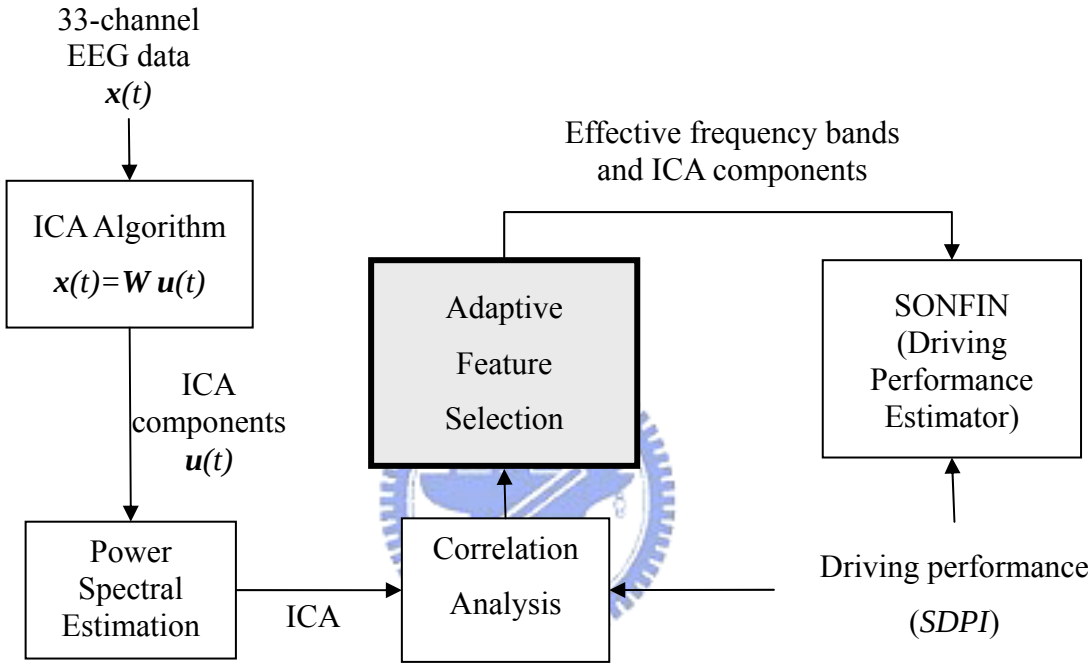

Figure 4-6. Signal flowchart of the adaptive alertness estimation system.

Adaptive Feature Selection Mechanism

Signal features in many studies are extracted according to experience and become a problem when applied for an on-line monitoring system. To solve this problem, an adaptive feature extracting mechanism is developed to extract useful frequency bands of representative ICA components according to the information of the correlation coefficients between log bandpower of ICA components and driving error index (*SDPI*). In this session, to extract the most representative ICA component and frequency bands, we first sort the correlation coefficients ***CC(i,k)*** in Eq. (2-19) in frequency bands *k* for each component *i* in descending

order by:

$$\boldsymbol{SC}(i,k) = \underset{k}{sort}(\boldsymbol{CC}(i,k)) = \left\lfloor \underset{k}{max}(CC(i,k)) \quad \cdots \quad \underset{k}{min}(CC(i,k)) \right\rfloor, \; i = 1, 2, \ldots, 33. \qquad (4\text{-}3)$$

The corresponding matrix indices $\boldsymbol{K}(i,k)$ is:

$$\boldsymbol{K}(i,k) = \arg \underset{k}{sort}(\boldsymbol{CC}(i,k)) = \left\lfloor \arg \underset{k}{max}(CC(i,k)) \quad \cdots \quad \arg \underset{k}{min}(CC(i,k)) \right\rfloor \qquad (4\text{-}4)$$

where the first five frequency bands with the largest correlation coefficients of i_{th} component are expressed as $\boldsymbol{SC}(i,1)$~$\boldsymbol{SC}(i,5)$ with frequency band index recorded in $\boldsymbol{K}(i,k)$, k=1~5.

We then sort the $\boldsymbol{SC}(i, k)$ in descending order in the column direction to select the ICA components having the maximum value in the summations of the largest 5 correlation coefficients in frequency bands as:

$$\overline{\boldsymbol{SC}}(i) = \underset{i}{sort}\left(\frac{1}{5} \sum_{k=1}^{5} \boldsymbol{SC}(i,k) \right), \; i = 1, 2, \ldots, 33. \qquad (4\text{-}5)$$

where the component indices in $\boldsymbol{K}(i,k)$ is also updated. Therefore, the first 2 ICA components with 5 largest correlation coefficients in the frequency bands can be derived as $\overline{SC}(1)$ and $\overline{SC}(2)$ with matrix index $\boldsymbol{K}(i,k)$, i = 1~2 and k = 1~5. An example of the adaptive feature selection mechanism for subject-3 is given in Fig. 4-7.

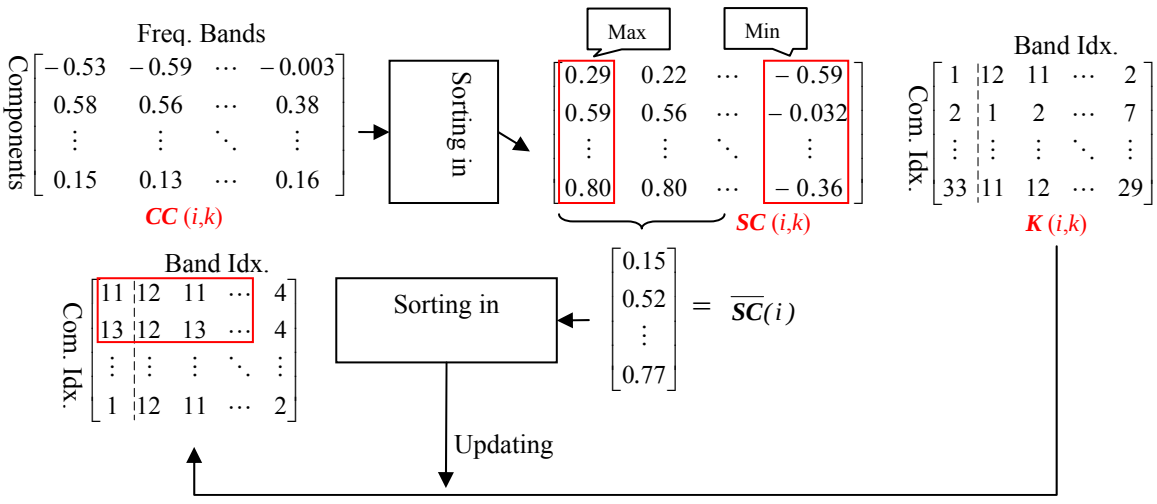

Figure 4-7. Example of the adaptive feature selection mechanism for subject-3. Note that

the band power of ICA components 11 and 14 in frequency bands 10-14 Hz are selected as input feature of the estimators.

4.6. Results and Discussions

4.6.1. Relationship between the EEG Spectrum and Subject Alertness

To investigate the relationship of minute-scale fluctuations in driving performance to concurrent changes in the EEG spectrum, we measured correlations between changes in the EEG power spectrum and driving performance by computing the correlation coefficients between the two time series at each EEG frequency. We refer to the results as forming a correlation spectrum. For each EEG site and frequency, we then computed spectral correlations for each session separately and averaged the results across all 10 sessions. Fig. 4-8 (A) showed the results for 40 frequencies between 1 and 40Hz. Note that the mean correlation between performance and EEG power is predominantly positive at all EEG channels below 20 Hz. We also investigated the spatial distributions of these positive correlations by plotting the correlations between EEG power spectrum and driving performance, computed separately at dominant frequency bins, 7, 12, 16 and 20Hz (cf. Fig. 4-8 (A) on the scalp (Fig. 4-8 (B). As the results in Fig. 4-8 (A) show the correlation coefficients plotted on the scalp maps are predominantly positive. The correlations are particularly strong at central and posterior channels, which are similar to the results of previous studies in the driving experiments [32, 34, 114]. The relatively high correlation coefficients of EEG log power spectrum with driving performance suggests that using EEG log power spectrum may be suitable for drowsiness (micro-sleep) estimation, where the subject's cognitive state might fall into stage one of the non-rapid-eye-movement (NREM) sleep. To be practical for routine use during driving or in other occupations, EEG-based cognitive assessment systems should use as few EEG sensors as possible to reduce the

preparation time for wiring drivers and computational load for estimating continuously the level of alertness in near real time. According to the correlations shown in Fig. 4-8 (B), we believe it is adequate to use the EEG signals at sites Cz and Pz to assess the alertness level of drivers continuously.

Next, we compared correlation spectra for individual sessions to examine the stability of this relationship over time and subjects. Fig. 4-9 and 4-10 plot correlation spectra at sites Fz, Cz, Pz and Oz, of two separate driving sessions for extreme cases from subjects A (best) and B (worst), respectively. The relationship between EEG power spectrum and driving performance is stable within the subjects, especially below 20 Hz. However, the relationship is variable from subject to subject (contrast Fig. 4-9 and 4-10). The time interval between the training and testing sessions of the lane-keeping experiments distributes over one day to one week long for the selected five subjects. The relationship between minute-scale fluctuations in driving performance and concurrent changes in the EEG spectrum appears to be stable within different sessions from the same subject, but differs between subjects.

The above analyses provide strong and converging evidence that changes in subject alertness level indexed by driving performance during a driving task are strongly correlated with the changes in the EEG power spectrum at several frequencies at central and posterior sites. This relationship is relatively variable between subjects, but stable within subjects, consistent with the findings from a simple auditory target detection task reported in [40, 51]. These findings suggest that information available in the EEG can be used for real-time estimation of changes in alertness of human operators performing monitoring tasks. However, for maximal accuracy the estimation algorithm should be capable of adapting to individual differences in the mapping between EEG and alertness.

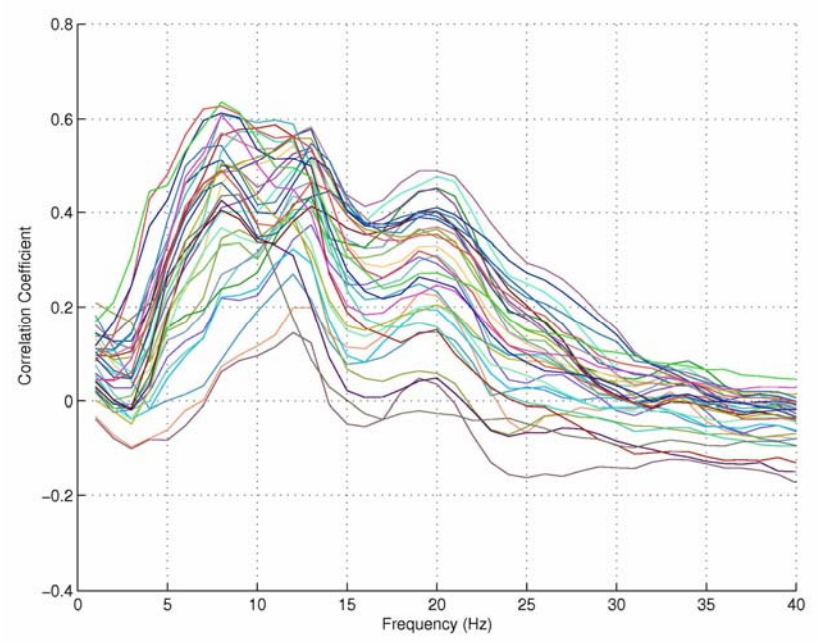

(A)

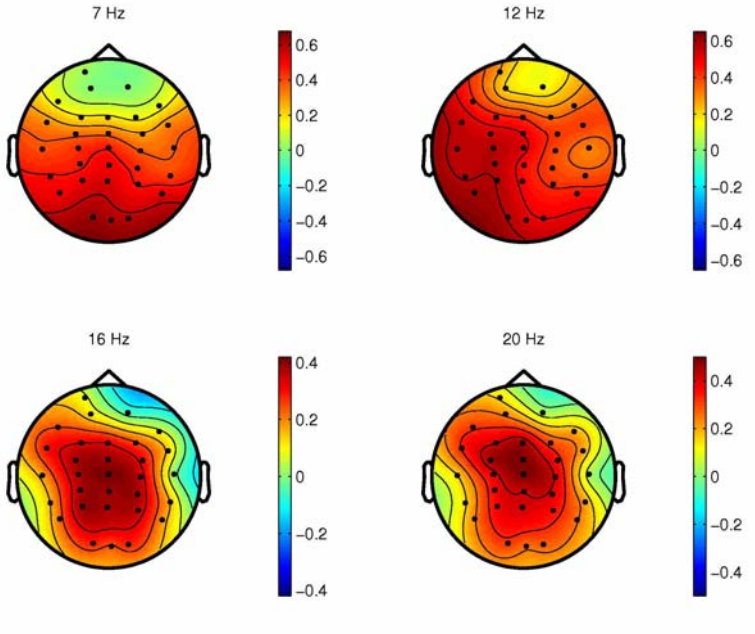

(B)

Figure 4-8. Correlation spectra. Correlations between EEG power and driving performance, computed separately for 40 EEG frequencies between 1 and 40 Hz. (A) Grand mean correlation spectra for 10 sessions on 5 subjects. (B) Scalp topographies of the correlations at dominant frequencies at 7, 12, 16 and 20 Hz.

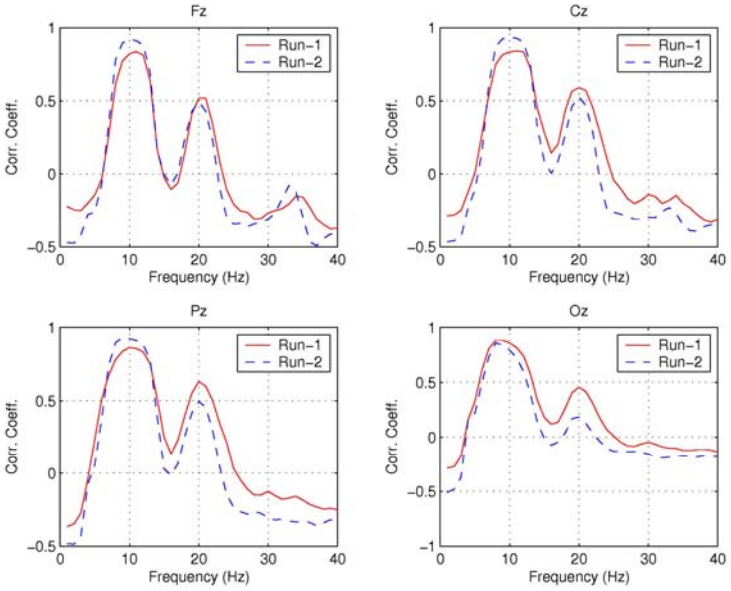

Figure 4-9. Correlation spectra between the EEG power spectrum and the driving performance at Fz, Cz, Pz, and Oz channels in two separate driving sessions from Subject A (best case). Note that the relationship between EEG power spectrum and driving performance is stable within this subject.

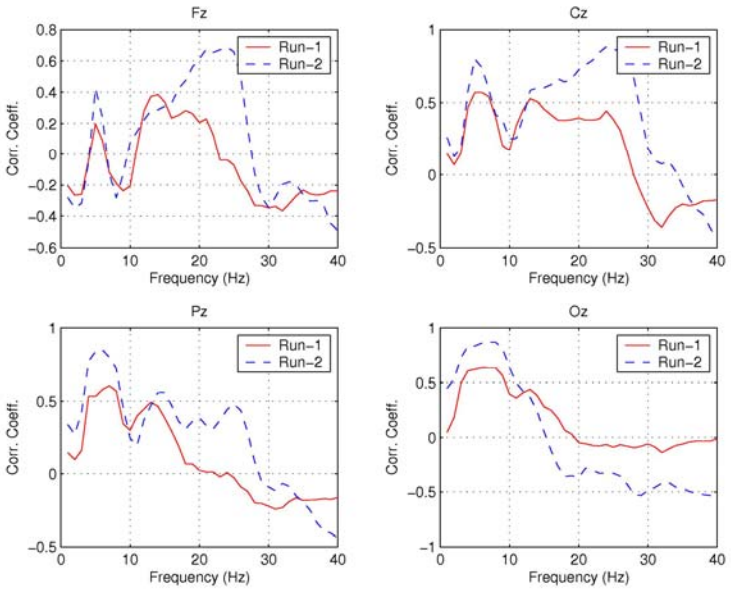

Figure 4-10. Correlation spectra between the EEG power spectrum and the driving performance at Fz, Cz, Pz, and Oz channels in two separate driving sessions from Subject B (worst case). Note that the relationship between EEG power spectrum and driving performance is stable within this subject, especially below 20 Hz. However, the relationship is variable from subject to subject (contrast Fig. 4-9 and 4-10).

4.6.2. EEG-based Driving Performance Estimation/Prediction

In order to estimate/predict the subject's driving performance based on the information available in the EEG power spectrum at sites Cz and Pz, a single 50-orders linear regression model $y = \sum_{i=1}^{N=50} a_i x_i + a_0$ with a least-square-error cost function is used, where y is the desired output, x is the input feature, N is the order (N=50 in this case), a_i's are the parameters, and a_0=1 is the constant. The input features are selected from the first 50 PCA-reduced EEG power spectra of two EEG channels (Cz and Pz) that showed the highest correlation between the EEG power spectrum and the driving performance because using all 33 channels may introduce more unexpected noise. Table 4-1 shows the driving performance estimation results using one single linear regression model for all subjects in the training and testing session. The resulting correlation rate between actual and estimated driving performance are not good enough (r=0.486 in the testing session) due to the large individualities between subjects. This result is consistent with previous studies [40, 42, 49, 67]. Therefore, we have to build an individual model for each subject (as discussed in Section 4.6.1). The resulting estimation driving performance using individual model for each subject are also shown in Table 4-1. Comparing to using one single model for all subjects, the correlation rate using individual model for each subject dramatically increased up to 10%. Fig. 4-11 plots the estimated and actual driving performance of a session from Subject 3. The linear regression model in this figure is trained with and tested against the same session, i.e. within-session testing. As can been seen, the estimated driving performance matched extremely well with the actual driving performance (r = 0.88). When the model was tested against a separate test session from the same subject as shown in Fig. 4-12, the correlation between the actual and estimated driving performance though decreased but remained high (r≒0.7). Across ten sessions, the mean correlation coefficient between actual driving performance time series and within-session

estimation is 89%, whereas the mean correlation coefficient between actual driving performance and cross-session estimation is 57.8%. Our results demonstrated that it is feasible to accurately estimate driving errors based on multi-channel EEG power spectrum estimation and principal component analysis algorithm. The computational methods we employed in this study were well within the capabilities of modern real-time embedded digital signal processing hardware to perform in real time using one or more channels of EEG data. Once an estimator has been developed for each driver, based on limited pilot testing, the method uses only spontaneous EEG signals from the individual, and does not require further collection or analysis of operator performance. The proposed methods thus might be used to construct and test a portable embedded system for a real-time alertness monitoring system.

Table 4-1. Comparisons of driving performance estimation using one single linear regression model for all five subjects and using individual model for each subject. Note that the input features are PCA-reduced EEG power spectrum from 1-40Hz in Cz and Pz channels.

		Sub-1	Sub-2	Sub-3	Sub-4	Sub-5	Average
Single Model	Training	76%	70%	66%	74%	80%	73.2%
	Testing	65%	42%	51%	41%	44%	48.6%
Individual Model	Training	89%	85%	88%	89%	94%	89 %
	Testing	69%	59%	70%	46%	45%	57.8%

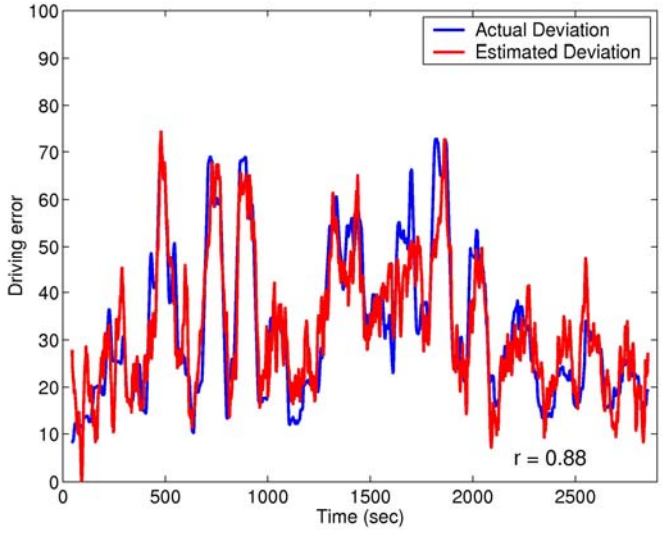

Figure 4-11. Driving performance estimates for a training session from Subject 3, based on a linear regression (red line) of PCA-reduced EEG log spectra at two scalp sites, overplotted against actual driving performance time series for the session (solid line). The correlation coefficient between the two time series is $r = 0.88$.

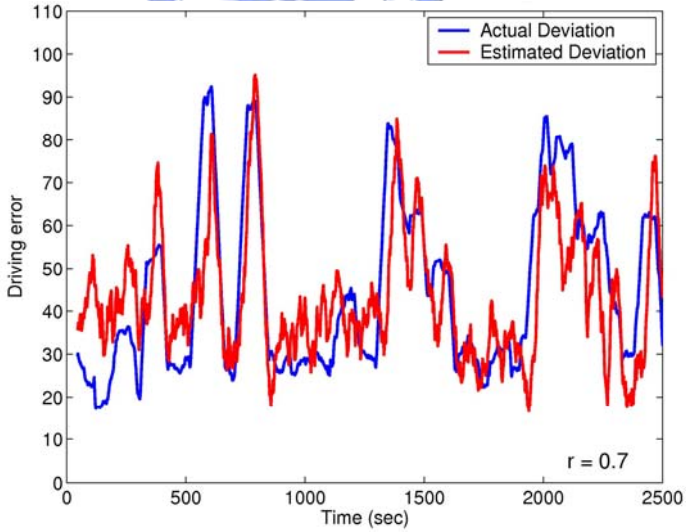

Figure 4-12. Driving performance estimates for a testing session of Subject 3, based on a linear regression (red line) of PCA-reduced EEG log spectra from a separate training session from the same subject, overplotted against actual driving performance time series of the test session (solid line). The correlation coefficient between the two time series is $r = 0.7$. Note that the training and testing data in this study were completely disjoined.

4.6.3. Relationship between the ICA Spectrum and Driving Performance

After ICA training and analysis of log subband power spectrum for each ICA components/EEG channels, we computed the spectral correlations between changes in the ICA/EEG log subband power spectrum and driving performance by computing the correlation coefficients between the two time series at each frequency band. Fig. 4-13 shows the resulting correlation spectra of subject 3 in (a) 33 EEG channels and (b) 33 ICA components. The horizon axis indexes frequency bands between 1 and 40 Hz and the vertical axis indexes the EEG channels/ICA components. In Fig. 4-13 (a), the correlation spectra show a strong evidence between fluctuations in EEG bandpower of frequency bands within 10~14Hz and driving performance with high positive correlations in most EEG channels. As driving error increases, so does EEG bandpower. We also investigated these relationships by plotting the correlations between bandpower of 33 ICA components and the driving performance. A similar monotonic relationship exists in a wide frequency band; especially the frequency bands from 9 to 25 Hz in ICA components 11 and 13 achieve a high positive correlation. Fig. 4-13 (c) and (d) show the spatial distributions in scalp topographies of weighting matrices for dominant ICA component 11 that was centered on Pz (28^{th}) channel and ICA component 13 that was centered on P4 (29^{th}) /O2 (33^{th}) channels. The correlations are particularly strong at central and posterior areas, which are similar to the results of previous studies in the driving experiments [32, 34, 115]. The relatively high correlation coefficients of near α-band (8-13 Hz) with driving performance suggests that alpha band frequencies (8-13 Hz) may be suitable for drowsiness (micro-sleep) estimation, where the subject's cognitive state might fall into stage one of the non-rapid-eye-movement (NREM) sleep. Next, we compared correlation spectra for individual subject to examine the stability of this relationship over the cross-sessions and cross-subjects. Fig. 4-14 shows the correlation spectra of subject 2. Comparing to subject 3, the characteristics of EEG measurements near α-band are consistent

but they differ in ICA components. By checking the dominant components 8 and 17 that have the highest correlation coefficients shown in Fig. 4-14 (b) and their spatial distributions of weighting matrices shown in Figs. 4-14 (c) and (d), we can observe that it is suitable to place the electrodes of non-invasive EEG measurement at parietal lobe and occipital lobe for the drowsiness estimation. For practice and routine application, EEG-based cognitive assessment systems should use as fewer EEG sensors as possible to reduce the preparation time for device wiring and computational cost for continuous alertness level estimation in near real time. According to the analysis shown in Figs. 4-13 and 4-14, we believe it is adequate to use the EEG signals at central and posterior sites to assess the alertness level of subjects continuously.

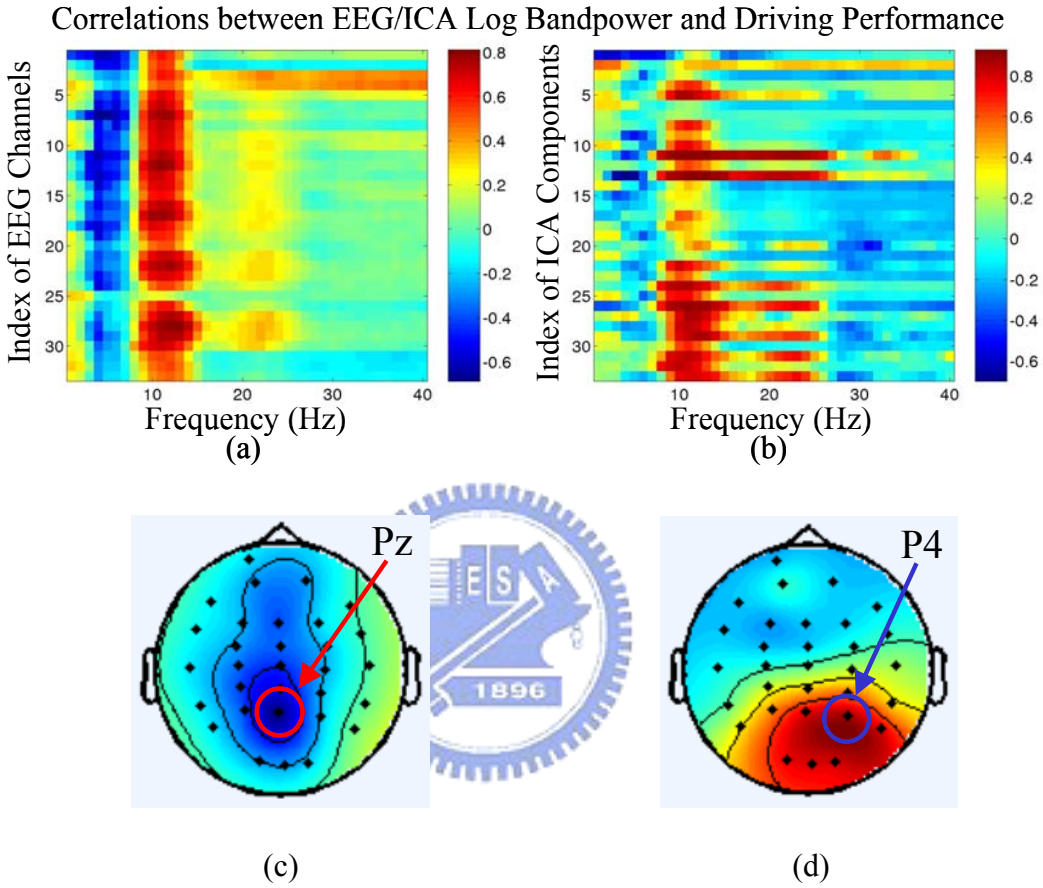

Figure 4-13. Correlation spectra between smoothed driving performance and log subband power spectra of (a) 33 EEG channels and (b) 33 ICA components for frequencies between 1 and 40 Hz of Subject-3. It is observed that the subband power spectra between frequency bands 10~14Hz have high positive correlation with driving performance in most EEG channels and both 11^{th} and 13^{th} ICA components. Figs. 4-13 (c) and (d) show the scalp topographies of weighting matrices for dominant ICA component 11 that was centered on Pz (28^{th}) channel and ICA component 13 that was centered on P4 (29^{th}) /O4 channels.

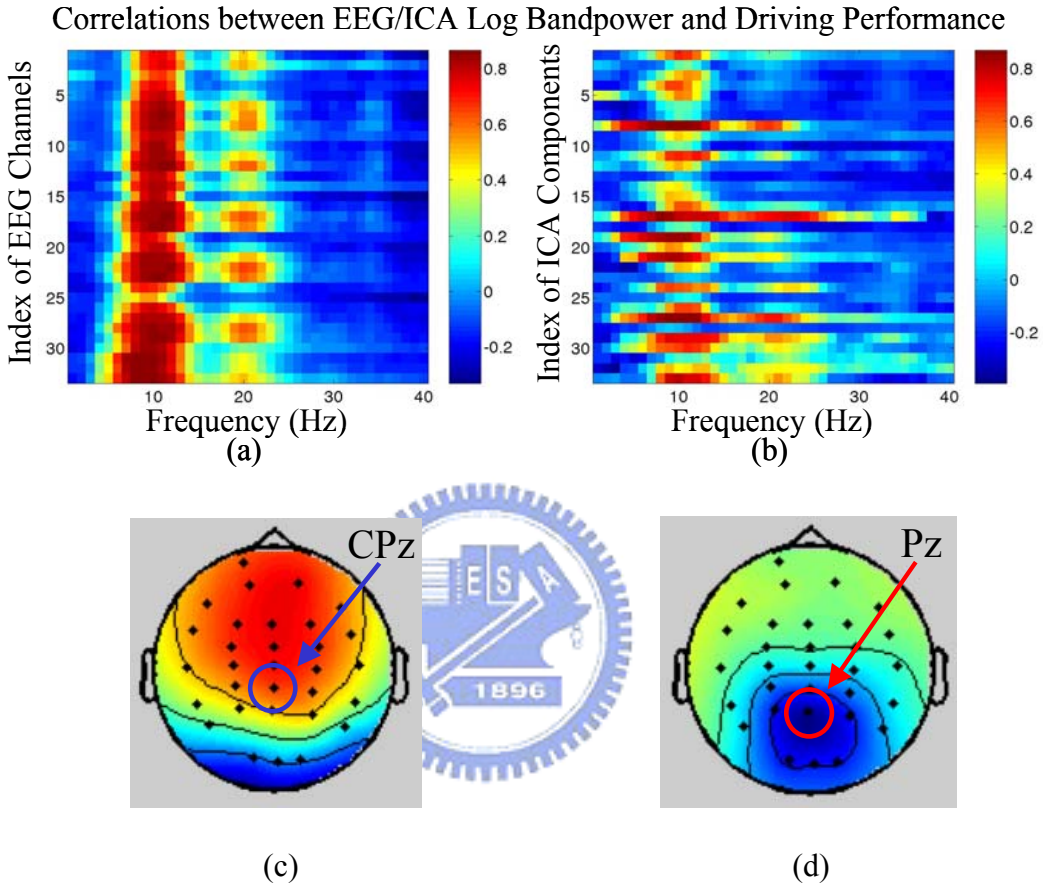

Figure 4-14. Correlation spectra between smoothed driving performance and log subband power spectra of (a) 33 EEG channels and (b) 33 ICA components for frequencies between 1 and 40 Hz of Subject-2. It is observed that the subband power spectra between frequency bands 8~13Hz have high positive correlation with driving performance in most EEG channels and both 8th and 17th ICA components. Figs. 4-14 (c) and (d) show the scalp topographies of weighting matrices for dominant ICA component 8 that was centered on CPz (22th)/Fz channels and ICA component 17 that was centered on Pz (28th) /Oz channels.

4.6.4. Noise Segmentation and Selection of Optimal Frequency Bands

During driving simulation, the subjects move their hands, torso, head, and eyes, which will create huge muscle movement, eye movement, and blink artifacts to the non-invasive measurement of brain potentials. The other noise includes the movement of the 6-DOF motion platform and line noise. Assume these noises of muscle activity, eye, and, cardiac signals are not time locked to the EEG activity, i.e., they are temporal independent; it is very suitable to use ICA to separate the EEG signals from the "mixed" recordings other than using low pass filter. In this chapter, after ICA training, we can obtain 33 ICA components ***u(t)*** decomposed from the measured 33-channel EEG data ***x(t)***. Fig. 4-15 shows the scalp topographies of ICA weighting matrix corresponding to each ICA component by spreading each $w_{i,j}$ into the plane of the scalp, which provides information about the location of the sources, e.g., eye activity was projected mainly to frontal sites, and the drowsiness-related potential is on the parietal lobe to occipital lobe, etc. We can observe that the most artifacts and channel noises included in EEG recordings are effectively separated into ICA components 1, 2, and 3 as shown in Fig. 4-15. The ICA components 8, 11, and 17 may be considered as effective "sources" related to drowsiness, which will be examined by the correlation analysis. It is more conservative estimation to just remove possible artifact components than choosing "sources" components only in avoidance of making erroneous judgments. Thus, the "corrected" EEG signals can be obtained by re-projection from the ICA components after removing possible "artifact" components using Eq. (4-6) as follows:

$$\boldsymbol{x}(t)=\begin{bmatrix} x_1(t) \\ x_i(t) \\ \vdots \\ x_{33}(t) \end{bmatrix}=\boldsymbol{W}\,\boldsymbol{u}(t)=\begin{bmatrix} w_{1,1} \\ w_{i,1} \\ \vdots \\ w_{33,1} \end{bmatrix}u_1(t)+\begin{bmatrix} w_{1,2} \\ w_{i,j} \\ \vdots \\ w_{33,2} \end{bmatrix}u_j(t)+\cdots+\begin{bmatrix} w_{1,33} \\ w_{2,33} \\ \vdots \\ w_{33,33} \end{bmatrix}u_{33}(t) \qquad (4\text{-}6)$$

Besides, the ICA can be used to locate possible positions of the "drowsiness" sources. Fig. 4-16 shows the resulting correlation spectra of subject 2 in 33 ICA components. The

horizon axis indexes frequency bands between 1 and 40 Hz and the vertical axis indexes the ICA components. The correlation spectra shows a strong evidence between fluctuations in ICA bandpower of frequency bands within 4 to 25 Hz and driving performance with high positive correlations in ICA components 8 and 17. As driving error increases, so does ICA bandpower. Fig. 4-17 show the spatial distributions in scalp topographies of weighting matrices for dominant ICA component 8 that was centered near CPz (22^{th}) channel and ICA component 17 that was centered on Pz (28^{th}) /Oz (32^{th}) channels. The correlations are particularly strong at central and posterior areas, which are similar to the results of previous studies in the driving experiments [32, 34]. For practice and routine application, EEG-based cognitive assessment systems should use as fewer EEG sensors as possible to reduce the preparation time for device wiring and computational cost for continuous alertness level estimation in near real time. According to the analysis shown in Figs. 4-16 and 4-17, the relatively high correlation coefficients with driving performance suggest that it is adequate to use the EEG signals at center position of dominant ICA components to assess the alertness level of subjects continuously.

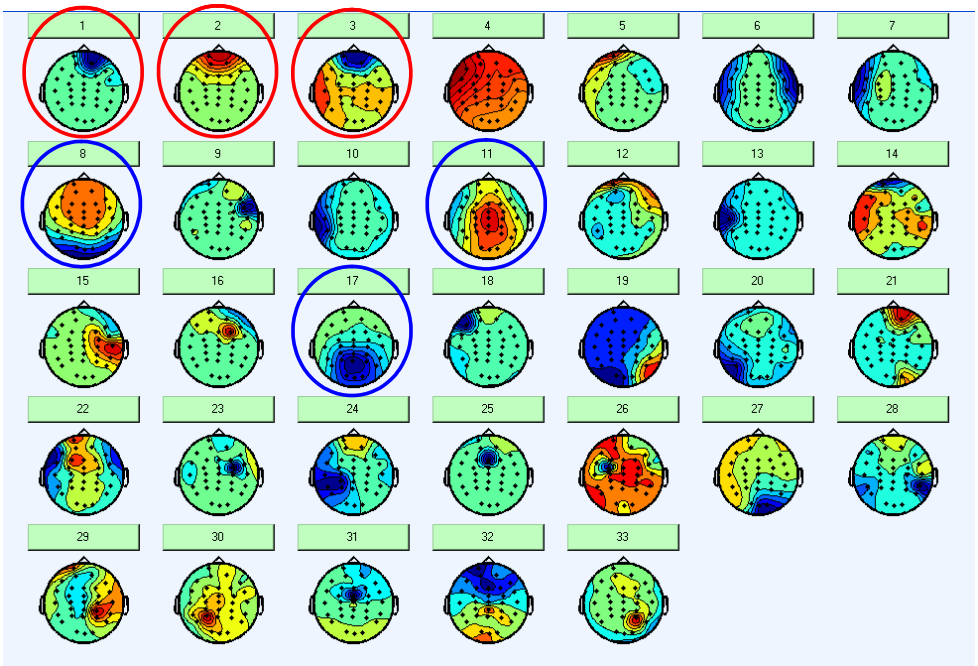

Figure 4-15. Scalp topography of ICA weighting matrix $w_{i,j}$ by spreading each $w_{i,j}$ into the plane of the scalp corresponding to the j_{th} ICA components based on International 10-20 system.

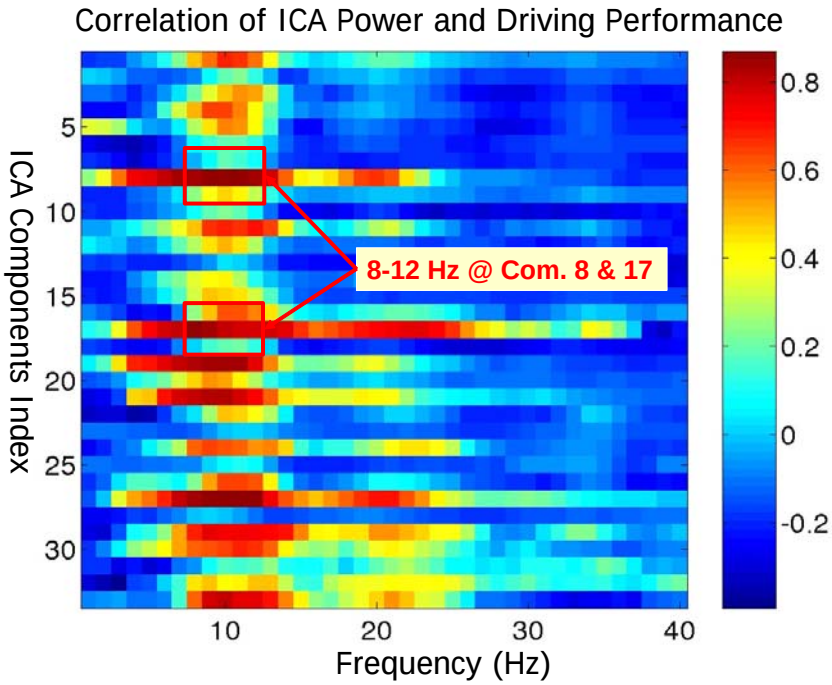

Figure 4-16. Correlation spectra between smoothed driving performance and log power spectra of 33 ICA components of Subject-2. It is observed that the bandpower spectra between frequency bands 8~12Hz have highest positive correlation with driving performance in both 8^{th} and 17^{th} ICA components.

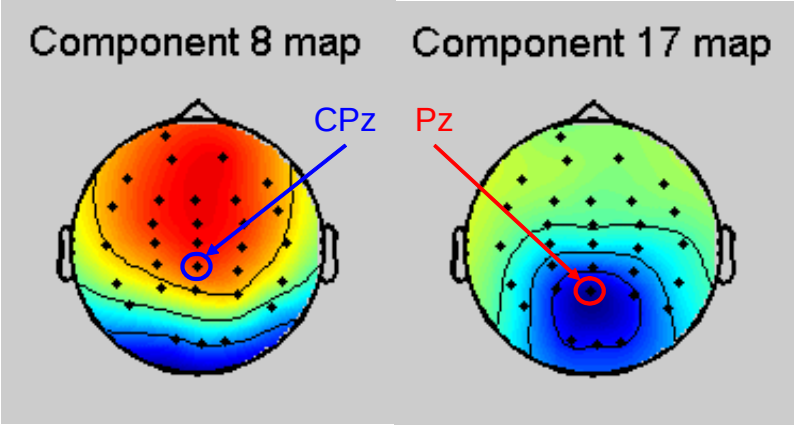

Figure 4-17. Scalp topographies of ICA weighting matrices for dominant components 8 and 17. Note that the CPz channel and Pz channels are at the center position of these two ICA components, respectively.

In this section, we compared the correlation between log subband power spectra and driving error for each frequency bands and individual ICA component to find the optimal subbands and localizations of electrodes according to the scalp topographies of ICA weighting matrices. Previous studies [40, 49-52] showed that it is not applicable to use full EEG frequency bands to accurately estimate individual changes in vigilance and driving error because of the artifacts and individual variability in EEG dynamics accompanying loss of alertness. Even though information about alertness may be distributed over the entire EEG spectrum. Table 4-2 shows the correlation coefficients between different frequency bands of the ICA component 11 or 13 and the driving error of subject-3 in different experimental sessions. The ICA weighting matrices after training were held and used in the testing sessions on different days. The results show the better frequency bands of ICA components 11 and 13 are from 10 to 14 Hz with the correlation rate up to 0.94. Table 4-3 lists the correlation results for training and testing sessions using frequency bands within 10~14 Hz in single ICA component. The statistical evidence shows that the ICA components 11 and 13 have the highest correlation coefficients than the other components (components 5, 24, 26, 29, and 31)

and their scalp topographies shown in Figs. 4-14 (c) and (d) demonstrated that the most alpha waves with positive correlation related to micro-sleep could be observed at occipital and central sites. Table 4-4 shows the optimal 2 ICA components and frequency bands ranges corresponding to different subjects according to the higher correlation coefficients between the log subband power spectra and the driving performance. The best frequency bands are 5-9 Hz both in 17^{th} and 28^{th} ICA components for subject 1, and 8-12 Hz both in 17^{th} and 8^{th} components for subject 2, etc. Table 4-4 demonstrated that the better frequency bands and the ICA components are not the same for different subjects.

The above analyses provide strong and converging evidence that changes in subject alertness level indexed by driving error during a driving task are strongly correlate with the changes in the ICA power spectrum at several frequencies located at central and posterior sites. This relationship is stable over time in different sessions of the same subject, but relatively variable between subjects. These results are consistent with the findings from a simple auditory target detection task reported in [18, 83]. These findings suggest that maximal accuracy the estimation algorithm should be capable of adapting to individual differences in the mapping between EEG and alertness..

Table 4-2. The correlation coefficients between the log subband power spectra and the driving error of subject 3 corresponding to different frequency bands from 8 to 15 Hz of ICA component 11 and 13 in the training and testing sessions using the same ICA weighting matrices obtained from the training session.

ICA Component Index \ Band		8 Hz	9 Hz	10Hz	11Hz	12Hz	13Hz	14Hz	15Hz
Com 11	Training	0.82	0.89	0.92	0.92	0.92	0.92	0.89	0.87
	Testing-1	0.86	0.88	0.88	0.88	0.87	0.86	0.83	0.82
	Testing-2	0.79	0.87	0.90	0.92	0.91	0.91	0.86	0.78
	Testing-3	0.78	0.90	0.93	0.93	0.93	0.94	0.94	0.91
Com 13	Training	0.77	0.88	0.90	0.91	0.92	0.91	0.90	0.86
	Testing-1	0.87	0.90	0.90	0.89	0.88	0.87	0.84	0.80
	Testing-2	0.75	0.87	0.87	0.90	0.90	0.88	0.85	0.79
	Testing-3	0.76	0.89	0.91	0.92	0.93	0.92	0.92	0.89

Table 4-3. The correlation coefficients between log subband power spectra and the driving error of subject 3 using five best frequency bands (from 10 to14 Hz) corresponding to different single ICA component. The same ICA weighting matrices obtained from the training session were used for testing session performed in the other day.

ICA component	5	11	13	24	26	29	31
Training	0.84	0.93	0.92	0.82	0.89	0.82	0.79
Testing	0.80	0.92	0.91	0.82	0.88	0.78	0.78

Table 4-4. The optimal 2 ICA components and frequency band ranges corresponding to different subjects according to the higher correlation coefficients between log subband power spectra and the driving performance.

Subject	Subject 1	Subject 2	Subject 3	Subject 4	Subject 5
ICA Components	17, 28	17, 8	11, 13	4, 5	22, 25
Bands	5-9 Hz	8-12 Hz	10-14 Hz	4-8 Hz	8-12 Hz

4.6.5. Drowsiness Estimation Based on Log Bandpower of ICA Components

In this study, we use a 10-order least-square linear regression model [113, 116] to estimate the subject's driving error based on the information obtained from the subband power spectra analysis of ICA components. The linear regression model attempts to model the relationship between the selected input features X by fitting a linear equation $y=AX+b$ to the observed output data y_d at each sampled data point. i.e., given the input data set X and desired output data y_d at each data point, the least-squared linear regression method is to find an optimal parameter set $\{A, b\}$, such that $y=AX+b$, subjected to minimizing the squared error cost function $\varepsilon = \sum(y_d-y)^2$. We used only 2 ICA components that performed the highest correlation between the ICA subband power spectrum and the driving error such that the most artifacts can be removed and the available information of drowsiness estimation is extracted. After moving-average spectra analysis of ICA components, we obtain the time series (stepping at 2 seconds), with a 40-point data set presenting bandpower of 1-40 Hz frequencies for each single ICA component. We also collected the corresponding smoothed driving error for each session. We selected 5-point bandpower of each component (e.g., 10-14 Hz in ICA component 11 for subject 3) and totally 10-point bandpower for 2 most important ICA components as the input data X of linear regression model. After training process, we get the

optimal parameter $\{A, b\}$ iteratively such that the output $y=AX+b$ of the linear regression model is very closed to observed output (driving error, y_d) with minimum $\varepsilon = \sum(y_d-y)^2$. The model was trained on one session and tested on the other session for each subject. The ICA weighting matrices obtained from the training sessions were used to spatially filter the features in the testing sessions so that all data were processed in the same way for the same subject before feeding to the estimation models. Fig. 4-18 plots the estimated and actual driving error of training/testing sessions from subject 3. The linear regression model in this figure is trained with one session (within-session) and tested against a separated session, i.e. cross-session testing. As can been seen, the estimated driving error matched well with the actual driving error with correlation coefficient r=0.93 in the training and r=0.92 in the testing. Fig. 4-19 plots the training/testing results of subject 2. The estimated driving error compared with the actual driving error is r=0.91 in the training and r=0.89 in the testing. Table 4-5 shows the statistics across ten sessions for five selected subjects. The mean correlation coefficient between actual driving error time series and within training session estimation is 0.908, whereas the mean correlation coefficient between actual driving error and cross testing session estimation is 0.848. These results suggest that continuous ICA-based driving error estimation using a small number of frequency bands is feasible, and can give accurate information about minute-to-minute changes in operator's alertness.

Table 4-5. Driving performance estimation using total 10 frequency bands in 2 dominant ICA components (5 frequency bands for each ICA component) as input features of the linear regression model for five subjects.

	Subject 1	Subject 2	Subject 3	Subject 4	Subject 5	Average
Training	91%	91%	93%	89%	90%	90.8 %
Testing	77%	89%	92%	86%	80%	84.8%

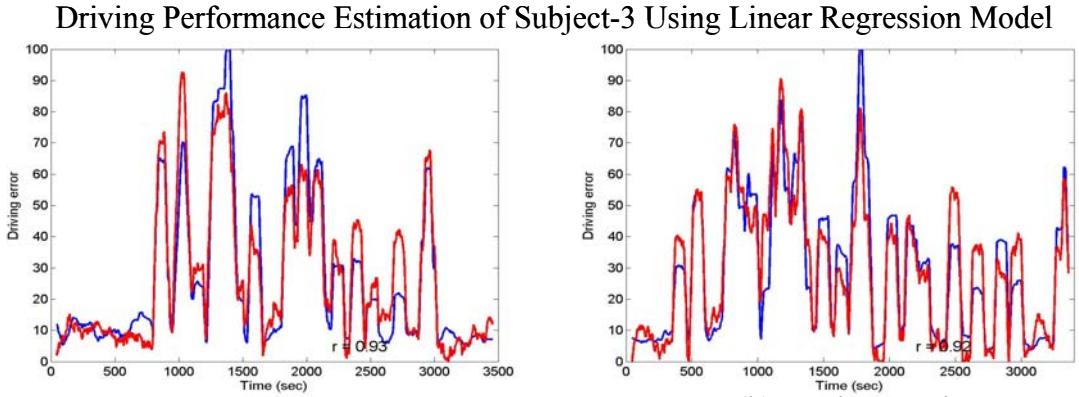

Figure 4-18. Driving performance estimates for training/testing sessions of subject 3, based on a linear regression model (red line) with subband log power spectra at frequency bands 10~14 Hz of ICA components 11 and 13 selected according to Table 4-4, overplotted against actual driving performance time series for the session (blue line). The correlation coefficient between the two time series is r=0.93 in the training session and r=0.92 in the testing session.

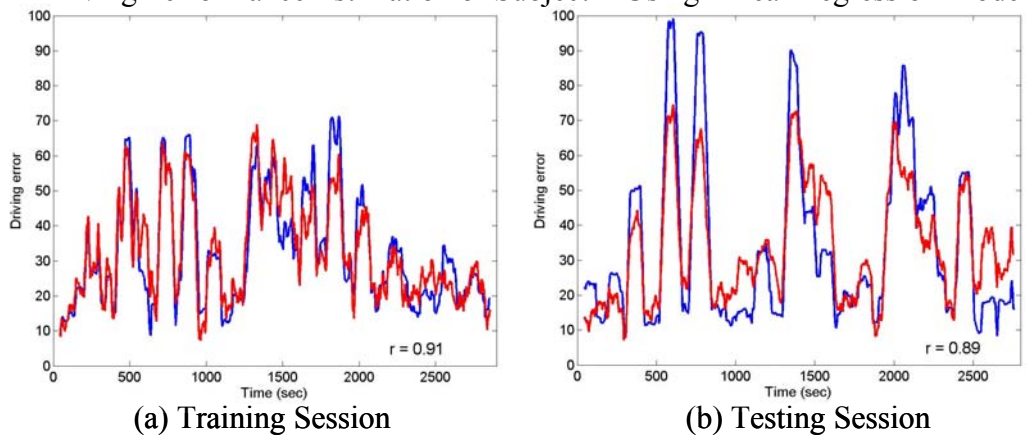

Figure 4-19. Driving performance estimates for training/testing sessions of subject 2, based on a linear regression model (red line) with subband log power spectra at frequency bands 8~12 Hz of ICA components 8 and 17 selected according to Table 4-4, overplotted against actual driving performance time series for the session (blue line). The correlation coefficient between the two time series is r=0.91 in the training session and r=0.89 in the testing session.

4.6.6. Drowsiness Estimation Based on EEG Log Bandpower

Experimental results discussed in the above sections demonstrated that it is feasible to accurately estimate driving error accompanying loss of alertness based on ICA algorithm and subband power spectrum analysis of multi-channel EEG signals. Since the proposed ICA-based drowsiness estimation method is a little complicated, we propose a alternative method to balance the tradeoff between accuracy of alertness monitoring and computational cost in this section. It uses only 10 frequency bands of 2 EEG channels located at central electrode positions of the 2 ICA components which have the better correlation coefficients between log subband power spectra and the driving error of the subject. This method needs multi-channel EEG signals to calculate their ICA weighting matrices in the training session which is used to locate the positions of 2 EEG electrodes and optimal frequency bands, and does not require collecting the EEG signals of the other EEG channels except the 2 selected ones in the testing sessions.

Table 4-6 shows the correlation coefficients between the log subband power spectra and the driving error of subject 3 using frequency bands from 10 to14 Hz of EEG channels located at Fz, FCz, Cz, CPz, P3, Pz, and P4 in the training/testing session. Comparing to the results of using ICA components listed in Table 4-3, the correlation coefficients is somewhat lower due to artifacts and other noise. We may observe that the results using Pz and P4, which are the central electrodes of ICA components 11 and 13, are better than the results by using other channels. The driving error estimation of subject 3 based on a linear regression model with frequency bands 10~14 Hz of EEG channels Pz and P4 as inputs (total 10 frequency bands) are shown in Fig. 4-20. The correlation coefficient between estimated and actual driving error is r=0.91 in the training session and r=0.87 in the testing session, which is just a little lower than those using corresponding ICA components. Table 4-7 shows the optimal 2 EEG channels and associated frequency band ranges of different subjects selected according to the

cortical locations corresponding to ICA components selected from Table 4-4. Table 4-8 shows the driving error estimation using total 10 frequency bands (5 for each EEG channel) as input features of linear regression model for five subjects. The mean correlation coefficient between actual driving error time series and within training session estimation is 0.882, whereas the mean correlation coefficient between actual driving error and cross testing session estimation is 0.79. Comparing Table 4-5 and Table 4-8, the accuracies of training and testing with ICA technique are a little better than those without ICA. This result suggests a compromise between computational cost and estimation accuracy.

Table 4-6. The correlation coefficients between log subband power spectra and driving error of subject 3 using bandpower in frequency bands from 10 to14 Hz corresponding to different single EEG channel in the training/testing session.

Index of EEG Channels	Fz	FCz	Cz	CPz	P3	Pz	P4
Training	0.75	0.77	0.77	0.78	0.74	0.80	0.79
Testing	0.67	0.69	0.69	0.72	0.69	0.77	0.72

Table 4-7. The optimal 2 EEG channels and the associated frequency band ranges corresponding to different subjects based on central electrode positions of 2 ICA components which have the better correlation coefficients between the log subband power spectra and the driving performance.

	Subject 1	Subject 2	Subject 3	Subject 4	Subject 5
Bands	5-9 Hz	8-12 Hz	10-14 Hz	4-8 Hz	8-12 Hz
EEG Channels	O1, O2	CPz, Pz	Pz, P4	O1, O2	P3, O1

Table 4-8. Driving error estimation using total 10 frequency bands (5 for each EEG channel) as input features of the linear regression model for five subjects.

	Subject 1	Subject 2	Subject 3	Subject 4	Subject 5	Average
Training	78%	90%	91%	88%	94%	88.2%
Testing	68%	86%	84%	84%	73%	79%

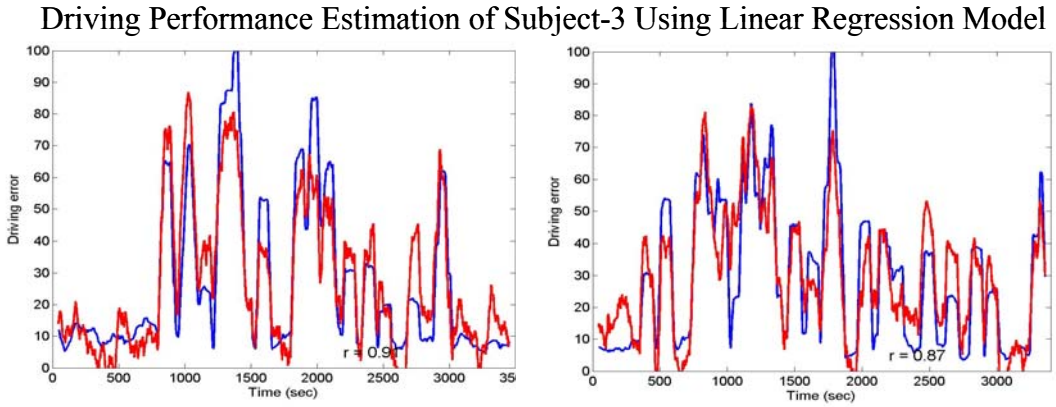

(a) Training Session (b) Testing Session

Figure 4-20. Driving error estimates for training/testing sessions of subject 3, based on a linear regression model (red line) with subband log power spectra at frequency bands 10~14 Hz of EEG channels Pz and P4 (selected according to Table 4-7), overplotted against actual driving error time series for the session (blue line). The correlation coefficient between the two time series is r=0.91 in the training session and r=0.87 in the testing session.

4.6.7. AFSM-based Driving Performance Estimation/Prediction

We also proposed a novel adaptive feature selection mechanism (AFSM) to solve the reliable and sorting problem of ICA components based on the correlation analysis between the time-frequency power spectra of ICA components and the driving performance. To reduce the computational loading within the capabilities of modern real-time embedded digital signal processing hardware for continuously estimating the level of alertness in near real time, we limited finally the number of the selected ICA components and the frequency bands of each

components to be two and five, respectively, by using AFSM. Table 4-9 shows the number of ICA components and optimal frequency bands selected manually and those by AFSM. Note that both selected ICA components and the frequency bands are almost the same but slightly different for each subject between manually selecting and AFSM. To verify the correctness and effectiveness of the AFSM method, the selected log bandpower spectra of the ICA components in these critical bands were feed as the input features of the linear regression models. We also used the Self-cOnstructing Neuro-Fuzzy Inference Network (SONFIN) [94] model to estimate and predict the individual driver's driving performance by taking the advantages of fuzzy reasoning and learning abilities, and flexibility of neural networks. Fig. 4-21 shows the driving performance estimation for training/testing sessions of subject 3, based on SOFNIN models (red line) with input features selected by AFSM method according to Table 4-10, overplotted against actual driving performance time series for the session (blue line). The correlation coefficient between the two time series is r=0.96 in the training session and r=0.94 in the testing session.

Table 4-10 shows the comparison results of driving performance estimation. Although the correlation coefficients between the two time series based on AFSM methods using linear regression models are somewhat lower than those selected manually. The adaptive feature selection mechanism has the advantages of saving time, and cost when the whole system is applied for on-line alertness monitoring. Table 4-11 shows the estimating results based on AFSM methods using SONFIN. Compared to the results using linear regression models, using fuzzy neural network models can achieve higher estimating results as shown in Fig. 4-21 for subject-3, and can compensate the slightly loss using AFSM in real-time applications.

Table 4-9. The optimal 2 ICA components and frequency bands selected manually and by AFSM corresponding to different subjects according to the higher correlation coefficients between log bandpower spectra and the driving performance.

		Subject 1	Subject 2	Subject 3	Subject 4	Subject 5
Manual	ICA Components	17, 28	17, 8	11, 13	4, 5	22, 25
	Freq. Bands	5-9 Hz	8-12 Hz	10-14 Hz	4-8 Hz	8-12 Hz
AFSM	ICA Components	17, 28	17, 8	11, 13	4, 5	22, 25
	Freq. Bands	4-8 Hz	8-12 Hz	10-14 Hz	5-9 Hz	9-13 Hz

Table 4-10. Driving performance estimation using total 10 frequency bands in 2 dominant ICA components selected manually and by AFSM methods shown in Table 4-9, as input features of the linear regression models for five subjects.

			Sub-1	Sub-2	Sub-3	Sub-4	Sub-5	Average
Manual	Linear Regression	Training	91%	91%	93%	89%	90%	90.8%
		Testing	77%	89%	92%	86%	80%	84.8%
AFSM	Linear Regression	Training	88%	91%	93%	88%	84%	88.8%
		Testing	72%	89%	82%	80%	76%	81.8%

Table 4-11. Driving performance estimation using total 10 frequency bands in 2 dominant ICA components selected by AFSM methods shown in Table 4-9, as input features of the linear regression models and SONFIN for five subjects.

			Sub-1	Sub-2	Sub-3	Sub-4	Sub-5	Average
AFSM	Linear Regression	Training	88%	91%	93%	88%	84%	88.8%
		Testing	72%	89%	82%	80%	76%	81.8%
	SONFIN	Training	89%	92%	96%	87%	91%	91%
		Testing	84%	89%	94%	83%	85%	87%

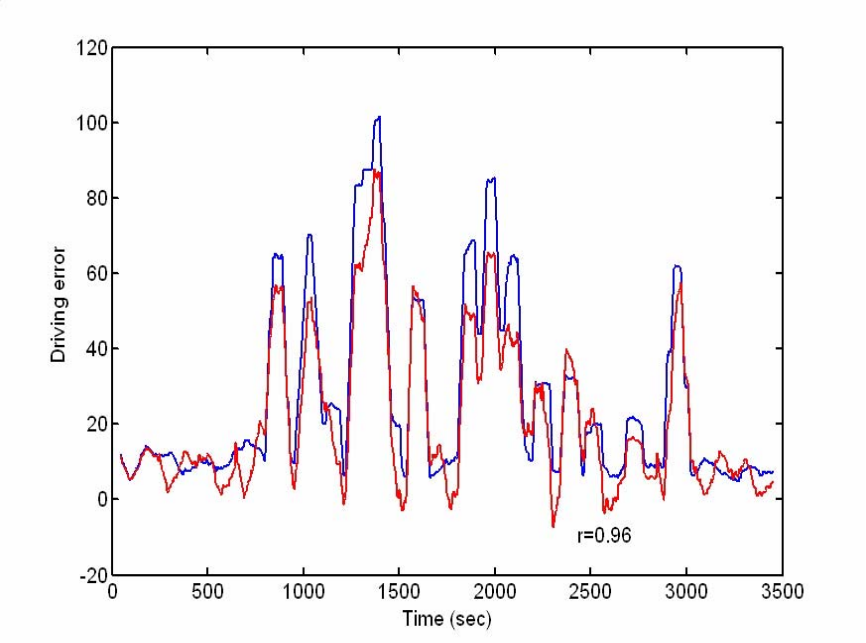

(a) Training Result

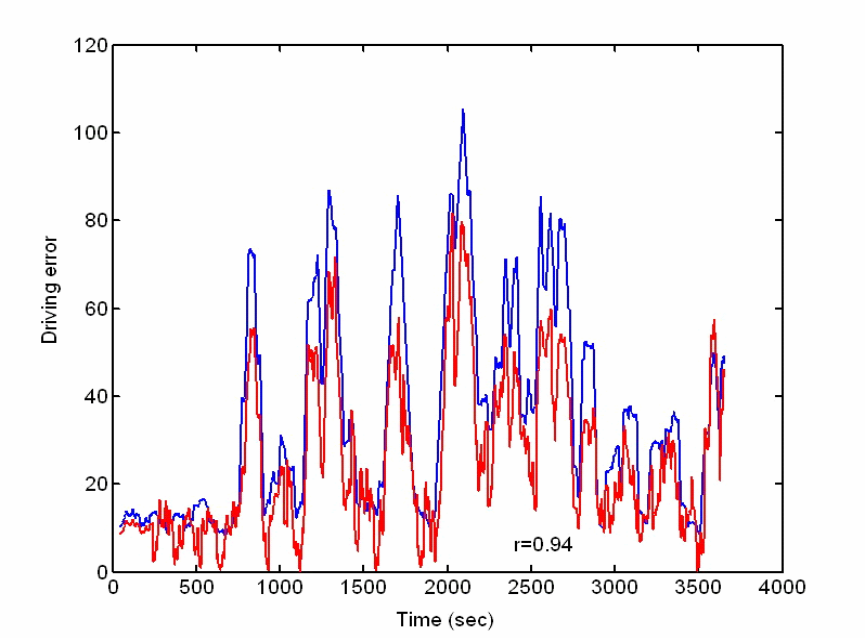

(b) Testing Result

Figure 4-21. Driving performance estimation for training/testing sessions of subject 3, based on SOFNIN models (red line) with input features selected by AFSM method according to Table 4-9, overplotted against actual driving performance time series for the session (blue line). The correlation coefficient between the two time series is r=0.96 in the training session and r=0.94 in the testing session.

4.7. Conclusion Remarks

In this chapter, we demonstrated a close relationship between minute-scale changes in driving performance and the EEG/ICA power spectrum. This relationship appears stable within individuals across sessions, but is somewhat variable between subjects. Four computational approaches were proposed to select effective features for drowsiness estimation based on the compromise of computational cost and estimating accuracies. The first approach combined EEG power spectrum estimation, correlation analysis, PCA, and linear regression to continuously indirectly estimate/predict fluctuations in human alertness level indexed by driving performance measurement, deviation between the center of the vehicle and the center of the cruising lane. Our results demonstrated that it is feasible to accurately estimate driving errors based on multi-channel EEG power spectrum estimation and principal component analysis algorithm. The computational methods we employed in this study were well within the capabilities of modern real-time embedded digital signal processing hardware to perform in real time using one or more channels of EEG data. Once an estimator has been developed for each driver, based on limited pilot testing, the method uses only spontaneous EEG signals from the individual, and does not require further collection or analysis of operator performance. The proposed methods thus might be used to construct and test a portable embedded system for a real-time alertness monitoring system. The other two approaches used ICA, power spectrum analysis, correlation analysis, and the linear regression model in a virtual-reality based driving environment. Experimental results show that the proposed analysis methods are feasible to accurately estimate individual driving error accompanying loss of alertness by linear regression model with 10 subband log power spectra near α-bands of 2 ICA components as inputs. Averaged accuracies of training and testing session for 5 subjects are 90.8% and 84.8%, respectively. We also propose an alternative method to save computational cost by selecting only 2 EEG channels located at central

electrodes of the corresponding ICA components. Average accuracies of training and testing session for 5 subjects are 88.2% and 79%, respectively. Although the accuracy is somewhat lower than those using ICA components, its does not require to collect more EEG channels data in testing session. Thus, this approach suggests a compromise between computational cost and estimation accuracy. Therefore, the proposed methods can be used to construct and test on an online portable embedded system for a real-time alertness monitoring system. In the last approach, we proposed a novel adaptive feature selection mechanism to solve the sorting problem of the ICA components and to extract useful frequency bands as input features. Experimental results show that the average accuracies of training and testing session for five subjects can achieve high to 88.8% and 81.8% as well as 91% and 87%, by using linear regression model and fuzzy neural network models, respectively. Although the accuracy using AFSM-based linear regression model is lower than those selected manually, the computational methods we employed in this study were well within the capabilities of modern real-time embedded digital signal processing hardware to perform in real time alertness monitoring system.

5. Conclusions

In this thesis, we develop quantitative techniques that combine independent component analysis, temporal matching filter, time frequency spectrum analysis, correlation analysis, adaptive feature selection mechanism, and fuzzy neural network models for ongoing assessments of the transient event-related brain dynamics and the level of alertness of drivers by investigating the neurobiological mechanisms underlying non-invasively recorded multidimensional electroencephalographic (EEG) brain dynamics in the virtual-reality-based cognitive driving tasks. We then apply these methodologies to the issue of driving safety and focus on two most frequent happened events on the roads, the visual traffic-light detection task and the continuous lane-keeping driving task in order to maintain the subject's maximum driving performance for preventing the traffic accidents and extend the applications of brain research to general populations (not limited to lock-in patients). In this thesis, we have made significant progresses in several aspects. (1) The use of virtual-reality technology not only allows subjects to interact directly with virtual objects, but also provides a well-controlled realistic experimental environment to avoid the risk of operating on the real world. (2) The computational approaches are capable of providing high spatial and temporal resolutions by using multidimensional EEG information obtained from an array of scalp electrodes and to model the dynamics of the underlying brain networks. (3) Comparing to the traditional time-domain overlap-added averaged methods, the introduced ICA algorithm can analyze brain activities in single trials correctly without first averaging on trials. The temporal independence and spatial stability make ICA to effectively remove non-brain artifacts to increase the amount of information contained in the EEG recordings and to find out the optimal location to wire EEG electrodes. (4) The proposed temporal matching filter can solve the time-alignment problems between trials and increase the recognition rates of ERP

classification. (5) We also use the moving-average time-frequency spectral analysis to avoid confounds caused by miscancellation of positive and negative potentials from different sources to the recording electrodes, and characterize the perturbations in the oscillatory dynamics of ongoing EEG. (6) The use of the correlation analysis can provide objective measurement of driver's cognitive state and is helpful to extract effective features. (7) For online applications, we proposed a novel adaptive feature selection mechanism combined with the Self-cOnstructing Neuro-Fuzzy Inference Network model to accuracy identify the transient brain response to different visual stimuli and estimate/predict the actual driving performance of individual subjects.

Experimental results demonstrated that the proposed ICA-based methods can achieve a high recognition rate on average up to 85% in classifications of the brain cognitive responses related to visual traffic-light detection task. These high-accuracy results can be further transformed as the control/monitoring signals of on-line brain computer interfaces in the driving-safety systems. Another proposed EEG-based technology for drowsiness estimation also showed that it is feasible to accurately estimate individual driving performance accompanying loss of alertness. In this study, we demonstrated a close relationship between minute-scale changes in driving performance and the EEG power spectrum. This relationship appears stable within individuals across sessions, but is somewhat variable between subjects. We also propose four strategies to explore the optimal and economic way to select effective EEG-based features. The first approach uses power spectrum of only 2 EEG channels, where once an estimator has been developed for each driver, based on limited pilot testing, the method uses only spontaneous EEG signals from the individual, and does not require further collection or analysis of operator performance. Another approach apply the ICA algorithm in the training session to locate the optimal position to wire EEG electrodes and uses 2 EEG channels located at central electrodes of the selected ICA components. Averaged accuracies

for 5 subjects achieve 79% using fuzzy neural network model. This method dramatically increases the accuracy than the first one and does not require collecting more EEG channels data in testing session. The third approach directly uses 10 log bandpower of 2 optimal ICA components as input features and achieves the maximum averaged accuracies to 84.8%. For the purpose of the online application, we proposed an automatic feature selecting mechanism combined with SONFIN to estimating driving performance and the averaged accuracies for five subjects can achieve high to 87%. Although the accuracy using adaptive feature selection mechanism is lower than those selected manually, the computational methods we employed in this study were well within the capabilities of modern portable embedded digital signal processing hardware to perform in real time alertness monitoring system.

Bibliography

[1] A. F. Kramer and D. L. Strayer, “Assessing the development of automatic processing: An application of dual-task and event-related brain potential methodologies,” *Biological Psychology*, Vol. 26, pp. 231-267, 1998.

[2] G. F. Wilson and F. Fisher, “Cognitive task classification based upon topographic EEG data,” *Biological Psychology*, Vol. 40, pp. 239-50, 1995.

[3] G. Pfurtscheller and A. Aranibar, “Event-related cortical desynchronization detected by power measurements of scalp EEG,” *Electroencephalography and Clinical Neurophysiology*, Vol. 42, pp. 817-826, 1977.

[4] G. Pfurtscheller and C. Andrew, “Event-Related changes of band power and coherence: methodology and interpretation,” *Journal of Clinical Neurophysiology*, Vol. 16, pp. 512-519, 1999.

[5] S. J. Williamson, L. Kaufman, S. Curtis, Z. L. Lu, C. M. Michel, and J. Z. Wang, “Neural substrates of working memories are revealed magnetically by the local suppression of alpha rhythm,” *Electroencephalography and Clinical Neurophysiology*. Supplement, Vol. 47, pp. 163-80, 1996.

[6] P. Sykacek, S. J. Roberts, and M. Stokes, "Adaptive BCI based on variational Bayesian Kalman filtering: An empirical evaluation," *IEEE Transactions on Biomedical Engineering*, Vol. 51, pp. 719-727, May, 2004.

[7] D. J. McFarland, G. W. Neat, R. F. Read, and J. R. Wolpaw, “An EEG-based method for graded cursor control,” *Psychobiology*, Vol. 21, No. 1, pp. 77-81, 1993.

[8] G. Pfurtscheller, D. Flotzinger, M. Pregenzer, J. Wolpaw, and D. McFarland, “EEG-based Brain Computer Interface (BCI),” *Medical Progress through Technology*, Vol. 21, pp. 111-121, 1996.

[9] T. M. Vaughan, J. R. Wolpaw, and E. Donchin, “EEG-based communication: prospects and problems," *IEEE Trans. on Rehabilitation Engineering*, Vol. 4, No. 4, pp. 425-430, 1996.

[10] L. A. Farwell and E. Donchin, “Talking off the top of your head: toward a mental prosthesis utilizing event-related brain potentials,” *Electroenceph. Clin. Neurophysiol.*, pp. 510-523, 1988.

[11] C. E. Davila and R. Srebro, "Subspace averaging of steady-state visual evoked potentials," *IEEE Transactions on Biomedical Engineering*, Vol. 47, pp. 720-728, Jun.

2000.

[12] T. J. Dasey and E. Micheli-Tzanakou, "Detection of multiple sclerosis with visual evoked potentials - an unsupervised computational intelligence system," *IEEE Transactions on Information Technology in Biomedicine*, Vol. 4, pp. 216-224, Sep. 2000.

[13] C. E. Davila, A. Abaye, and A. Khotanzad, "Estimation of single sweep steady-state visual evoked potentials by adaptive line enhancement," *IEEE Transactions on Biomedical Engineering*, Vol. 41, pp. 197-200, Feb. 1994.

[14] X. R. Gao, D. F. Xu, M. Cheng, and S. K. Gao, "A BCI-based environmental controller for the motion-disabled," *IEEE Transactions on Neural Systems and Rehabilitation Engineering*, Vol. 11, pp. 137-140, Jun. 2003.

[15] J. Klopp, K. Marinkovic, P. Chauvel, V. Nenov, and E. Halgren, "Early widespread cortical distribution of coherent fusiform face selective activity," *Human Brain Mapping*, Vol. 11, pp. 286-293, 2000.

[16] E. Basar, *EEG-brain dynamics: relation between EEG and brain evoked potentials*, Elsevier/North-Holland Biomedical Press, New York, 1980.

[17] R. Barry, S. Kirkaikul, and D. Hodder, "EEG alpha activity and the ERP to target stimuli in an auditory oddball paradigm," *International Journal of Psychophysiology*, Vol. 39, No.1, pp. 39-50, 2000.

[18] A. von Stein, C. Chiang, and P. Konig, "Top-down processing mediated by interareal synchronization," *Proceedings of the National Academy of Sciences, USA*, Vol. 97, No. 26, pp. 14748-14753, 2000.

[19] S. Thorpe, D. Fize, and C. Marlot, "Speed of processing in the human visual system," *Nature*, Vol. 381, No. 6582, pp. 520-2, 1996.

[20] H. Ueno, M., Kaneda, and M. Tsukino," Development of drowsiness detection system,**"** *Proceedings of the 1994 Vehicle Navigation and Information Systems Conference*, Vol. 31, pp. 15–20, Sep. 1994.

[21] G. Hamouda, and F. F. Saccomanno, "Neural network model for truck driver fatigue accident detection," *Proceedings of the 1995 Electrical and Computer Engineering Canadian Conference*, Vol. 1, pp. 362-365, Sep. 1995.

[22] M. Eriksson, and N. P. Papanikotopoulos, **"**Eye-tracking for detection of driver fatigue,**"** *Proceedings of the 1997 IEEE Conference on Intelligent Transportation System,* pp. 314–319, Nov. 1997.

[23] R. Grace, A. Guzman, J. Staszewski, B. A. Peters, M. Mallis, and D. F. Dinges, "The

Carnegie Mellon TruckSim: a tool to improve driving safety," *Proceedings of the 1998 IEEE 17th Conference on Digital Avionics Systems*, Vol. 2, pp. I35/1 - I35/831, Nov. 1998.

[24] R. Grace, V. E. Byrne, D. M. Bierman, J. M. Legrand, D. Gricourt, B. K. Davis, J. J. Staszewski, and B. Carnahan, " A drowsy driver detection system for heavy vehicles" *Proceedings of the 1998 the 17th AIAA/IEEE/SAE Conference on Digital Avionics Systems,* Vol. 2, pp. I36/1-I36/8, Nov. 1998.

[25] C. A. Perez, A. Palma, C. A. Holzmann, and C. Pena, "Face and eye tracking algorithm based on digital image processing," *Proceedings of the 2001 IEEE International Conference on Systems, Man, and Cybernetics,* Vol. 2, pp.1178-1183, Oct. 2001.

[26] T. Pilutti, and G. Ulsoy, "Identification of driver state for lane-keeping tasks," *IEEE Trans. Syst, Man, Cybern., Part A: Systems and Humans,* Vol. 29, pp. 486-502, Sep. 1999.

[27] J. C. Popieul, P. Simon, P. Loslever, "Using driver's head movements evolution as a drowsiness indicator," *Proceedings of the 2003 IEEE International Intelligent Vehicles Symposium*, pp. 616–621, Jun. 2003.

[28] J. Qiang, Z. Zhiwei, P. Lan, "Real-time nonintrusive monitoring and prediction of driver fatigue," *IEEE Transactions on Vehicular Technology,* Vol. 53, Issue: 4, pp. 1052– 068, Jul. 2004.

[29] K. Van Orden, W. Limbert, S. Makeig, and T. P. Jung, "Eye Activity correlates of workload during a visualspatial memory task," *Human Factors*, Vol. 43, No. 1, pp. 111-21, 2001.

[30] R. S. Huang, C. J. Kuo, L. L. Tsai, and O. T. C. Chen, "EEG pattern recognition-arousal states detection and classification," *Proceedings of the 1996 IEEE Conference on Neural Networks,* Vol. 2, pp. 641-646, Jun. 1996.

[31] A. Vuckovic, V. Radivojevic, A. C. N. Chen, and D. Popovic, "Automatic recognition of alertness and drowsiness from EEG by an artificial neural network," *Medical Engineering and Physics* Vol. 24, pp. 349-360, Jun. 2002.

[32] S. Roberts, I. Rezek, R. Everson, H. Stone, S. Wilson, and C. Alford, "Automated assessment of vigilance using committees of radial basis function analysers," *IEE Science Measurement and Technology,* Vol. 147, pp. 333–338, Nov. 2000.

[33] K. B. Khalifa, M. H. Bedoui, R. Raytchev, and M. Dogui, "A portable device for alertness detection," *Proceedings of 2000 1st Annual International IEEE-EMBS Special Topic Conference on Microtechnologies in Medicine and Biology,* pp. 584–586, Oct.

2000.

[34] B. J. Wilson, and T. D. Bracewell, ”Alertness monitor using neural networks for EEG analysis,” *Proceedings of the 2000 IEEE Signal Processing Society Workshop on Neural Networks for Signal Processing X,* Vol. 2, pp. 814-820, Dec. 2000.

[35] J. Santamaria and K. Chiappa, “The EEG of drowsiness in normal adults,” *J. Clin. Neurophysiol.*, Vol. 4, No. 4, pp. 327-382, 1987.

[36] Rechtschaffen, A., Kales, A. (Eds.): “A manual of standardized terminology in techniques and scoring system for sleep stages of human subjects,” *BIS/BRI*, UCLA, Los Angeles, CA, 1968.

[37] R. B. Berry, (Series Editors:) S. A. Sahn, and J. E. Heffner, “Sleep medicine pearls”, Hanley and Belfus Inc., Philadelphia, 1999.

[38] P. Parikh, and E. Micheli-Tzanakou, “Detecting drowsiness while driving using wavelet transform” *Proceedings of the IEEE 30th Annual Northeast on Bioengineering Conference*, pp. 79-80, Apr. 2004.

[39] H. Park, “Automated sleep stage analysis using hybrid rule-based and case-based reasoning,” Ph. D. Dissertation, Seoul National University, Aug. 2000.

[40] T. P. Jung, S. Makeig, M. Stensmo, and T. J. Sejnowski, “Estimating alertness from the EEG power spectrum,” *IEEE Trans. Biomed Eng*, Vol. 44, No. 1, pp. 60-69, 1997.

[41] S. Makeig, “Auditory event-related dynamics of the EEG spectrum and effects of exposure to tones,” *Electroencephalog. clin. Neurophysiolog*., Vol. 86, pp. 283-93, 1993.

[42] S. Makeig, and M. Inlow, “Lapses in alertness: Coherence of fluctuations in performance and EEG spectrum,” *Electroencephalography and Clinical Neurophysiology*, Vol. 86, pp. 23-35, 1993.

[43] S. Makeig, M. Westerfield, J. Townsend, T. P. Jung, E. Courchesne, and T. J. Sejnowski, “Independent components of early event-related potentials in a visual spatial attention task,” *Philosophical Transactions: Biological Sciences*, Vol. 354, pp. 1135-1144, 1999.

[44] S. Makeig, S. Enghoff, T. P. Jung, and T. J. Sejnowski, “Moving-window ICA decomposition of EEG data reveals event-related changes in oscillatory brain activity,” *The 2nd Int'l Workshop on Indeppendent Component Analysis and Signal Separation*, pp. 627-632, 2000.

[45] R. Verleger, T. Gasser, and J. Mocks, “Correction of EOG artifacts in event-related potentials of EEG: aspects of reliability and validity,” *Psychoph.*, Vol. 19, No. 4, pp. 472-80, 1982.

[46] J. C. Woestenburg, M. N. Verbaten, and J .L. Slangen, "The removal of the eye-movement artifact from the EEG by regression analysis in the frequency domain," *Biological Psychology*, Vol. 16, pp. 127-47, 1983.

[47] P. J. Oster and J. A. Stern, "Measurement of eye movement electrooculography," *Techniques in Psychophysiology*," Wiley Chichester, pp. 275-309, 1980.

[48] T. P. Jung, C. Humphries, T. W. Lee, S. Makeig, M. J. McKeown, V. Iragui, and T. J. Sejnowski, "Extended ICA removes artifacts from electroencephalographic recordings," *Advances in Neural Information Processing Systems* Vol. 10, pp. 894-900, 1998.

[49] S. Makeig and T. P. Jung, "Tonic, phasic and transient EEG correlates of auditory awareness in drowsiness," *Cogn. Brain Res.* Vol. 4, pp. 15-25, 1996.

[50] M. Treisman, (J. Gibbon and L. Allan. Eds.) "Temporal rhythms and cerebral rhythms," *Timing and Time Perception*, New York: Academic, Vol. 423, pp. 542-565, 1984.

[51] S. Makeig and T. P. Jung, "Changes in alertness are a principal component of variance in the EEG spectrum," *NeuroReport*, Vol. 7, pp. 21316, 1995.

[52] J. Beatty, A. Greenberg, W. P. Deibler, and J. O'Hanlon, "Operant control of occipital theta rhythm affects performance, in a radar monitoring task," *Science*, Vol. 183, pp. 871-873, 1974.

[53] L. Evans, *Traffic Safety and the Driver*, van Nostrand Reinhold (ed.), New York, 1991.

[54] L. Y. Chang and F. Mannering, "Analysis of injury severity and vehicle occupancy in truck-non-truck-involved accidents," *Accident Analysis and Prevention*, Vol. 31, pp. 579-592, 1999.

[55] L. P. Kostyniuk, F. M. Streff, and J. Zakarajsek , "Identifying unsafe driver actions that lead to fatal car-truck crashes," *AAA Foundation for Traffic Safety*, 2002.

[56] J. Hendrix, "Fatal crash rates for tractor-trailers by time of day," *Proceedings of the International Truck and Bus Safety Research and Policy Symposium*, pp. 237-250, 2002.

[57] URL: http://www.nhtsa.dot.gov/

[58] URL: http://www.sleepfoundation.org/

[59] J. Cremer, J. Kearney, and Y. Papelis, "Driving simulation: challenges for VR technology," *IEEE Computer and Applic.*, Vol. 16, No. 5, pp. 16-20, 1996.

[60] F. P. Brooks, "What's real about Virtual Reality?" *IEEE Computer Graphics and Applic.*, Vol. 19, No. 6, pp. 16-27, 1996.

[61] C. F. Hsu, C. T. Lin, T. Y. Huang, and K. Y. Young "Development of multipurpose

virtual-reality dynamic simulator with force-reflection joystick," *Journal of Systems and Control Engineering*, 2004.

[62] C. T. Lin, I. F. Chung, and J. Y. Lin, "Multipurpose virtual-reality-based motion simulator," *Proceeding of 2001 IEEE International Conference on Systems, Man, and Cybernetics*, Tucson, AZ, Oct. 2001.

[63] C. T. Lin, Y. T. Wang, T. Y. Huang, and C. F. Hsu, "Research of multi-function hla-based virtual-reality simulation system," *National Defense Conference*, pp. 185-196, R.O.C., 2003.

[64] *WorldToolKit Reference Manual, Release 7*, SENSE8 Corporation, Mill Valley, USA, 1997.

[65] P. Comon, "Independent component analysis — A new concept?" *Signal Processing*, Vol. 36, pp. 287–314, 1994.

[66] J. F. Cardoso, and B. Laheld, "Equivariant adaptive source separation," *IEEE Transactions on Signal* Processing, Vol. 45, pp. 434–444, 1996.

[67] C. T. Lin, R. C. Wu, S. F. Liang, and T. P. Jung, "Monitoring driver's alertness based on the driving performance estimation and the EEG power spectrum," *Proc of the 27th Int'l Conference of the IEEE Engineering in Medicine and Biology Society*, Shanghai, 2005.

[68] D. Ghahremani, S. Makeig, T. P. Jung, A. J. Bell, and T. J. Sejnowski. "Independent component analysis of simulated EEG using a three-shell spherical head model," *Tech Rep. INC-9601*, Institute for Neural Computation, University of California, San Diego, 1996.

[69] S. Makeig, T. P. Jung, D. Ghahremani, and T, J, Sejnowski, "Independent component analysis of simulated ERP data," *Tech Rep. INC-9606*, Institute for Neural Computation, University of California, San Diego, 1996.

[70] M. Scherg, and DVon Cramon, "Evoked dipole source potentials of the human auditory cortex," *Electroencephalography and Clinical Neurophysiology*, Vol. 65, No. 5, pp. 344-60, 1996.

[71] A. M. Dale, and M. I. Sereno, "Improved localization of cortical activity by combining EEG and MEG with MRI cortical surface reconstruction: A linear approach," *Journal of Cognitive Neuroscience*, Vol. 5, pp. 162-176, 1993.

[72] R. M. Chapman, and J. W. McCrary, "EP component identification and measurement by principal components analysis," *Brain and Cognition*, Vol. 27, No. 3, pp. 288-310, 1995.

[73] S. Makeig, T. P. Jung, A. J. Bell, D. Ghahremani, and T. J. Sejnowski. “Blind separation of event-related brain responses into independent components,” *Proc. Natl. Acad. Sci.*, Vol. 94, pp. 10979-84, USA, 1997.

[74] S. Makeig, M. Westerfield, J. Townsend, T. P. Jung, E. Courchesne, and T. J. Sejnowski, “Independent components of early event-related potentials in a visual spatial attention task,” *Philosophical Transactions: Biological Sciences*, Vol. 354, pp. 1135-44, 1999.

[75] S. Makeig, S. Enghoff, T. P. Jung, and T. J. Sejnowski, “An efficient basis for brain-actuated control,” *IEEE Trans Rehab Eng.,* Vol. 8, pp. 208-211, 2000.

[76] S. Makeig, T. P. Jung, and T. J. Sejnowski, “Awareness during drowsiness: dynamics and electrophysiological correlates,” *Canadian J. Experimental Psychology*, Vol. 54, No. 4, pp. 266-73, 2000.

[77] T. P. Jung, S. Makeig, M. Westerfield, J. Townsend, E. Courchesne, and T. J. Sejnowski, “Analyzing and visualizing single-trial event-related potentials,” *Advances in Neural Information Processing Systems*, Vol. 11, pp. 118-24, 1999.

[78] T. P. Jung, S. Makeig, C. Humphries, T. W. Lee, M. J. McKeown, V. Iragui, T. J. Sejnowski, “Removing electroencephalographic artifacts by blind source separation,” *Psychophysiology*, Vol. 37, pp. 163-78, 2000.

[79] R. N. Vigário, “Extraction of ocular artifacts from EEG using independent component analysis,” *Electroencephalography and Clinical Neurophysiology*, Vol. 103, No. 3, pp. 395-404, 1997.

[80] T. P. Jung, S. Makeig, M. Westerfield, J. Townsend, E. Courchesne, and T. J. Sejnowski, “Removal of eye activity artifacts from visual event-related potentials in normal and clinical subjects,” *Clinical Neurophysiology*, Vol. 111, No. 10, pp. 1745-58, 2000.

[81] M. J. McKeown, S. Makeig, G. G. Brown, T. P. Jung, S. S. Kindermann, A. J. Bell, and T. J. Sejnowski, “Analysis of fMRI data by blind separation into independent spatial components,” *Human Brain Mapping*, Vol. 6, No. 3, pp. 160-88, 1998.

[82] P. Nunez, *Electric Fields of the Brain*, Oxford University Press, 1981.

[83] P. Fries, J. Reynolds, A. Rorie, and R. Desimone, “Modulation of oscillatory neuronal synchronization by selective visual attention,” *Science*, Vol. 291, No. 5508, pp. 1560-63, 2001.

[84] E. Werth, P. Achermann, and A. A. Borbély, “Fronto-occipital EEG power gradients in human sleep,” *Journal of Sleep Research*, Vol. 6, No. 2, pp. 102-12, 1997.

[85] A. J. Bell and T. J. Sejnowski, “An information-maximization approach to blind separation and blind deconvolution,” *Neural Computation*, Vol. 7, pp. 1129–1159,

1995.

[86] T. W. Lee, M. Girolami, and T. J. Sejnowski, “Independent component analysis using an extended infomax algorithm for mixed sub-Gaussian and super-Gaussian sources,” *Neural Computation*, Vol. 11, pp. 606–633, 1999.

[87] A. Papoulis, “Minimum bias windows for high resolution spectral estimation,” *IEEE Trans. Inform. Theory*, Vol. IT-19, pp. 9-12, 1973.

[88] M. Steriade, “Central core modulation of spontaneous oscillations and sensory transmission in thalamocortical systems,” *Current Opinion in Neurobiol.*, Vol. 3, No. 4, pp. 619-625. 1993.

[89] A. Destexhe, D. Contreras, and M. Steriade, “Spatiotemporal analysis of local field potentials and unit discharges in cat cerebral cortex during natural wake and sleep states,” *J Neurosci*, Vol. 19, pp. 4595-4608, 1999.

[90] P. Achermann, and A. A. Borbely, “Low frequency oscillations in the human sleep electroencephalogram,” *Neuroscience*, Vol. 81, pp. 213-222, 1997.

[91] E. Werth, P. Achermann, D. J. Dijk, A. A. Borbely, “Spindle frequency activity in the sleep EEG: individual differences and topographic distribution,” *Electroencephalogr Clin Neurophysiol*, Vol. 103, pp. 535-542, 1997.

[92] D. Gervasoni, S. C. Lin, S. Ribeiro, E. S. Soares, J. Pantoja, and M. A. L. Nicolelis, “Global forebrain dynamics predict rat behavioral states and their transitions,” *Journal of Neuroscience*, Vol. 24, pp. 11137–11147, Dec. 2004.

[93] C. T. Lin and C. S. G. Lee, *Neural Fuzzy Systems: A Neuro-Fuzzy Synergism to Intelligent Systems*, Prentice Hall, 1996.

[94] C. F. Juang and C. T. Lin, “An on-line self-constructing neural fuzzy inference network and its applications,” *IEEE Trans. on Fuzzy Systems*, Vol. 6, No. 1, pp. 12-32, 1998.

[95] A. Kemeny and F. Panerai1, “Evaluating perception in driving simulation experiments,” *TRENDS in Cognitive Sciences*, pp. 31-37, Vol. 7, No. 1, Jan. 2003.

[96] S. Makeig, A. Delorme, M. Westerfield, J. Townsend, E. Courchense, and T. J. Sejnowski, “Electroencephalographic brain dynamics following visual targets requiring manual responses,” *PLOS Biology*, Vol. 2, No. 6, pp. 747-62, 2004.

[97] Z. Duric, W. D. Gray, R. Heishman, L. Fayin, A. Rosenfeld, M. J. Schoelles, C. Schunn, and H. Wechsler, “Integrating perceptual and cognitive modeling for adaptive and intelligent human-computer interaction,” *Proceedings of the IEEE*, Vol. 90, Jul. 2002.

[98] A. Yasuta, O. Kubo, M. Takahashi, H. Yoshikawa, K. Sasaki, T. Itoh, M. Matsumiya, and Y. Yamanaka, “An experimental study on the estimation of plant operators'

cognitive behavior at man-machine interface," *Proceedings of 4th IEEE International Workshop on Robot and Human Communication*, pp. 71-76, TOKYO, Jul. 1995.

[99] K. Murano, "Estimation of a plant operator's cognitive state," *Proceedings of International Conference on Industrial Electronics, Control, and Instrumentation*, pp. 371-375, Vol. 1, Nov. 1993.

[100] M. Takahashi, O. Kubo, M. Kitamura, H. Yoshikawa, "Neural network for human cognitive state estimation," *Proceedings of the IEEE/RSJ/GI International Conference on Intelligent Robots and Systems*, Vol. 3, pp. 2176-2183, Sep. 1994.

[101] M. LeCavalier, G. E. Miller, and W. R. Klemm, "Analysis of evoked EEG patterns from controlled cognitive states," *Proceedings of the Annual International Conference of the IEEE Engineering in Medicine and Biology Society*, Vol. 3, pp. 1196-1197, Nov. 1988.

[102] D. D. Schmorrow and A. A. Kruse, "DARPA's augmented cognition program-tomorrow's human computer interaction from vision to reality: building cognitively aware computational systems," *Proceedings of the 2002 IEEE 7th Conference on Human Factors and Power Plants*, pp. 7/1-7/4, Sep. 2002.

[103] H. V. Rosvold, A. F. Mirsky, I. Sarason, E. D. Bransome Jr., and L. H. Beck, "A continuous performance test of brain damage," *J. Consult. Psychol.*, Vol. 20, 1956.

[104] H. V. Semlitsch, P. Anderer, P. Schuster, and O. Presslich, "A solution for reliable and valid reduction of ocular artifacts applied to the P300 ERP," *Psychophy.*, Vol. 23, pp. 695-703, 1986.

[105] T. Kohonen, G. Barna, and R. Chrisley, "Statistical pattern recognition with neural networks: benchmarking studies," *Proceedings of the International Conference on Neural Networks*, pp. 61-68, Los Alamitos, 1988.

[106] T. Kohonen, *Self-Organizing Maps*, Springer, Berlin, 1995.

[107] H. Demuth and M. Beale, *Neural Network Toolbox For Use with MATLAB, 3ed*, The MathWorks Inc., 1998.

[108] C. T. Lin, *Neural Fuzzy Control Systems with Structure and Parameter Learning*, World Scientific, 1994.

[109] M. S. Lewicki, "A review of methods for spike sorting: the detection and classification of neural action potentials," *Network: Computation Neural Syst.*, Vol. 9, pp. 53-78, 1998.

[110] J. H. Choi, D. Kim, and T. Kim, "A new overlapping resolution method for multi-channel spike sorting," *The 2nd IEEE EMBS Conference on Neural Engineering,* Mar. 2005.

[111] A. M. Mamlouk, H. Sharp, K. Menne, U. G. Hofmann, and T. Martinetz, “Unsupervised spike sorting with ICA and its evaluation using genesis simulations,” *Neurocomputing*, 2005.

[112] P. Philipa, J. Taillarda, E. Kleinb, P. Sagaspeb, A. Charlesb, W. L. Daviesc, C. Guilleminaultd, and B. Bioulaca, “Effect of fatigue on performance measured by a driving simulator in automobile drivers,” *Journal of Psychosomatic Research*, Vol. 55 pp. 197-200, 2003.

[113] S. Chatterjee and A. S. Hadi, “Influential observations, high leverage points, and outliers in linear regression,” *Statistical Science*, pp. 379-416, 1986.

[114] C. M. Bishop, *Neural Networks for Pattern Recognition*, Oxford University Press, Oxford, 1995.

[115] D. K. McGregor, and J. A. Stern, “Time on task and blink effects on saccade duration,” *Ergonomics*, Vol. 39, pp. 649–660, 1996.

[116] N. R. Draper and H. Smith, *Applied Regression Analysis,* Wiley Series in Probability and Statistics, 1998.

姓名: 吳瑞成

性別: 男

生日: 中華民國 62 年 4 月 1 日

籍貫: 台灣省高雄縣

論文題目: 中文: 基於腦波之駕駛員認知反應估測及其在安全駕駛的應用

英文: EEG-Based Assessment of Driver Cognitive Responses and Its Application to Driving Safety

學歷:

1. 民國 84 年 6 月國立清華大學核子工程系畢業。
2. 民國 86 年 6 月國立交通大學控制工程研究所碩士班畢業。
3. 民國 94 年 7 月國立交通大學電機及控制工程研究所博士班。

已刊登或被接受之期刊論文：(總共 7.4 點)

[1] C. T. Lin, R. C. Wu, S. F. Liang, W. H. Chao, Y. J. Chen, and T. P. Jung, "EEG-based Drowsiness Estimation for Safety Driving Using Independent Component Analysis" *IEEE Transactions on Circuit and System, Part I*, In Press, 2005. (2.4 點)

[2] C. T. Lin, R. C. Wu, T. P. Jung, S. F. Liang, and T. Y. Huang, "Estimating Driving Performance Based on EEG Spectrum Analysis," *EURASIP Journal on Applied Signal Processing*, In Press, 2005. (1.2 點)

[3] C. T. Lin, R. C. Wu, J. Y. Chang, and S. F. Liang, "A Novel Prosodic-information Synthesizer Based on Recurrent Fuzzy Neural Network for the Chinese TTS System," *IEEE Trans. Systems, Man, and Cybernetics, Part B*, Vol. 34, pp. 309-324, Feb. 2004. (2.4 點)

[4] C. T. Lin, R. C. Wu, and G. D. Wu, "Noisy Speech Segmentation/Enhancement with Multiband Analysis and Neural Fuzzy Networks," *International Journal of Pattern Recognition and Articial Intelligence*, Vol. 16, No. 7, pp. 927-955, 2002. (1.4 點)

待審之期刊論文：

[1] C. T. Lin, R. C. Wu, and S. F. Liang, "EEG-based Assessment of Driver Cognitive Responses in a Dynamic Virtual-Reality Driving Environment," submitted to *IEEE Transactions on Biomedical Engineering*, Mar., 2005.

[2] C. T. Lin, R. C. Wu, Y. C. Chen, S. F. Liang, and Yu-Jie Chen, "Automatic EEG-based Alertness Estimation System Using Fuzzy Neural Networks," submitted to *IEEE Transactions on Systems, Man, and Cybernetics Part A*, Jun., 2005.

[3] C. T. Lin, R. C. Wu, S. F. Liang, and Yu-Jie Chen, "Monitoring Alertness Level with

Changes in Driving Performance Based on the EEG Power Spectrum Analysis," submitted to *IEEE Transactions on Biomedical Engineering*, Jun., 2005.

研討會論文：

[1] C. T. Lin, D. J. Liu, R. C. Wu, and G. D. Wu, "Noisy Speech Segmentation/Enhancement with Multiband Analysis and Neural Fuzzy Networks," *Proceedings of the 2002 AFSS International Conference on Fuzzy Systems. Calcutta: Advances in Soft Computing*, Calcutta, India, 2002.

[2] R. C. Wu, S. F. Liang, and C. T. Lin, "Analysis of Event-Related Potential Signals for Brain Computer Interface," *The Joint Conference on AI, Fuzzy System, and Grey System*, Taipei, Taiwan, 2003.

[3] R. C. Wu, S. F. Liang, C. T. Lin, and C. F. Hsu, "Applications of Event-Related -Potential- Based Brain Computer Interface to Intelligent Transportation Systems," *IEEE International Conference on Networking, Sensing and Control*, Session TA5-1, Taipei, Taiwan, 2004.

[4] R. C. Wu, C. T. Lin, S. F. Liang, T. Y. Huang, Y. C. Chen, and T. P. Jung, "Estimating Driving Performance Based on EEG Spectrum and Fuzzy Neural Network," *IEEE International Joint Conference on Neural Networks*, Budapest, Hungry, 2004.

[5] C. T. Lin, S. F. Liang, R. C. Wu, Y. C. Chen, and T. Y. Huang, "Driving Performance Estimation with EEG Spectrum and Neural-Fuzzy Network," *The 20th National Conference on Fuzzy Theory and Its Applications*, I-Lan, Taiwan, 2004.

[6] R. C. Wu, C. T. Lin, S. F. Liang, T. Y. Huang, and T. P. Jung, "EEG-Based Fuzzy Neural Network Estimator for Driving Performance," *IEEE International Conference on Systems, Man and Cybernetics*, Hague, Netherlands, Oct. 10-13, 2004.

[7] S. F. Liang, C. T. Lin, R. C. Wu, W. H. Chao, and T. Y. Huang, "Classifications of Driver Cognitive Responses From EEG Analysis," *IEEE International Symposium on Circuits and Systems*, Kobe, Japan, May 23-26, 2005.

[8] C. T. Lin, Y. C. Chen, R. C. Wu, S. F. Liang, and T. Y Huang, "Assessment of Driver Vigilance and Performance Using EEG-based Fuzzy Neural Networks," *IEEE International Symposium on Circuits and Systems*, Kobe, Japan, May 23-26, 2005.

[9] C. T. Lin, R. C. Wu, S. F. Liang, Y. C. Chen, T. Y. Huang, and T. P. Jung, "Monitoring Alertness with Driving Performance from Changes in the EEG Spectrum," *The 27th Annual International Conference of the IEEE Engineering in Medicine and Biology Society*, Shanghai, China, Sep. 1-4, 2005.

[10] C. T. Lin, Y. C. Chen, R. C. Wu, S. F. Liang, T. Y Huang, and Y. J. Chen, "Adaptive Feature Extractions in an EEG-based Alertness Estimation System," *IEEE International Conference on Systems, Man and Cybernetics*, Hawaii, USA, Oct. 10-12, 2005.